AQUEOUS PHASE PROCESSING OF LIGNOCELLULOSIC BIOMASS FOR BIOFUEL PRODUCTION

A Dissertation
Presented to
The Academic Faculty

by

Wei Mu

In Partial Fulfillment
of the Requirements for the Degree
Doctor of Philosophy in the
School of Chemical & Biomolecular Engineering

Georgia Institute of Technology
December, 2014

AQUEOUS PHASE PROCESSING OF LIGNOCELLULOSIC BIOMASS FOR BIOFUEL PRODUCTION

Approved by:

Dr. Yulin Deng, Advisor
School of Chemical & Biomolecular Engineering
Georgia Institute of Technology

Dr. Carsten Sievers
School of Chemical & Biomolecular Engineering
Georgia Institute of Technology

Dr. Christopher W. Jones
School of Chemical & Biomolecular Engineering
Georgia Institute of Technology

Dr. Preet M. Singh
School of Materials Science and Engineering
Georgia Institute of Technology

Dr. Pradeep K. Agrawal
School of Chemical & Biomolecular Engineering
Georgia Institute of Technology

Date Approved: Nov 3, 2014

In memory of my beloved grandma.

ACKNOWLEDGEMENTS

The Ph. D study at the Georgia Institute of Technology is a memorable journey in my life. It is filled with happiness, surprise, as well as frustrating, disappointing, just as our life. I would not get through it without the support from lots of people. There is no doubt that it will always be a treasurable experience to me.

Foremost, I would like to express my sincere gratitude to my advisor Prof Yulin Deng, for his support, patience, enthusiasm, and immense knowledge. I appreciate his great help in my Ph. D study, research and writing of this thesis. I could not have imagined having a better advisor and mentor.

Besides my advisor, I would like to express my sincere thanks to my thesis committee: Prof. Christopher Jones, Prof. Pradeep Agrawal, Prof. Carsten Sievers, Prof. Preet Singh and Prof. Arthur Ragauskas, for their encouragement, insightful comments, and hard questions.

I appreciate all the colleagues and co-workers at Georgia Tech, especially Dr. Zeshan Hu. His dedicated work greatly facilitated my research work. I also want to thank the visiting scholars, Dr. Jian Gong, Dr. Hongli Cai, Wei Liu, etc. Last but not the least, I would like to thank all our group members. I feel lucky to have all of you around.

I reserve my deepest gratitude to Jie Pan, my dearest and adorable girlfriend. Meeting her is one of the best things (things) that ever happened to me in my life. We shared a great many fantastic moments during the last couple years and we will collect a lot more in the future.

I am grateful to my family for giving birth to me and their spiritual supporting since the first day. My parents have been the most influential person in my life. I appreciate all the sacrifices they made to raise me. I would also like to thank all my friends in China for the wonderful times we once enjoyed together.

Here I would like to especially express my appreciation to Ms. Shiow-Meei Lai and Dr. Lei Kerr, who brought me into the Ph. D program. All these would not happen without their generous help.

At last, I want to acknowledge the financial support from the Paper Science and Engineering fellowship program at the Renewable Bioproducts Institute (RBI).

TABLE OF CONTENTS

LIST OF TABLES

LIST OF FIGURES

LIST OF ABBREVIATIONS

Ar	Aromatic
BET	Brunauer, Emmett and Teller
BJH	Barret-Joyner-Halenda
CAT	Catechol
$CDCl_3$	Chloroform, deuterated
D	Polydispersity
DEPT	Distortionless Enhancement by Polarization Transfer
DMSO	Dimethyl sulfoxide
EOL	Ethanol Organosolv Lignin
FTIR	Fourier Transform infrared
GC	Gas Chromatography
GPC	Gel Permeation chromatography
GUA	Guaiacol
HDO	Hydrodeoxygenation
HSQC	Heteronuclear Single-Quantum Correlation
HW	Hardwood
HYD	Hydrogenation
M_n	Number average molecular weight
MS	Mass Spectroscopy
M_w	Weight average molecular weight
NMR	Nuclear Magnetic Resonance
Pd	Palladium
Ph	Phenol

Pt	Platinum
ppm	part per million
Rh	Rhodium
RT	Room Temperature
Ru	Ruthenium
SEM	Scanning Electron Microscopy
SW	Softwood
T	Temperature
T1	Spin-lattice relaxation time
TEM	Transmission Electron Microscopy
TGA	Thermogravimetric Analysis
THF	Tetrahydrofuran
TPR	Temperature programmed reduction
UV	Ultraviolet
XRD	X-ray Diffraction
1 D	1 dimensional
2 D	2 dimensional

SUMMARY

Depleting fossil fuel reserves and increase of energy demands drive people to find alternative and sustainable energy resources such as wind, solar, tidal, geothermal, and biomass. Among all these sustainable energy resources, biomass is the only one that we can be used for chemicals and liquid fuel production. The advantages of using biomass include fast production, high efficiency, and ease of harvesting and transportation. The major compositions of lignocellulosic biomass are cellulose, hemicellulose, and lignin. The former two are widely studied and due to the relatively uniform and unique chemical structures, some of the processes have undergone commercialization. However lignin, as the second most abundant biomass component, receives little attention. The US paper industry produces approximately 50 million tons of lignin annually and over 98 percent of these are burned directly. The major problems with lignin are poor thermal stability and a complex structure. It tends to form coke under high temperatures, which makes the conversion process extraordinarily difficult. Its complex structure also results in complications in product characterization.

Thermochemical methods are commonly used in biomass decomposition, such as gasification, pyrolysis and direct combustion. Pyrolysis is an economically feasible method. It can undergo operation under an ambient atmosphere, so the equipment investment is low. The major products from pyrolysis are gases, pyrolysis oils and char. However, one cannot use pyrolysis oil directly because of its poor thermal stability, and

high acidity; therefore, it requires further upgrading is required. Catalytic hydrodeoxygenation (HDO) is a general approach for oil upgrading. Evaluating catalysts, optimizating reaction conditions, and understanding of reaction mechanisms are critical to its application.

This thesis studied the catalytic upgrading of pyrolysis oil derived from both ethanol organosolv (EOL) lignin and whole biomass. There are four major components of this thesis.

(1) In the first part, several lignin model compounds and the commonly used noble metal catalysts were evaluated. During the reaction, coke formation deactivated several catalysts. The catalysts were characterized with BET and a great reduction in the surface area was observed. The reaction pathway of the coke formation was proposed. Ruthenium/activated carbon can hydrogenate the aromatic ring and remove the methoxyl group as well. The reaction mechanism was deduced based on the products distribution of the model compounds.

(2) The second part of this study focuses on the catalytic HDO reaction with real EOL pyrolysis oil. To confirm whether the mechanism obtained from model compounds is applicable to pyrolysis oil, two catalysts were picked to react with EOL pyrolysis heavy oil. The results indicate the reaction mechanism with EOL pyrolysis oil is similar to the results of the model compound study.

Further investigation was carried out with the ruthenium catalyst, which displayed the highest reactivity in the previous study. Due to the deactivation of the Ru/C catalyst by tar produced during the upgrading, two-step hydrodeoxygenation at different temperature was adopted in this study. In this part, the first-step is discussed. The upgraded pyrolysis oil was analyzed using GC-MS, ^{1}H, ^{13}C, and HSQC ^{2}D NMR. Deuterium gas was used to elucidate the fundamental principle in the hydrogenation reaction because the deuterium atom is invisible in the regular ^{1}H-NMR. The comparison between the products upgraded by deuterium and hydrogen provides an intuitive and accurate result.

(3) The third part focuses on the product analysis from the second-step HDO. In the second-step HDO, all the products were completely hydrogenated. The molecular weight of the upgraded oil is in the monomer range and the GC-MS study provided detailed compound structures. However, some of them still contain oxygen atoms. To produce completely deoxygenated products, ZSM-5 was used as a supporting material. The experiment with the model compound (guaiacol) showed alkali treated ZSM-5 was effective in catalyzing the dehydration reaction and producing deoxygenated compounds.

(4) In the fourth part, light oil derived from whole biomass also underwent treatment under the same hydrodeoxygenation reaction conditions as those used in upgrading EOL pyrolysis oil. In this reaction, the biomass were separated into three components: stem, residue and bark. The contents of

cellulose, hemicellulose and lignin are different in the three components. The compound structures of the three different types of light oil were analyzed by GC, ^{1}H and ^{1}H-^{13}C HSQC-NMR. Then the light oil was processed under the same condition as the heavy oil upgrading. The reaction mechanisms with cellulose and hemicellulose were also studied. These results will be of value in developing of complete hydrogenation of whole biomass pyrolysis oils.

CHAPTER 1: INTRODUCTION

In the past century, energy consumption has grown 17-fold worldwide, [1] and is predicted to increase another 50 percent by 2025 [2]. According to data from the U.S. Energy Information Administration (EIA), the production of crude oil increased from 420 million barrels a year in 1920 to 2700 million barrels a year in 2013 [3]. The major products from petroleum refinery process are transportation fuels and chemicals. However, there are several inherent problems with the petroleum industry. First, during the refinery process, a tremendous amount of CO_2 releases into the atmosphere. CO_2 is a greenhouse gas (GHG) and it absorbs the thermal radiation from the earth and re-radiates it back to the ground, hence causing the increase of atmospheric temperature. Second, the petroleum reserves are limited. Nowadays the drilling stations extend from onshore to offshore, even in the middle of the ocean. Nonetheless, all the petroleum resources will deplete eventually. Many countries recognize this problem and have shown efforts to search for alternative sustainable energy resources. For example, the study conducted by the National Renewable Energy Lab (NREL) indicated 80 percent of the electricity in the United States could be generated from renewable energy by 2050. The US Department of Agriculture and the US Department of Energy also established a vision to derive 25 percent of chemicals and 20 percent of transportation fuels from biomass before 2030 [4].

Biomass proves to be the only feasible renewable source for liquid transportation fuel production. [4] The energy generated from biomass recently surpassed the hydroelectric and it became the single largest renewable energy resource. The biomass used for energy

production increased from 184 million dry tons in 2005 to 200 million dry tons in 2009. Meanwhile the fraction of biofuels increased from 10 percent to 31 percent. [4] The lignocellulosic biomass seems to be an ideal candidate because it is a CO_2-neutral, widely distributed, and readily usable renewable energy. It is the most abundant source of carbohydrates in the world. The annual forest resource potential is 368 million dry tons each year. Currently, the total annual consumption is approaching 190 million dry tons, which include the agricultural feedstock. Thus the amount of forest resource is enough to cover the consumption of the agricultural products. The path forward for biofuels and biomaterials, published by the leading experts in this field, has predicted that "the integration of agro-energy crops and biorefinery manufacturing technologies offers the potential for the development of sustainable biopower and biomaterials that will lead to a new manufacturing paradigm." [2].

There are three major compositions in lignocellulosic biomass: cellulose, hemicellulose and lignin. Researchers have intensively stidied the previous two in various approaches. However, lignin, as the second most abundant natural-made polymer, has received less attention because of its complex structure and poor thermal stability. The US paper industry produces over 50 million tons of lignin per year. Over 98 percent of these are burned directly. [5] Another major source of lignin is bioethanol plants. Regardless of the technology employed, almost all bioprocessing approaches result in forming a process stream of waste lignin. [6] Different from other biomass wastes, lignin is energy-rich. Therefore, it is pragmatic and desirable to find an efficient approach to convert lignin into fuels and useful chemicals.

Intensive researches and developments have been carried out in the biomass utilization. The most common methods for biomass conversion to liquid fuels include: (1) gasification followed by Fischer–Tropsch reaction, [7] (2) pyrolysis and catalytic upgrading, [8] and (3) enzymatic fermentation [9]. Among these methods, pyrolysis is regarded as a promising technique to convert biomass into liquid products, such as aromatic chemicals and biofuels. [10] It is a thermochemical process that heats biomass in the absence of oxygen.

One of the major challenges towards industrializing biomass pyrolysis is the poor properties of pyrolysis oil, such as low volatility, high oxygen content, high acidity and viscosity, corrosiveness, etc. [11] Therefore, upgrading raw pyrolysis oils is a necessary and critical step. In this dissertation, the conversion of biomass to liquid fuel through pyrolysis and catalytic upgrading is systematically studied.

The major focuses of this dissertation are summarized as follows:

- Using lignin model compounds to screen the proper catalyst for HDO upgrading, and studying the reaction mechanisms (Chapter 4)

- Catalytic upgrading of lignin derived pyrolysis heavy oil. (Chapter 5, 6). The reaction mechanisms of the noble metals catalyzed heavy oil upgrading are in

accordance with the reaction pathways deduced from the model compounds study.

- Production of cyclohexanol and 4-methyl-cyclohexanol from the lignin pyrolysis heavy oil upgrading. (Chapter 6)

- Convert lignin into gasoline-compatible fuels from the aqueous phase HDO of the heavy oil derived from the lignin pyrolysis. (Chapter 6)

- Structure analysis of the light oils derived from different components of the woody biomass (stem, residue and bark). The reaction mechanisms of the upgrading of these light oils were studied. (Chapter 7)

CHAPTER 2: LITERATURE REVIEW[1]

Biomass pyrolysis oil is a potential renewable biofuel precursor. The particular research regarding to the lignin pyrolysis process has not been widely studied until recently. Lignin is the second most abundant biomass component and the primary renewable aromatic resource in nature. The pyrolysis chemistry and mechanism of lignin are significantly different from the pyrolysis of cellulose or entire biomass. This chapter reviewed the background of biofuels, the composition of biomass, the pyrolysis and catalytic upgrading process, and the common liquid oil characterization methods.

2.1 Background

The growth of the domestic energy consumption makes the accommodation of the alternative resources become an inevitable step in the future. The annual energy review reported by the U.S Department of Energy highlighted several key facts related to the energy consumption in the United States, [12, 13] including:

- The domestic energy consumption has increased by 28% in last 37 years. The total energy consumption is 97 quadrillion Btu in 2010. A large percentage of the energy (28% in 2010) was consumed for transportation.

---

[1] Part of this chapter was published in BioEnergy Research, 2013. It is entitled as "Lignin Pyrolysis Components and Upgrading—Technology Review". Reproduced by permission of Springer Science and Business Media.

- Annual energy consumption of renewable resources in 2012 is twice the value of 2001.
- Until recently, the energy from renewable sources exceeded the domestic consumption of nuclear electric power.
- The consumption of the ethanol fuel has more than tripled in last six years. The annual consumption of biodiesel is doubled within one year.

The remarkable growth of the domestic renewable fuels is due to the transformations in economic, political policies and consumers' demands. The energy independence is closely related to the national security. Environmentalists and scientists also concern about how to reduce the emission of carbon dioxide, which contributes to the global warming and cause changes to farming practices. [14-19]

The potential supply of renewable biomass from forest and agricultural lands are tremendous throughout the world. In the land of the United States alone, the annual capacity of renewable biomass is higher than 1.3 billion dry tons of biomass, which is readily available for bio-refineries. [20] Therefore, the conversion of renewable biomass into other useful products such as fuels, specialty chemicals, and plastics, attracts many scientists and great efforts are contributed towards developing the process as well as advancing the fundamental science. It is claimed that the annual energy potential of the sustainable global biomass is approximately ~10^{20} J and approximately 40% is being used. [21] Due to the high bulk density and low moisture content, woody biomass is an ideal feedstock for the biomass conversion process. All fractions of the tree can be

directly used for chemical production that a great deal of researches is related to the fermentation of cellulose and hemicellulose to produce bio-ethanol. Meanwhile, lignin, as the second most abundant natural-made biopolymer, receives much less attention. Most of the lignin is burned directly as agricultural waste.

Biomass pyrolysis is regarded as a promising approach for renewable chemicals and fuels production and it has been proven at commercial scale. However, several drawbacks have not been addressed. The components of biomass pyrolysis oils are very complicated and it directly determines the properties of bio-oil. In this review chapter, the details about pyrolysis oil components, particularly those from lignin pyrolysis processes, are discussed. Due to the poor physical and chemical property, the lignin pyrolysis oil has to be upgraded before use. The most common upgrading approach is hydrodeoxygenation (HDO). Catalysts have been widely used during the pyrolysis bio oil upgrading.

2.2 Lignocellulosic Biomass

Lignocellulosic biomass captures the solar energy and stores it as chemical energy. The sugar building blocks are firstly produced by absorbing carbon dioxide and water. Then, the sugar chains keep growing and gradually exhibit a polymer form. Such type of molecules is the most abundant organic matter on the earth. Table 2.1 provides several examples of productivity and solar energy capture of several types of biomass.

Table 2.1 Productivity and solar energy capture of some biomass (selected) [22]

Location	Biomass Community	Annual Yield dry matter (t/ha-year)	Average insolation (W/m^2)	Solar energy capture efficiency (%)
Minnesota	Willow and hybrid poplar	8-11	159	0.30 - 0.41
Texas	Switchgrass	8-20	212	0.22 - 0.56
Nova Scotia	Sublittoral seaweed	32.1	133	1.34
England	Coniferous forest	34.1	106	1.79
Israel	Maize	34.1	239	0.79
Germany	Temperate reedswamp	46.0	133	1.92
West Indies	Tropical forest, mixed ages	59.0	212	1.55
Java	Sugarcane	86.8	186	2.59
Thailand	Green algae	164	186	4.90

The major compositions of lignocellulosic biomass are cellulose, hemicellulose and lignin. Other components, such as tannin, pigments, resin, etc., are in relatively minor quantity. The chemical compositions of some common biomasses are summarized in Table 2.2 and some of them are very different.

Table 2.2 Chemical Composition of different Wood Species[23]

Constituent	Scots Pine (Pius Sylvestris)	Spruce (Picea Glauca)	Eucalyptus (Eucalyptus Camaldulensis)	Silver Birch (Betula Verrucosa)
Cellulose (%)	40.0	39.5	45.0	41.0
Hemicellulose				
-Glucomannan (%)	16.0	17.2	3.1	2.3
-Glucuroxylan	8.9	10.4	14.1	27.5
-Other Polysaccarides	3.6	3.0	2.0	2.6
Lignin	27.7	27.5	31.3	22.0
Total Extractives (%)	3.5	2.1	2.8	3.0

2.2.1 Cellulose

Cellulose is a polysaccharide consisting of many thousands of D-glucose monomers. Figure 2.1 shows the chemical structure of cellulose. The linkages between monomers are β-1,4 glycoside. The molecular weight of cellulose is typically distributed between 300,000 and 500,000. The annual production of cellulose through photosynthesis is approximately 100 billion metric tons. Cellulose is the skeletal structure of most lignocellulosic biomass due to the highly organized structure and hydrogen bonds. The crystallinity of cellulose is generally between 50-70% [24].

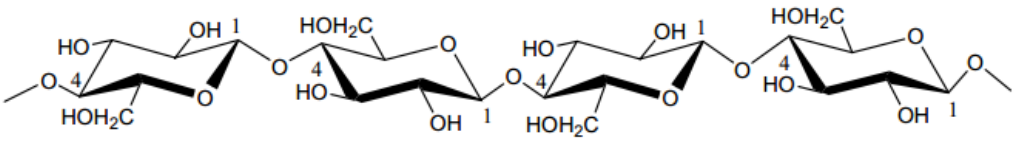

Figure 2.1 Chemical structure of cellulose.

2.2.2 Hemicellulose

Hemicellulose is another type of polysaccharide polymer. As listed in table 2.2, hemicellulose typically constitutes 20 to 40 wt.% of the biomass. Hemicellulose contains five different monomers. These monomers can be divided into two groups: five-membered ring (xylose and arabinose) and six-membered ring (galactose, glucose, mannose). The most abundant sugar in hemicellulose is xylose. Unlike cellulose, hemicellulose is amorphous and it is relatively easier to hydrolyze. Figure 2.2 is an example of the chemical structure of hemicellulose in softwood.

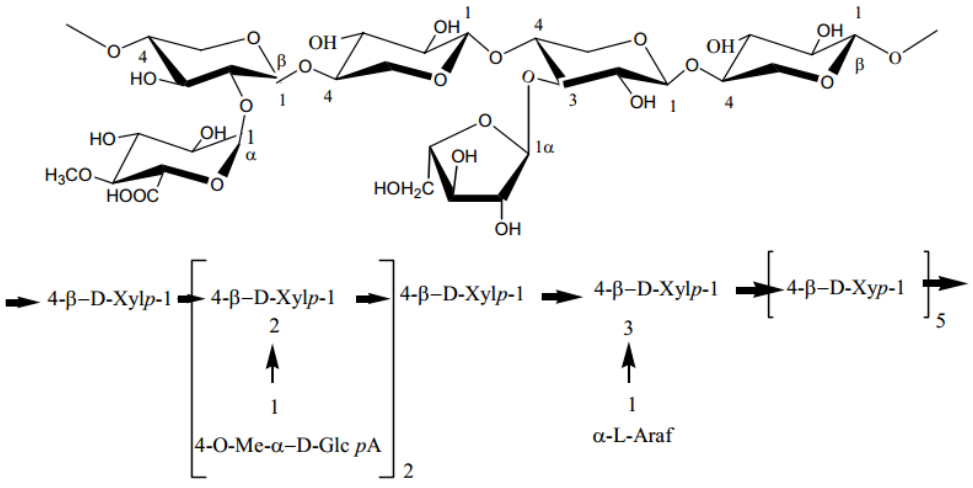

Figure 2.2 Hemicellulose Principal Structure: Arabinoglucuronoxylan in Softwood [25]

2.2.3 Lignin

Lignin is also abundant in the lignocellulosic biomass. The mass percent of lignin is normally 10 – 25 wt.%. The chemical structure of lignin is highly branched mononuclear aromatic and the aromatic ring is often highly substituted. Lignin mainly exists in the cell wall, especially in the woody biomass. There are three major functions of lignin: (1) conducting water in plant stems; (2) providing mechanical support and structure; (3) resisting attack by most microorganisms. [26] Figure 2.3 is an illustrations of the structures of lignin in softwood and hardwood.

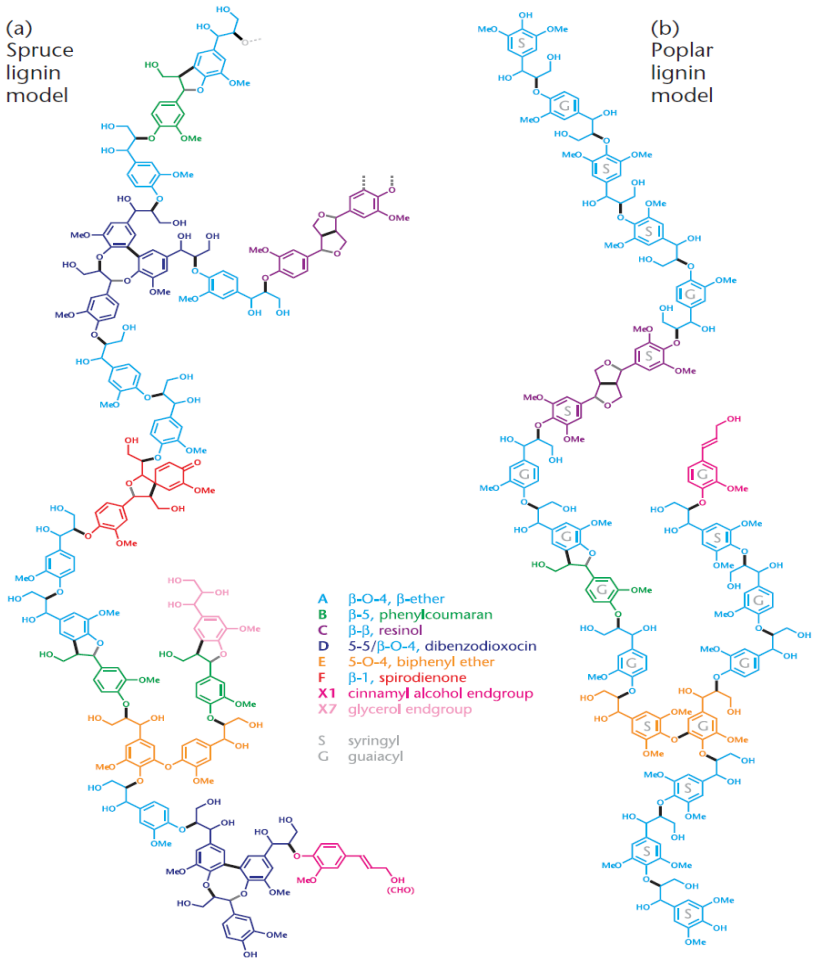

Figure 2.3 Examples of lignin structure in (a) Softwood and (b) Hardwood [27]

There are three building block monomers of lignin: *p*-coumaryl, coniferyl and sinapyl. As shown in Figure 2.4 (a), all three building blocks have aromatic structure. The major difference is the number of the methoxyl group. These monomers interact with each other and form various types of interlinkages. Figure 2.4 (b) are the ten most general linkages between lignin monomers. Table 2.3 summarizes the ratios of *p*-coumaryl (H), coniferyl (G) and sinapyl (S) in several biomasses.

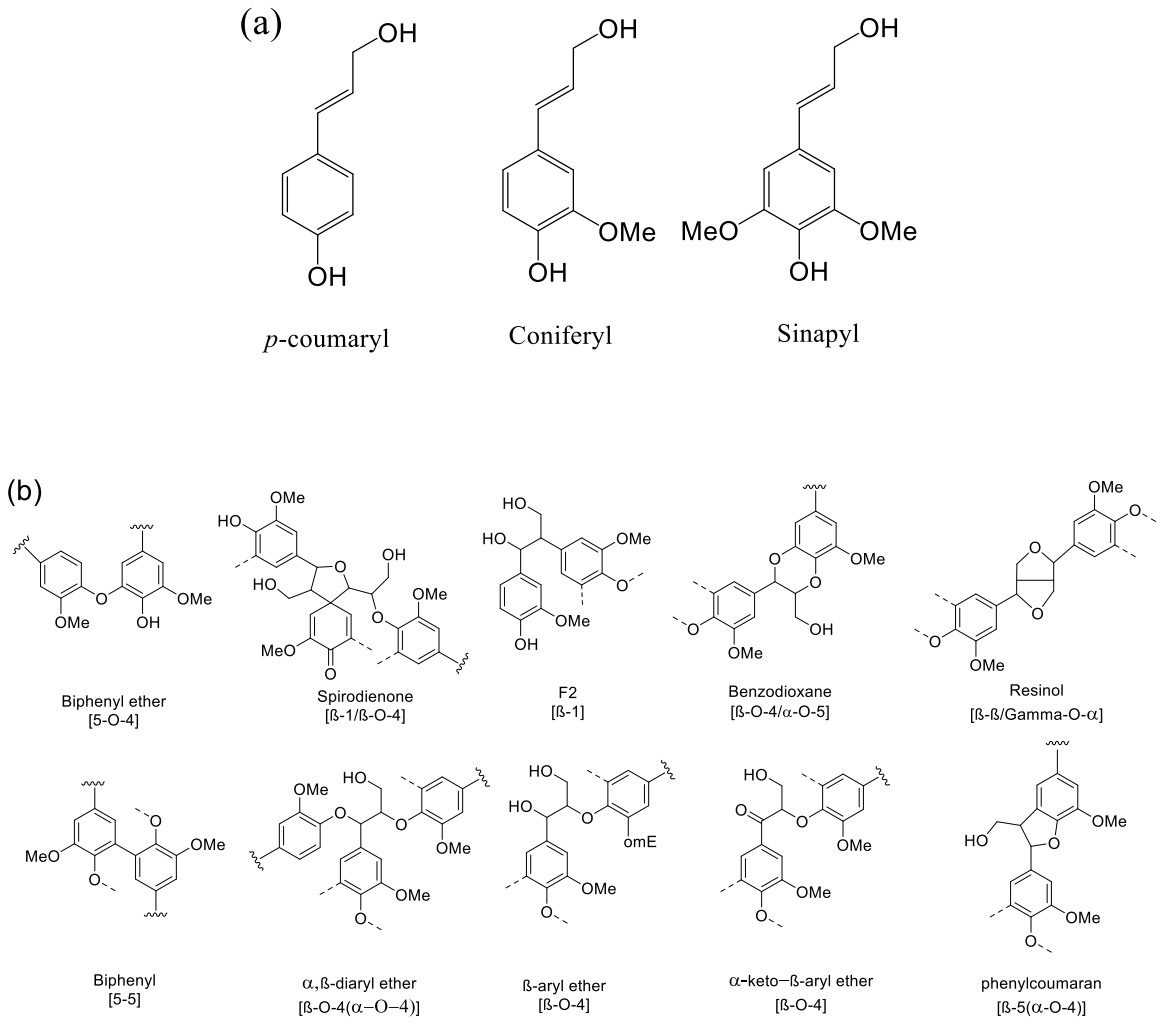

Figure 2.4 (a) Building block of lignin and (b) common linkages between lignin monomers [27]

Table 2.3 Lignin Composition of several biomass and the G:S:H distribution [28].

	Lignin %	G	S	H
Loblolly pine	29	86	2	12
Spruce	28	94	1	5
Eucalyptus globus	22	14	84	2
Eucalyptus grandis	27	27	69	2
Birch penclula	22	29	69	2
Beech	26	56	40	4

The molecular weight of lignin is normally distributed in a wide range. The separation process of lignin will decompose lignin to smaller fragments. Table 2.4 is the summarization of molecular weights of various lignin. The carbon/oxygen ratio of lignin is typically around 3:1 and the carbon/hydrogen ratio is slightly less than 1.

Table 2.4 Molecular weight distribution of lignin in selected biomass and the calculated polydispersity (D) [29].

	M_w(g mol^{-1})	M_n(g mol^{-1})	D
Douglas fir	49500	7700	6.4
White fir	57000	7700	7.4
E. globules	23400	6500	3.6
E. grandis	27700	7500	3.7

2.3 Brief introduction to pyrolysis process

During the pyrolysis process, biomass is heated in the absence of oxygen. The major products are gases, pyrolysis oil and char. Pyrolysis normally carries out under ambient atmosphere without reducing gas, which lowers the capital investment and operation expense. Although the cost of pyrolysis oil is relatively low, the quality of the fuel obtained from the process is inferior that it cannot be used directly in conventional gasoline and diesel engine. Due to the high oxygen content, the pyrolysis oil is immiscible with gasoline fuel. It also has several poor properties such as low volatility, instability, high viscosity, high acidity and low heating value. These properties are mainly attributed to the large amount of unsaturated bonds (mainly the olefin and aldehyde structure) and oxygen atoms in the pyrolysis oil. [13] Therefore, upgrade the pyrolysis oil to remove the oxygen and hydrogenate the unsaturated bonds is a necessary step. A summary of lignin pyrolysis conditions and the yields of pyrolysis products are shown in Table 2.5.

Table 2.5. Summary of lignin pyrolysis conditions and the yield of pyrolysis products

Lignin	Reactor	Temperature (K)	Tar (wt.%)	Char (wt.%)	Gas (wt.%)
Kraft lignin (wheat straw and sarkanda grass) [30]	Fluidized bed	773	31	49	6
	Fluidized bed	683-833	31	34	12
	Fluidized bed	748-798	50	42	8
	Entrained flow	973	37	35	28
	Batch	753	22	48	30
Kraft lignin (pine)	Fluidized bed[31]	823	23	41	39
Lignoboost^{TM} (pine)			22	29	49
EOL (*pinus radiate*)			16	63	21
Kraft lignin	Fixed bed[32]	1073	3-5	43-48	49-52
EOL			14-21	35-44	41-44
Kraft lignin	Fix bed[33]	923	13	47	40
EOL			19	39	42
Klason lignin (almond shells)[34]	Micro pyroprobe reactor	773	53	34	7
		873	64	20	9
		973	55	17	17
		1073	50	15	22
		1173	43	14	29

2.4 Chemical composition and NMR characterization methods of lignin derived pyrolysis oil

2.4.1 GC-MS analysis of lignin pyrolysis oil

Most of the pyrolysis works employed GC-MS to analyze the liquid pyrolysis products. [30, 35-49] By using pyrolysis(Py)-GC-MS, Jimenez et al. [49] indicated that softwood lignin yielded guaiacyl derivatives, coniferaldehyde and coniferyl alcohol as the major products; hardwood lignin was converted to guaiacyl and syringyl derivatives, syringaldehyde, coniferyl alcohol and sinapyl alcohol. Pyrolysis of bamboo lignin produced p-vinylphenol as the major compound. Similarly, Jiang et al. [39] also used Py-GC-MS to analyze pyrolysis products of lignin over a temperature range of 673-1073 K and indicated that the maximum yield of phenolic compounds was obtained at 873 K. Most of the phenolic compounds had an individual yield of less than 1 wt.% of lignin on an ash free basis. Greenwood et al. [45] pyrolyzed *Douglas* fir and *Q. nigra* water oak lignin in a laser micropyrolysis-GC-MS system. They found that guaiacol, 4-methyl-guaiacol, vinylguaiacol, eugenol, vanillin and coniferylaldehyde were the major components in the pyrolysis oil produced from the *Douglas* fir lignin. For the *Q. nigra* water oak lignin pyrolysis oil, guaiacol, 4-methyl-guaiacol, vinylguaiacol, syringol, eugenol, 3,5-dimethoxyacetophenone, 4-methyl 2,5-dimethoxy benzaldehyde, 4-allyl-dimethoxylphenol, syringaldehyde, 2,6-dimethoxyl-2-propylphenol and sinapaldehyde were found as the major components. Jegers et al. [47] also showed that guaiacol, 4-methylguaiacol, 4-ethylguaiacol, catechol, 4-methylcatechol, 4-ethylcatechol, phenol,

cresol and 4-ethylphenol were the major products of lignin pyrolysis. As the most abundant products, the content of guaiacol and 4-methylguaiacol are ~5 wt.% of dry lignin. Lou et al. [41] examined the effect of temperature on the composition of pyrolysis products and indicated that the contents of methoxyl contained components, such as guaiacol, 4-methylguaiacol, 4-vinylguaiacol and syringol decreased at higher pyrolysis temperature. In contrast, the contents of non-methoxyl contained compounds, like cresols, ethyl-phenol, and 2, 6-dimethyl-phenol, increased with the increasing treatment temperature.

To understand the possible decomposition pathways of lignin during the pyrolysis process, and to find an effective upgrading method, many researchers use pyrolysis oil model compounds to simplify the simulation model. To facilitate this part of work, the GC-MS detected components in the lignin pyrolysis oils are summarized in Appendix I [30, 39, 44-48]. There are approximately a hundred compounds and almost all of them contain a phenol structure. Furthermore, phenol, acetovanillone, cresols, guaiacol, 4-ethylphenol, syringaldehyde, acetosyringone, 4-methylguaiacol, catechol, 3-methylcatechol, 4-methylguaiacol, 4-vinylguaiacol, vanillin, syringol, eugenol, isoeugenol and acetovanillone have been reported in more than four references and many of them were also reported in other references.[37, 40-42] Therefore, these components can be used as potential candidates in the model compounds study of lignin pyrolysis. The possible decomposition pathways are shown in Figure 2.5.

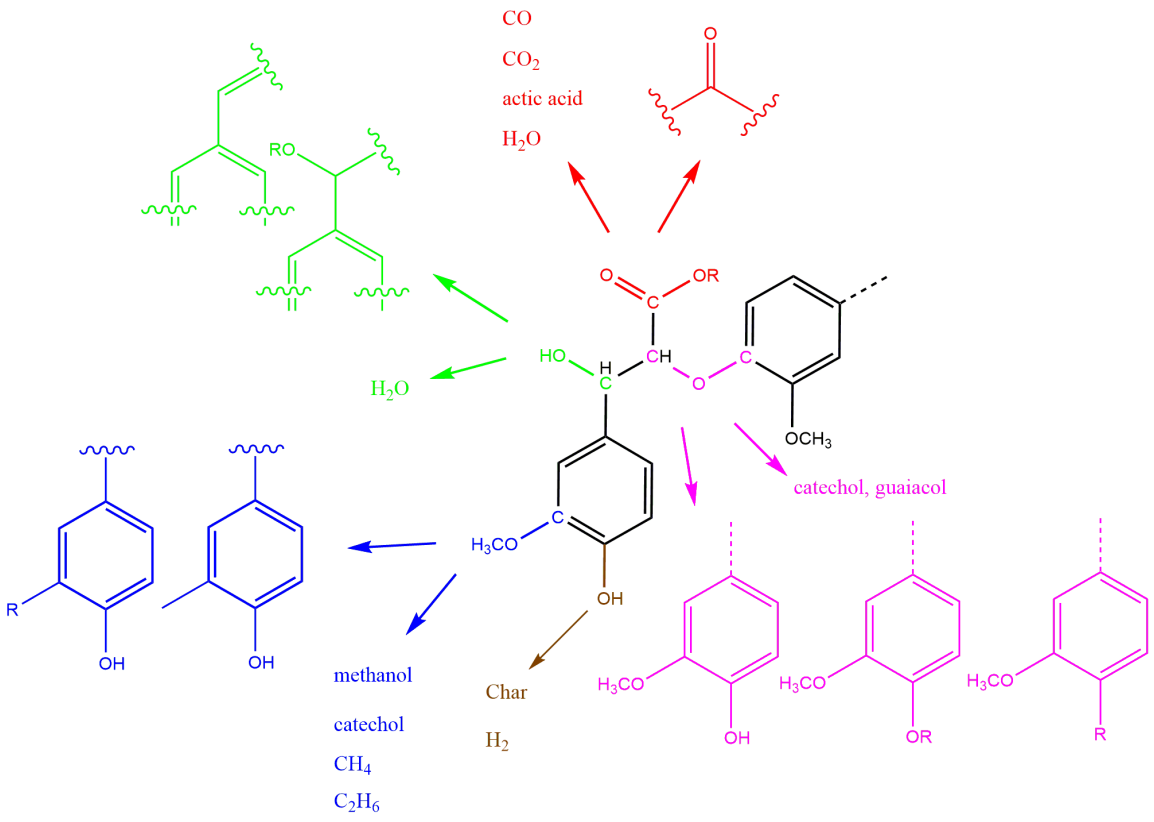

Figure 2.5. The possible decomposition pathways of lignin during the pyrolysis [50-57]

2.4.2 NMR analysis of lignin pyrolysis oil

Most recently, several research works [58-70] introduced NMR, including the quantitative ^{1}H, ^{31}P, ^{13}C-NMR, and semi-quantitative ^{1}H-^{13}C HSQC-NMR, to characterize the pyrolysis oils. Mullen et al. [58] analyzed various pyrolysis oils produced from switchgrass, alfalfa stems, corn stover, guayule (whole plant and latex-extracted bagasse), and chicken litter by ^{1}H, ^{13}C, and ^{13}C-DEPT NMR. They found that pyrolysis oil from chicken litter had the lowest overall amount of methyl groups and had the highest ketone content among all the pyrolysis oils studied. The ^{13}C and DEPT-NMR analysis indicated that the pyrolysis oils from corn stover and switchgrass had the fewest

aliphatic carbons. The large amount of methine (CH_1) groups in the corn stover pyrolysis oil suggested that its aliphatics were highly branched. However, there were almost the same amounts of methyl (-CH_3) groups as its methine groups, while the percentage of -CH_2- was low. It was surmised that these branches were very short which could mostly be methyl groups. Conversely, pyrolysis oil from switchgrass appeared to have more straight-chain aliphatics. The authors also indicated that the aromatic region of these pyrolysis oils had CH_0:CH_1 ratios of >2:1, which represented highly complex substituted (at least four substituents) benzene rings.

In a previous publication, ^{31}P and ^{13}C-NMR were used to characterize pyrolysis oils produced from softwood (SW) kraft lignin at 673, 773, 873 and 973 K [69]. A ^{13}C-NMR database was created to provide a more accurate chemical shift assignments for the analysis of pyrolysis oils. This analysis showed that the carbonyl group content was reduced after pyrolysis, and methoxyl groups were significantly eliminated after pyrolysis, especially at higher pyrolysis temperatures. Nearly 70%-80% of the carbons from a water insoluble portion of pyrolysis oil (heavy oil) were aromatic carbon. By using ^{31}P-NMR, the results indicated that the heavy oils contained less aliphatic hydroxyl group and carboxyl acid group. The decreased concentration of aliphatic hydroxyl and acid groups was significant as it indicated that the lignin side chain hydroxyl groups were readily eliminated during the thermal treatment. In contrast, the contents of guaiacyl, p-hydroxyphenyl and catechol type hydroxyl groups were increased after pyrolysis. The ^{31}P-NMR results for the water soluble part of pyrolysis oil (light oil) showed that it

contained nearly 80 w/w% water and another 10 w/w% is methanol, catechol and acetic acid.

To solve spectral overlapping problems when using ^{13}C-NMR to analyze the pyrolysis oils, the previous work [68] demonstrated that ^{1}H-^{13}C HSQC-NMR was uniquely well suited to analyze various C-H bonds present in the pyrolysis oils. The fingerprint analysis of ^{1}H-^{13}C HSQC-NMR spectral data provides chemical shift assignment of twenty-seven (fourteen from lignin pyrolysis oil) different types of C-H bonds presented in the pyrolysis oils produced from cellulose, lignin and pine wood. The ^{1}H-^{13}C HSQC-NMR for the lignin pyrolysis oils showed that there were two different types of methoxyl groups presented in the pyrolysis oils, which indicated that the native methoxyl group in the kraft lignin rearranged to another type during the thermal treatment. The contents of aromatic C-H and aliphatic C-H bonds in the lignin pyrolysis oils increased with increasing pyrolysis temperature, which was attributed to the rearrangement and the cleavage of the ether bonds or methoxyl groups in the lignin. Table 2.6 summarized the functional groups presented in the lignin pyrolysis oils that could be analyzed by NMR.

Table 2.6. NMR detectable functional groups in lignin pyrolysis oils. [58-70]

^{1}H-NMR[58-60, 63, 70]	^{31}P-NMR[60, 62, 64, 65, 67, 69]	^{13}C-NMR[58, 60-70]	HSQC[68]	
-C**H**O, -COO**H**	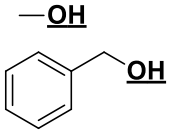	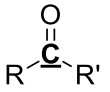	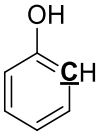	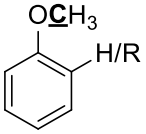
Ar**H**, **H**C=C-	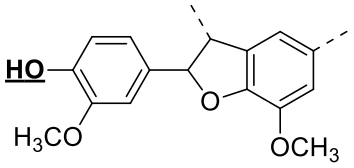	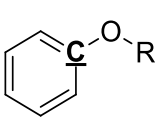	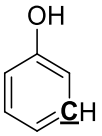	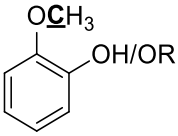
-C**H**$_n$-O- , C**H**$_n$-O-	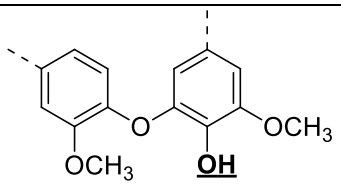	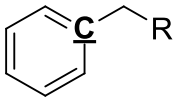	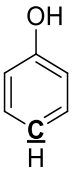	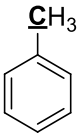
-C**H**$_3$, -C**H**$_n$-	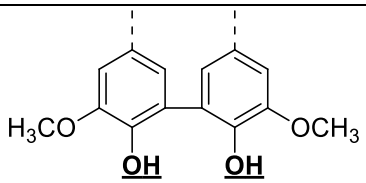	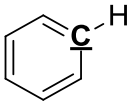	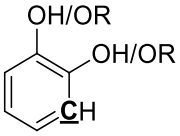	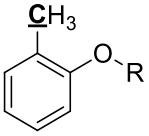
	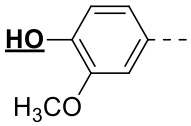	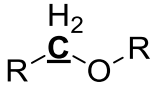	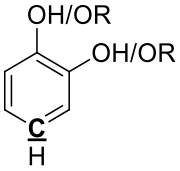	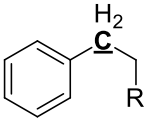
	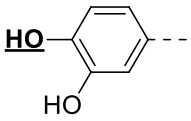	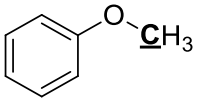	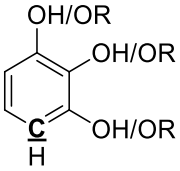	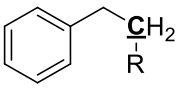
	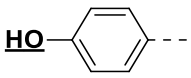	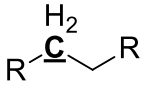	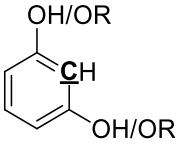	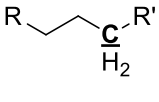
	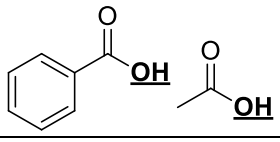	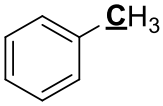		
		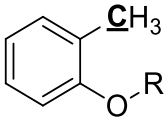		

2.5 Catalytic Upgrading

The major products in the lignin derived pyrolysis oil are covered in sections 2.4. However, the produced oil cannot be used directly as fuel due to several poor properties, such as thermal instability, corrosiveness, poor volatility, high coking tendency, low heating value, and immiscibility with petroleum fuels. [71] Two key differences between the biomass pyrolysis oil and the crude oil are a large number of oxygen-containing functional groups and unsaturated bonds. Therefore, upgrading is a necessary step for the lignin derived pyrolysis oil to meet the fuel specification.

The catalytic bio-oil upgrading involves a series of complex reactions. Generally speaking, the upgrading process stabilizes the bio-oil, reduces or eliminates the poor properties mentioned above, and makes the bio-oil compatible with gasoline. The most common upgrading approaches are hydrodeoxygenation (HDO) and zeolite cracking. Mortensen et al. gave a detailed review of the upgrading of whole biomass derived bio-oil by HDO and zeolite cracking. [72] Huber and Corma et al. also reviewed the synthesis of transportation fuels from the whole biomass and both upgrading methods were introduced in the bio-oil upgrading section. [73] Briefly speaking, HDO process produces high quality oil, but it requires pressurized hydrogen as reactant. The cost for hydrogen and pressurized reactor are significant barriers for the promotion of HDO process. Zeolite cracking only needs a low amount hydrogen and a regular non-pressurized reactor. However, the produced oil is in inferior quality (low H/C ratio) and the coking problem is much more prominent than that in the HDO process. [74] Moreover, although zeolites are

effective in the deoxygenation of small oxygenates (such as aldehydes and ketones), their capability for phenolics deoxygenation is limited because these phenolic compounds are too large to diffuse into the small pore opening. [75-77] This thesis work focuses the catalytic HDO reaction and related reaction mechanisms.

Hydrodeoxygenation reaction is the removal of the oxygen-containing functional groups with the presence of hydrogen. It often accompanies with hydrogenation reaction. The common features of the model compounds for lignin pyrolysis oil are phenolic hydroxyl group, methoxyl group, and aromatic ring. The purpose for HDO is to hydrogenate the unstable unsaturated bonds and to reduce the oxygen content in the pyrolysis oil. Research showed that the pyrolysis oil tended to repolymerize under 448 - 523 K with the absence of a catalyst or hydrogen, followed by char formation within a couple minutes. [78] However, in the presence of the catalyst and hydrogen, the pyrolysis oil converted to stable compounds under the same condition.

2.6 Review of noble metal catalyst for HDO reaction

Two types of catalysts are commonly used in the HDO process. The first type is sulfide catalysts, such as NiMoS/Al_2O_3, CoMoS/Al_2O_3, etc. Such type of catalysts has been widely used in the petroleum industry for decades. [72, 79, 80] The technique is mature and the reaction mechanisms are well studied. The cost for this type of catalysts is much lower than the second type of catalysts. Oxygen atoms in phenolic compounds can be effectively removed by these sulfide catalysts with high yields of aromatic and saturated

products. [79-84] However, bio-oil is different to the conventional fossil feedstock. The bio-oil from biomass pyrolysis contains a large amount of water and a negligible amount of sulfur. Although the sulfide catalysts are good at oxygen removal, the high amount of oxygen can cause rapid catalyst deactivation during the HDO. [85] Second, the water in biomass derived bio-oil also induces catalyst deactivation. Therefore, most of the reactions catalyzed by sulfide catalysts were conducted in the gas phase. [86] The high coking formation also reduced the life of the catalysts. [86-88] Some of the catalysts required sulfur during the reaction which causes sulfur contamination. [89]

The second type of catalysts is the transition metal catalysts, including platinum, palladium, ruthenium, rhodium, etc. This category of catalysts is tolerant to the aqueous solvent. Therefore, the HDO reaction can be carried out with the existence of water steam or even in the aqueous phase. Generally speaking, noble metal catalysts have higher reactivity than the sulfide catalyst that it requires a less severe reaction condition. [90, 91] One of the disadvantages of noble metal catalyst is that it is sensitive to sulfur that sulfur removal is a necessary step. Among the common lignin separation approaches, kraft pulping process is the only one which induces a large amount of sulfur. For other processes, noble metal catalyst will not encounter such problem. The cost of the noble metal catalyst is high, so that the catalyst recycle technique is also challenging.

2.6.1 Platinum

Platinum is the most extensively studied catalyst in this category. It was widely used in various HDO reactions and showed robust reactivity. [71, 74, 78, 89, 92-99] This section only focuses on its catalytic behavior during the reaction.

Overall speaking, platinum has high reactivity in the aromatic ring hydrogenation. To remove the oxygen in the compound, in most cases, a bifunctional catalyst is necessary because the removal of oxygen requires acid sites on the support material. Lobo et al. used $Pt/\gamma\text{-}Al_2O_3$ catalyst to hydrogenate meta-cresol under 533 K. [92] The platinum metal only hydrogenated the aromatic ring and the acid site on the support promoted the dehydration reaction after the hydrogenation reaction. The kinetics study showed that phenolic ring saturation was the rate-limiting step. Increasing the dispersion of platinum enhanced the hydrogenation activity. [74] The dispersion of platinum is not only determined by the surface area, but also by the surface chemistry of the support material. Jones et al. [93] found that platinum catalyst was efficient at ring saturation under 473 K. However, it could not remove the hydroxyl group from both phenol and cyclohexanol. Bicyclic molecules were produced in the reaction, which indicated the occurrence of the ring-coupling reaction on the metal surface. Not only the hydroxyl group, during the hydrogenation of guaiacol under 523 K, both methoxyl and hydroxyl group could not be removed by platinum catalyst alone. [94]

However, another research demonstrated that under some conditions, the oxygen could be partially or completely removed by using platinum catalyst. Gates et al. [71] carried out HDO experiments with four model compounds using Pt/γ-Al_2O_3 catalyst under 573 K. Both HDO and hydrogenolysis reactions were observed under the condition. The author defined the two terms as following: hydrodeoxygenation indicated that the oxygen atom was removed from the aromatic ring, and hydrogenolysis meant that the oxygen atom was still attached to the aromatic ring after the C-O cleavage (Figure 2.6). The kinetic data were calculated on the basis of the experimental results and hydrogenolysis reaction is predominant in anisole and 4-methylanisole. For guaiacol, the reaction rate of hydrogenolysis was still higher than that of the HDO reaction. Once the aromatic ring was saturated, the Pt catalyst could not effectively deoxygenate the cyclohexanone and cyclohexanol under this condition.

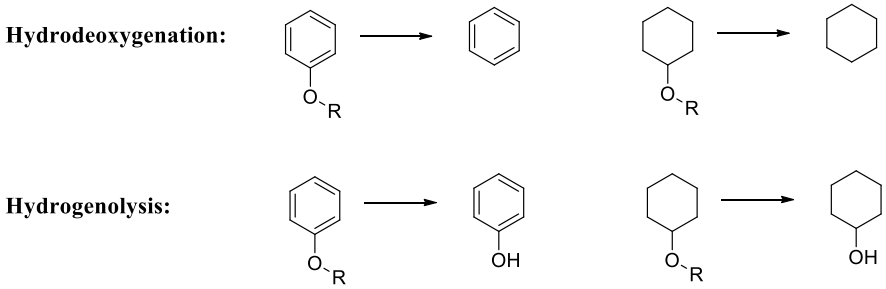

Figure 2.6 Difference between Hydrogenolysis and Hydrodeoxygenation[71]

Fukuoka et al. [97] used Pt/activated carbon (AC) catalyst to study the HDO reaction of 4-propyl-phenol in the aqueous phase at 553 K under acid-free condition. The aromatic structure was hydrogenated initially on the metal surface, and then the deoxygenated products are produced. In the NH_3-TPD (temperature programmed desorption) profile,

Pt/AC showed no peak, which meant that there was very few acidity sites on the surface. Therefore, the acid-site catalyzed dehydration reaction was not observed during the reaction. The hydrogenolysis reaction occurred on the platinum surface. This catalyst was reused for three times and no deactivation was observed.

Besides hydrogenation and deoxygenation reactions, platinum is also able to catalyze the methyl removal/transfer reaction. Resasco et al. [95] did the HDO of anisole under 673 K using Pt/Hβ zeolite as the catalyst. On the platinum surface, demethylation of the anisole was the primary reaction. The platinum catalyst showed low activity towards the hydrogenation reaction under this condition. The presence of Pt also improved the coke tolerance that the coke amount of the Pt/ Hβ was lower than that with the Hβ zeolite. Krause et al. [78] performed guaiacol HDO experiment at 373 and 573 K and the methyl transfer reaction was only observed under low temperature.

Not all types of aromatic compounds can be effectively hydrogenated by platinum catalyst. In the study by Liang et al., [99] Pt/silica-alumina neither hydrogenated the aromatic ring, nor removed the oxygen for benzofuran at 553 K. 2-methyl-2-pentenal is introduced as a special case here. Although it is not a model compound of the lignin pyrolysis oil, it contains C=O and C=C bonds. Both bonds exist in the bio-oil. Mallinson et al. [96] performed the experiment under 473 K and Pt/SiO_2 was used as the catalyst. Pt showed high reactivity with the model compounds. The calculated rate constants indicated that platinum mainly catalyzed the hydrogenation of C=C bond that the reaction rate of C=O bond was much slower. The preference for C=C bond hydrogenation was

also reported in two other publications. [100, 101] In the meantime, the aliphatic-OHs could be cleaved under this condition.

Table 2.7 Reaction condition for experiments using platinum catalyst

Model Compounds (MC)	Temp	Hydrogen pressure		Support Material	Solvent	Reaction Type	Ref
		Absolute	H_2 to MC ratio				
Guaiacol, Anisole, 4-methyl-anisole, cyclohexanone	573 K	0.14 MPa (30% H_2, 70% N_2)	-	γ-Al_2O_3	-	HYD[a], HDO	[102]
Meta cresol	533 K	0.05 MPa	-	γ-Al_2O_3	-	HYD	[103]
dibenzofuran	473 K	4 MPa	-	γ-Al_2O_3, ZSM-5, MZ-5(MS[b])	tridecane	HYD	[103, 104]
Phenol	473-523 K	4 MPa	-	HY, ZSM-5, Hβ, γ-Al_2O_3, SiO_2	Water	HYD, ring coupling	[105]
Guaiacol	523 K	4 MPa	-	γ-Al_2O_3, SiO_2, NAC[c]	n-decane	weak HYD	[106]
Anisole	673 K	0.1 MPa	50	SiO_2,Hβ	-	HDO, HYD demethylation	[81]
4-Pr-Phenol	553 K	4 MPa	-	AC, ZrO_2,	water	HYD, HDO	[107]

				TiO_2,CeO_2			
Guaiacol	373 K 573 K	8 MPa	-	ZrO_2	hexadecane	HYD Deoxygen	[108]
Benzofuran	553 K	3 MPa	-	SiO_2-Al_2O_3	decalin	HYD, HDO	[86]
2-methyl-2-pentenal	473 K	0.1 MPa	12	SiO_2	-	HYD	[82]

* a: Hydrogenation, b: Mesoporous, c: Nitric acid treated carbon black,

Table 2.7 summarizes the catalysts, reaction conditions, model compound studies, and reaction types included in this section. It is easy to find that temperature plays a key role. Under 373-533K, platinum mainly hydrogenates the aromatic structure. Almost all of the model compounds listed were fully hydrogenated under this temperature. Deoxygenation occurs at a temperature over 553 K. Krause et al. [78] performed guaiacol HYD/HDO experiment at 373 K and 573 K. At 373 K, hydrogenated oxygen-containing compounds were the major products. When the temperature increased to 573 K, benzene became the predominant product. The author explained that the high temperature suppressed the hydrogenation reaction and the amount of hydrogen adsorbed on the catalyst surface at different temperatures was proposed to be the major cause. A related study showed that hydrogen adsorption was an exothermic reaction. [109] Low hydrogen coverage on the catalyst surface at high temperature reduced the reaction rate for both HYD and DO. [78] According to the experimental results, the reaction rate of the HYD reaction was significantly reduced because it required a lot more hydrogen than the deoxygenation

reaction. On the other side, it was more conducive to ring saturation under a high hydrogen pressure and a low temperature. [95]

How the model compounds interact with the catalyst surface directly determines the behavior of catalyst. Pt(111) is the most stable facets of the Pt crystal. [89] The adsorption of the anisole and its derivatives on Pt(111) surface was studied. [110] Anisole was less strongly bonded to the Pt(111) surface compared to the parent molecule benzene, probably due to the steric hindrance of the methoxyl group. The most stable configuration between anisole and Pt surface is the horizontal configuration that the organic molecule adsorbs in parallel to the metal surface with both aromatic ring and oxygen above the bridge sites. The binding energy for this configuration is 2.23 eV for Pt(111). The vertical configuration results in a much weaker adsorption. The binding energy is only 1.09 eV. The adsorption on the stepped surface has also been studied because it is often considered as the preferable sites for catalysis. The binding energy of Pt(211) is only 0.64 eV. The dissociation of phenol into phenoxy is endothermic on Pt(111) with reaction energy equal to 0.26 eV.

The addition of promoter is widely used to enhance the catalytic reactivity. Pt catalyst doped with 3*d* metals shows superior performance than monometallic Pt in the hydrogenation reaction. [111, 112] Adding Ni or Co into the Pt not only increased the HDO activity, but changed the products distribution as well. [92] The deoxygenation selectivity was also higher on bimetallic catalysts, probably due to the additional active sites generated. The EXAFS study showed that Pt-Ni and Pt-Co coordination number

clearly reflected the bimetallic structure. If the number was greater than one, the Pt atom was surrounded by more Ni or Co atoms than Pt atoms. The DFT study suggested that the Pt terminated surface had weaker bonding with hydrogen and hydrocarbon adsorbates than it is with the monometallic Pt surface, which resulted in more optimal binding energies and higher rates of hydrogenation. [111-113] Rh doping was also studied that PtRh alloy catalyzed guaiacol HDO had higher conversion than that of the monometallic Pt catalyst. [78, 99] On the other hand, some dopant may cause adverse effects. For example, adding Pd into platinum catalyst reduced the guaiacol conversion due to the reduced active surface area. [78]

2.6.2 Palladium

Palladium is another widely used HDO catalyst. Under 423 K, Pd effectively hydrogenated phenol, anisole, catechol and guaiacol in aqueous phase. [114] With the presence of the phosphoric acid, Pd/C catalyst converted phenolic and guaiacol-based compounds into aliphatic molecules in the aqueous phase under 353 K. The turnover frequency (TOF) is very high (>1000 hr^{-1}) and the recyclability is excellent. No catalyst deactivation was observed in 6 hours after the reaction begins. [115] For the phenolic dimers connected in various linkages (including α-O-4, 4-O-5, β-1, 5-5, β- β), the Pd/C and solid acid HZSM-5 achieved 100% hydrogenation and deoxygenation at 473 K in aqueous phase. [116]

Sometimes the palladium catalyst shows similar behavior as platinum catalyst. Therefore, both catalysts are often compared in some study. The activity of these two catalysts is highly depended on the reaction condition. In the study by Liang et al., the metal dispersion of Pd was only half as the Pt catalyst, but the CO uptake amount of the Pd catalyst was 50% higher than the Pt catalyst. [99] The Pd catalyst also showed higher activity than the Pt catalyst in both hydrogenation and HDO of benzofuran. The study indicated that the HYD of benzofuran and the cleavage of C-O were easier with Pd than those with Pt. In some other cases, Pt showed better performance than Pd. In the HDO of 4-propyl-phenol under 553 K in acid-free aqueous solution, Pd/active carbon (AC) was used as catalyst. [97] Compared with Pt, Ru and Rh, Pd showed superior reactivity in the hydrogenation reaction, but not the hydrogenolysis of the C-O bond. More than half of the aliphatic-OH bonds were left intact. Another example was that under 373 K and 8.0 MPa H_2, Pd was not effective in either the hydrogenation or the hydrodeoxygenation of guaiacol. Half of the methoxyl groups were removed under this condition. [78]

Understanding how the metal particles are dispersed in the supporting material is helpful in the catalyst optimization. In the study by Suzuki et al, [117] CeO_2 and ZrO_2 were used as the supporting materials. The amount of H_2 chemisorbed on the Pd metal surface increased abruptly when Pd loading increased from 1 to 3 wt.%. On the other hand, the Pd crystallite size increased almost linearly. These two facts indicate that 1) deposition is more on the external surface as the load increases, 2) Pd first preferentially occupies the internal surface. The increasing in the Pd loading increases the *d*-spacing of CeO_2 mesoporous structure, which means Pd particles expand the pore size. For CeO_2 support,

the increasing loading led to higher conversion, but lower TOF value. [117, 118] Cyclohexanone was the major product under low Pd loading and the yields of hexanol and hexane increased with higher Pd loading. The temperature effect has also been studied that maximum conversion was obtained under 333 K. Above 333 K, the overall conversion decreased monotonously with the increasing temperature. Other two researchers also found that the maximum conversions were obtained at 333 K. [118, 119] When the temperature went higher, more cyclohexane, cyclohexanone and less cyclohexanol were produced. [117, 120] For ZrO_2 support, the result was much simpler that the conversion of phenol is similar to that with Pd/CeO_2 and the selectivity towards cyclohexanone was above 90%.

Pd_4Pt_1 has been synthesized to study the alloy effect. [99] The dispersion of Pd_4Pt_1 was twice more than the Pd monometallic catalyst and the CO uptake amount of Pd_4Pt_1 was also doubled. The selectivity of Pd_4Pt_1 towards deoxygenated products was 80% and the selectivity with Pd monometallic catalyst was only 37%. The TOF of Pd_4Pt_1 was 16.88, which was much higher than the TOF of Pd 2.15. After alloying with Pt, there were two major changes with the Pd catalyst: the bonding length and the electronic density. From the CO chemisorption change, these factors enhanced the exposure of active sites on the catalyst surface.

Orita and Itoh studied the formation of phenol from benzene on the surface of Pd(111). [121] Pd(111) is the most stable facet for palladium. Even in polycrystalline Pd, it is still the most abundant. The adsorption of phenol on the Pd surface is less stable than that of

benzene. The adsorption energy of phenol on Pd(111) is −7.85 eV. When one hydrogen atom is attached to the C-1, the adsorption energy of the intermediate increases to -6.85 eV. The O-atom and benzene are both adsorbed on one unit cell. The co-adsorption system becomes more stable (−7.06 eV). The last step is C-O bond cleavage. The sum of adsorption energies of the oxygen atom and benzene in separate domains is −7.26 eV, (benzene adsorption energy is -1.43 eV and oxygen adsorption energy is -5.83 eV).

2.6.3 Rhodium

Rhodium is a relatively newly developed catalyst compared with the platinum and palladium catalysts. However, it shows excellent performance in some cases. Under 553 K in acid-free aqueous solution, Rh/activated carbon (AC) effectively catalyzes the HDO of 4-propyl-phenol. [97] The conversion is 100% and over 83% of the aliphatic-OH bonds are cleaved. The hydrogenation of guaiacol occurs at 331-381 K and the deoxygenation reaction occurred over 523 K. [94] Both temperatures were lower than those required by platinum catalyst. This indicates the high reactivity of Rh in the HDO experiment. In another guaiacol HDO experiment conducted under 373 K, the predominant product with Rh catalyst is 1-methyl-1,2-cyclohexanediol. [78] The hydrogenation conversion was 100%. However, the Rh catalyst was not effective in C-O hydrogenolysis. The superior catalytic performance of Rh is probably due to the high amount of irreversible chemisorption of H_2 on the Rh surface.

The temperature effect of guaiacol HDO has also been studied with Rh catalyst. [122] The temperature range studied is 573 - 673 K. The increasing temperature led to higher cyclohexane yield. The coke formed on Rh decreased with the increasing temperature. The $C_xH_yO_2$ compound decreased dramatically in the temperature range (especially between 623 and 673 K). The yields of both mono-oxygen molecules and aliphatic molecules increased. At 673 K, the aliphatic yield was almost 50%. RhPt and RhPd were both synthesized and the monometallic Rh catalyst had higher HDO reactivity than both of them.

Rh(111) is the most stable facets of Rhodium.[89] Phenol shows strong adsorption on Rh(111) with a binding energy of 2.79 eV under the horizontal configuration. Under vertical configuration, the binding energy is 1.15 eV, which is much weaker than that of the horizontal configuration. On the stepped surface Rh(211), the binding energy reduces to 1.79 eV. The dissociation of phenol to phenoxyl is -0.27 eV, which indicates the exothermic reaction. However, for finite coverage, the dissociation reaction on Rh(111) requires a lower temperature than it is on Pt(111). [123, 124]

2.6.4 Ruthenium

Ruthenium on activated carbon was used to catalyze the HDO of 4-propyl-phenol under 553 K in acid-free aqueous solution. [97] In this study, the ruthenium catalyst achieved 100% hydrogenation, but the deoxygenation capability of Ru was weaker than the Rh and Pt catalysts that only 50% aliphatic-OH bonds were cleaved.

The performance of ruthenium is highly affected by the supporting material. Although this phenomenon is also generally observed for other metal catalysts, the effect is much stronger for ruthenium. In the study by Park et al., platinum, rhodium, palladium and ruthenium were compared in guaiacol HDO with three different support materials. [94] When using γ-Al_2O_3/SiO_2-Al_2O_3/nitric acid treated carbon black as the supports, the highest product yields for ruthenium catalysts are cyclohexanol, cyclohexane, and 2-methoxycyclohexanol respectively. The selectivity of the ruthenium was the best among all four catalysts.

The HDO of phenol and anisole using Ru/charcoal was studied by Kluson and Cerveny. [125] The reaction network was proposed and kinetics data were calculated. The reaction network are discussed in detail in the model compounds study review. The results indicated that ruthenium was able to remove the aliphatic-OH groups through dehydration reaction. When there was a carbonyl group attached to the aromatic ring, the C=O bond was hydrogenated first, then the hydrogenation of aromatic ring happened.

Zhang et al. studied the hydrotreating of eugenol with ruthenium catalyst. [126] The major crystal facet of ruthenium is Ru(101) and the major facet of Pd is Pd(111). Under the similar condition, ruthenium showed much higher activity than palladium, which was in accordance with the study by Greenfield. [127] The reactivity of catalyst had no loss after two runs with model compounds. When the distillate fraction from bio-oil was used as the reactant (major components were phenolic compounds, such as phenol, 2-

methoxyphenol, 4-ethylphenol, 4-methyl-2-methoxyphenol, 4-ethyl-2-methoxyphenol), Ru catalyst lost its activity rapidly. The BET study showed the reduction in both surface area and pore volume, which indicated the coke or tar formation in pore channels. The study further revealed that Ru^0 is the major role in HYD reaction.

Heeres et al. studied the hydrotreatment of the fast pyrolysis oil using Ru/C at 623 K and 20 MPa H_2 pressure. [128] The ruthenium catalyst was highly effective in the deoxygenation initially. The O/C molar ratio decreased from 0.45 to 0.02 within the first hour. However, it increased again from 0.02 to 0.07 in the following five hours, probably due to the low O/C ratio compounds transferring from the oil phase to the gas phase. The H/C ratio was 1.35 for the pyrolysis oil. It dropped to 1.05 in the first hour, and then increased to 1.32 after six hours. The initial drop was probably caused by the loss of hydrogen for dehydration.

2.6.5 Support effect

The surface acidity is a key feature of the support material. Acid sites on HBeta are well known for catalyzing the alkyl transfer reaction. [77] In the paper published by Resasco et al, the inter-molecule methyl transfer was observed with HBeta zeolite support. When the SiO_2 was used as the support, methyl were rapidly hydrogenated to form methane. The results suggest that the methyl group is stable on the zeolite surface, but unstable on the SiO_2 surface. Not only HBeta zeolite, both γ-Al_2O_3 [71] and HY zeolite [129, 130] induced intramolecule- and intermolecule-methyl-group-transfer reaction, especially with

HY zeolite catalyst. The transalkylation reaction was the only kinetically significant reaction class with the HY catalyst. Besides catalyzing alkyl transfer reaction, the total number of acid sites significantly affects the rate of dehydration. Under 373 K, the acid sites on ZrO_2 surface were not enough to dehydrate the cyclohexanol produced by guaiacol and only the methyl transfer was observed in this reaction. [78] HY zeolite was also used under the same condition and the results illustrated that the acid protons were necessary for the dehydration reaction. [93] Furthermore, the HY and Hβ zeolite-supported catalyst have higher selectivity towards bicyclics than that of the HZSM-5 zeolite, because of the micropores structure induced shape selective effects with the HZSM-5 zeolite.

Acidic supporting materials sometimes show synergistic effect with the metal catalyst. In the study by Ha et al., [94] Rh/Al possessed 10 times more active sites compared with Rh/SiAl. However, the Rh/SiAl catalyst exhibited much better HDO activity. The even mechanical mix of metal-deposited non-acid support and noble-metal-free SiAl enhanced the deoxygenation reactivity. When using Pt/ZrO_2 as the catalyst, only negligible deoxygenated products were produced.

Besides the acid-sites on the solid support, the mineral acids also show similar effect. For example, several noble metal catalysts are used for phenol HDO reaction and a variety of the supporting material, includes sulfated zirconia, Amberlyst 15, $Nafion/SiO_2$ and $Cs_{2.5}H_{0.5}PW_{12}O_{40}$, were studied. All these catalysts reach fully conversion and 90% selectivity towards cycloalkane in the aqueous phase HDO. [116] The activation energy

of the five solid acids are below 120 kJ/mol, which is almost equal to the activation energy of H_3PO_4 in aqueous phase reaction. HZSM-5 is a special case. HZSM-5 (Si/Al ratio 45) produces 93% cycloalkanes due to the lower activation energy of dehydration (approximately 95 kJ/mol). Therefore, HZSM-5 is able to catalyse the dehydration reaction under lower temperature.

The acid sites on the surface further affect the interaction between the reactant and the support material. The chemisorption of guaiacol was measured with ZrO_2 and γ-Al_2O_3 supports. [122] No special response of the guaiacol desorption on γ-Al_2O_3 surface was observed. ZrO_2 exhibited at least three peaks in the desorption profile. The total surface area of ZrO_2 was larger than that of γ-Al_2O_3, which indicated that the bonding strength between guaiacol and ZrO_2 was weaker than that between guaiacol and γ-Al_2O_3. Due to the acid strength of γ-Al_2O_3 was stronger than ZrO_2, the results indicated that the stronger acid strength resulted in firmer bonding with the model compound. In another study, [131] ZrO_2 showed better catalytic activities toward C_{arom}-O hydrogenolysis through demethoxylation and direct deoxygenation than TiO_2 and Al_2O_3.

Not only the acid strength, but also the porous structure affects the activity of the catalyst. The porous supporting material with large pore size can increase the diffusion rate of model compounds inside the catalyst. As mentioned above, zeolites are better than alumina and silica in the phenol HDO because of their stronger acidity. However, small pore opening often causes diffusion limitation, especially for the large compound. [93] Therefore, mesoporous zeolite is an ideal material. It has the advantages of both zeolites

and mesoporous material. The MZ-5 zeolite used in the paper possessed intra-crystalline wormhole mesopore channels. The reaction rate increased with the larger pore size, due to the enhancement of the diffusion. 2-methyl-2-pentene isomerization was used as a model compound to compare the acidity of the catalyst and the results demonstrated that MZ-5 and ZSM-5 had higher acidity than γ-Al_2O_3. Pt/γ-Al_2O_3 catalyst exhibited high HYD reactivity due to the high Pt dispersion and mesoporous nature. But the mild acidity of the supporting material limited the dehydration reaction. Pt/ZSM-5 showed limited hydrogenation ability due to the small pore size. Overall speaking, MZ-5 exhibited high reaction rate in both hydrogenation and dehydration reactions.

Suzuki et al. [117] compared the reactivity of Pd deposited on MgO, γ-Al_2O_3, mesoporous CeO_2 and mesoporous ZrO_2. Pd/MgO was very active and it had high selectivity toward cyclohexanone. However, MgO had very poor mechanical strength, which inhibited it from being used in industrial scale. γ-Al_2O_3 was the least active and most selective among these supports. Mesoporous CeO_2 and mesoporous ZrO_2 were equally active. The high catalytic activity of mesoporous supports compared to that of the commercial microporous supports was attributed to the high dispersion of the palladium particle and small crystallite size of the supporting material, which was validated by the high BET surface area. ZrO_2 had relatively stronger acids and bases than those in CeO_2. When the system was heated up between 473 and 673 K, the surface reduction of CeO_2 began and it became CeO_2-x/Ce_2O_3-like non-stoichimetric oxide with anion vacancies, thus the Lewis acidic and basic sites were formed. Phenol was adsorbed in non-planar fashion. The redox property of CeO_2 also facilitated the alkylation of phenol with

propanol. [132] ZrO_2 had a stable structure that it did not reduce under the hydrogen atmosphere. The hydrogen molecules were adsorbed dissociatively on the solid surface as Zr-OH, Zr-H and ZrHZr [133] that the surface hydroxyl groups had the acidic or basic character with Brønsted centers, depending on the polarization of the OH group. Carbon deposition during the alkylation and hydrogenation of phenol on these Brønsted center is one major cause of the activity decay. [134, 135]

The structure change of the support material during the reaction is one of the major causes for catalyst deactivation, especially when the reaction is carried out in the aqueous phase. Both SiO_2 and γ-Al_2O_3 tend to degrade with water and water vapor. In the study by Aprile et al. [136], the pore structure in SiO_2 support collapsed after the reaction in aqueous phase, which led to the complete deactivation of catalyst. The solubility of the amorphous silica in water was also measured, but the amount was relatively minor. [137] The transformation of γ-alumina had been investigated by Lefevre et al. [138] The study revealed that γ-alumina transforms to bayerite (β-$Al(OH)_3$) gradually with the presence of water and most of the acidity sites were disappeared, which resulted in the low reactivity of the catalyst.

2.7 Reaction mechanism of lignin model compounds HDO

2.7.1 Phenolic based compound

Phenol is the most commonly studied model compounds in lignin derived bio-oil upgrading. [89, 93, 97, 114, 115, 117] It is the simplest compound which consisted

aromatic structure and phenolic hydroxyl group. The understanding of the phenol HDO reaction path can reveal the fundamental reaction mechanism of other related compounds.

In the study of Lercher et al., [114, 115] the reaction path is proposed as follows: 1) aromatic ring was partially hydrogenated to cyclohexanone or fully hydrogenated to cyclohexanol, 2) the cyclohexanone was further hydrogenated to cyclohexanol, 3) the –OH of cyclohexanol was removed through dehydration, 4) the C=C double bond of cyclohexene was finally hydrogenated and cyclohexane was produced. The authors believed that the phenol and cyclohexanol could not be directly deoxygenated. The detailed reaction pathways were marked in (1) – (4) in Figure 2.7.

Jones et al. proposed another reaction pathway in phenol HDO [93]: a) Phenol was converted into cyclohexenol as an intermediate product, b) the cyclohexenol was converted to cyclohexanone or further hydrogenated to cyclohexanol, c) cyclohexanol was dehydrated to cyclohexene, d) cyclohexene was finally hydrogenated to cyclohexane. Two extra proposed steps were e) directly HDO of phenol to form benzene and f) hydrogenolsysis of the C=O bond of cyclohexone, which produced cyclohexane in one step. These reactions are marked in (a) – (f) in Figure 2.7.

The Gibbs energy in each step for phenol HDO was calculated by Keane et al. under 498 K. [135] The values were listed below the arrows in Figure 2.7 and the unit is kJ/mol. Besides the partial hydrogenation of benzene to cyclohexene, the standard free energies of all other HYD/hydrogenolysis reactions were negative. Therefore, all of the

hydrogenolysis steps and the benzene hydrogenation steps were considered to be irreversible. Cyclohexanone was produced by hydrogenation of cyclohexeneol followed by a tautomerism, but the Gibbs energy was not able to be calculated due to the missing of thermodynamic data for this reaction.

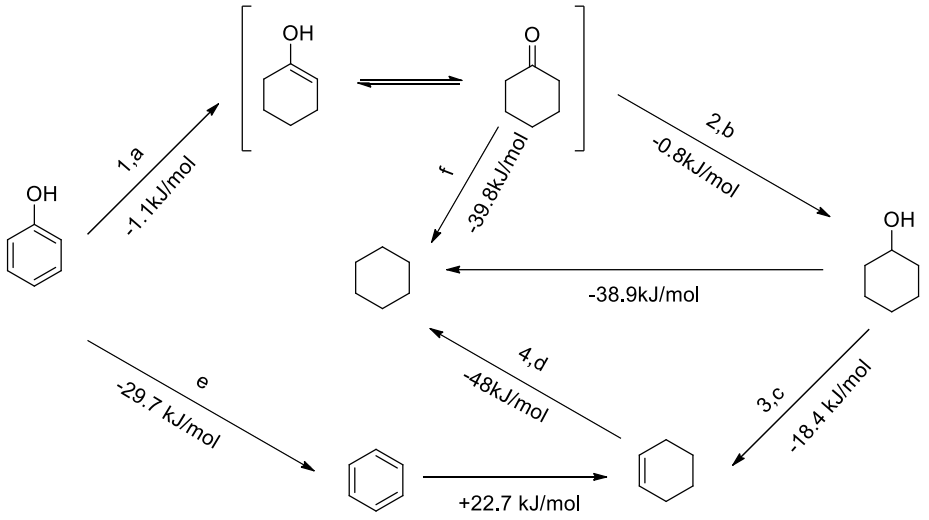

Figure 2.7 Reaction network proposed for phenol HDO and the calculation of Gibbs energy in each step. [117]

Reaction condition: 0.5 gram of Pd/CeO_2 or Pd/ZrO_2 catalyst, phenol and benzene mixture flowrate 0.3 cm^3/h, hydrogen flow 20 cm^3/min, temperature 433 - 503 K.

How the phenol is adsorbed on the catalyst surface has also been discussed. [89] After phenol is adsorbed on the metal surface, the C-C bond is slightly stretched, which makes it more close to the sp^3 hybrid than the sp^2 hybrid. The C-O bond is slightly shifted away from the horizontal benzene and the bonding length is also increased. Both changes increase the reactivity of C=C and C-O bond and make the hydrogenation and HDO reactions possible. Suzuki et al. [117] studied the formation of cyclohexanone and cyclohexanol from benzene. The results suggested that the selectivity toward

cyclohexanone or cyclohexanol depended on the configuration of phenol adsorption on the metal surface. Cyclohexanone was produced if phenol was adsorbed non-planar to the surface. If the phenol was adsorbed co-planar to the surface, cyclohexanol was produced directly. The configuration of phenol adsorption was governed by the nature of the support, mainly the acid-base properties. [119, 134]

2.7.2 Anisole based compounds

Compared with phenol, anisole has one more methyl group attached to the oxygen. One common reaction of anisole is transalkylation reaction, in which the methyl group transfers from the methoxyl group to the aromatic ring. Resasco et al. observed the acidic catalyzed transalkylation reaction, yielding phenol, cresols and xylenols as the major products. [95] The reaction was carried out in gas phase under 673 K and an atmospheric hydrogen pressure. The noble metal catalyst was able to cleave the PhO-CH_3 bond and generates phenol and methane. The phenol was further hydrodeoxygenated and yielded benzene or cyclohexane. The presence of the noble metal and acid support also had a synergistic effect that the methyl group was transferred to the aromatic ring first, then the HDO reaction occurred, which reduced the carbon loss as methane. The reaction path was presented in Figure 2.8.

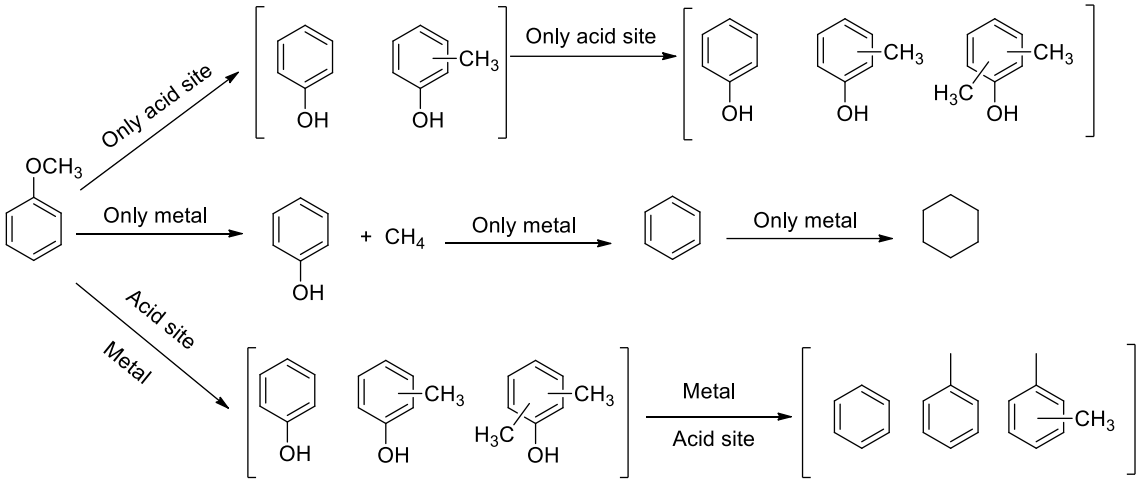

Figure 2.8 Reaction path of anisole HDO on a) only acid site, b) only metal and c) metal and acid site. [95]

Reaction condition: Pt/HBeta catalyst (5-240 mg), anisole flowrate 0.03 – 0.48 mL/hour, H_2/Anisole molar ratio was 50, temperature 673 K.

With the existence of water, the reaction path is slightly different. In aqueous phase reaction, methanol was produced through acid hydrolysis. [114] Weckhuysen et al. carried out the HDO reaction of anisole under 573 K and 5.0 MPa hydrogen pressure. [139] The selectivity of anisole toward phenol and methyl phenol were > 35% and 10-35%, respectively.

2.7.3 Catechol based compounds

Two major reaction paths for catechol HDO are a) hydrogenation first, then deoxygenation reaction, and b) removal of one hydroxyl group first, and the following reaction mechanisms are the same as phenol. [114, 139] The reaction pathways are drawn in Figure 2.9. Under 473 K and 5.0 MPa hydrogen pressure, the selectivity of catechol towards 2-hydroxycyclohexanone was 80% in aqueous phase. [114] The following

dehydration of 2-hydroxycyclohexanone was a fast step under acid condition and cyclohexanone was formed via two parallel reactions. The major reaction pathways were ketone hydrogenation and alcohol dehydration.

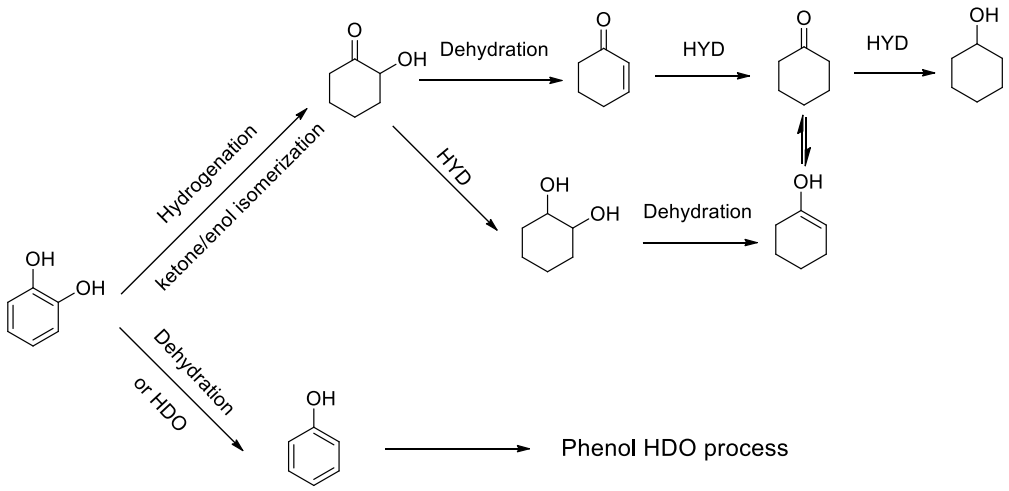

Figure 2.9 Reaction path of catechol HDO. [114]

Reaction condition: aqueous phase HDO. Metal: Pd, Pt, Ru, Rh; catalyst support: C, Al_2O_3, SiO_2; temperature: 423, 473, 523 K. In a specific run, 40 mg 5wt.% catalyst was added to the autoclave. The reactions were conducted at 473 K for 0.5 h.

2.7.4 Guaiacol based compound

Guaiacol is the most representative model compound for lignin and lignin-derived bio-oil. Compared with phenol, there is one more methoxyl group attaching to the aromatic ring. This small change makes the reaction network of guaiacol much more complex than that of phenol. During the reaction, HDO, hydrogenolysis, transalkylation, bimolecular

transalkylation, and hydrogenation are all observed. [71] The complete reaction network is shown in Figure 2.10 and the reaction rate constants are marked next to the arrow.

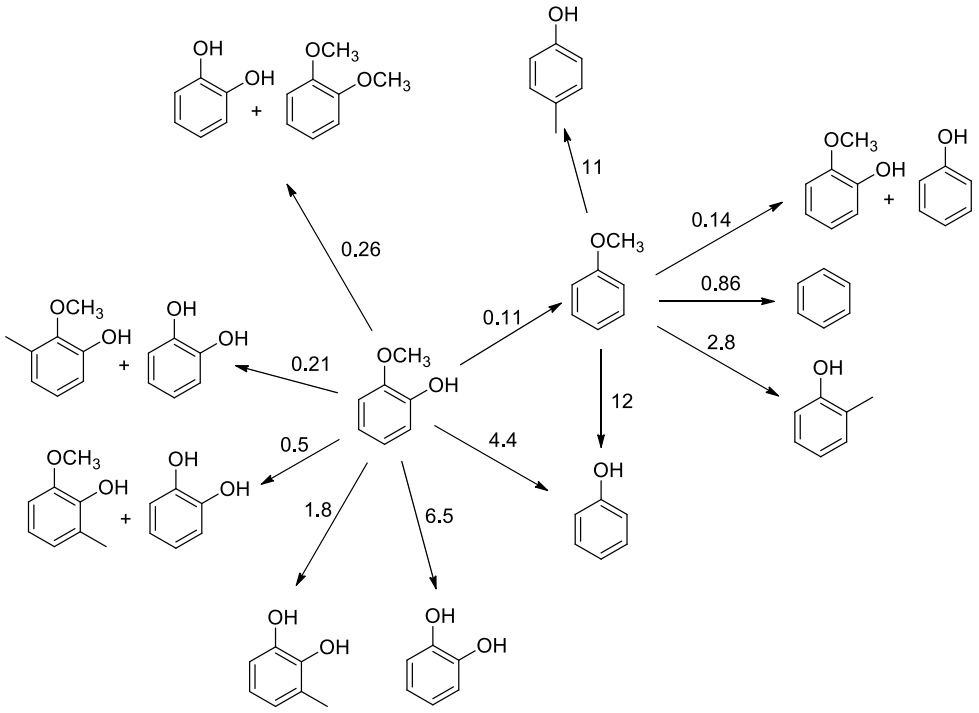

Figure 2.10 Part of the Reaction network for guaiacol HDO. [71]

Reaction condition: Catalyst loading 0.001 - 0.100 g Pt/ γ -Al_2O_3, liquid reactant (guaiacol, anisole, 4-methylanisole or cyclohexanone) flowrate was 0.030 mL/min. The reactor temperature was 573 K and the pressure was 140 KPa.

Following conclusion can be extracted from the information above.

1) The methyl group in the guaiacol is very unstable. The acid support can transfer the methyl intermolecularly or intramolecularly. The transferred methyl groups often attach to the aromatic ring or generate the methane gas.
2) The methoxyl or hydroxyl group of the guaiacol is cleaved in one step. Both products can be further HDO to produce benzene.

3) Guaiacol cannot be hydrogenated in one step under this condition. Normally it is converted to anisole or phenol first, and then the aromatic ring is hydrogenated.
4) Cyclohexane is produced via two major routes. The first is from the hydrogenation of phenol, which is the HDO product of guaiacol. Second is the hydrogenolysis of cyclohexanol and cyclohexanone.

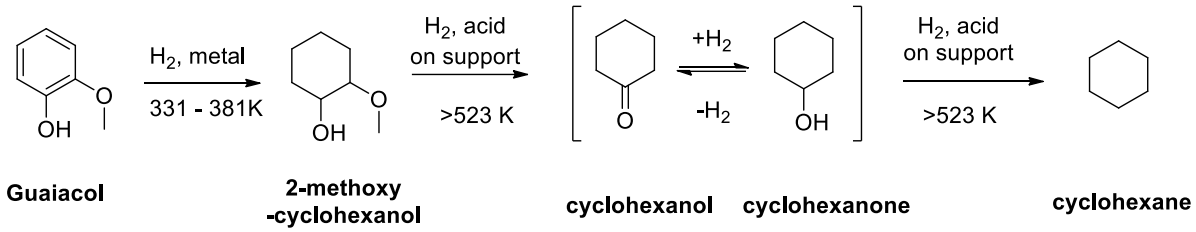

Figure 2.11 Guaiacol HDO reaction path proposed by Park et al. [94]

Reaction condition: Metal: Pd, Pt, Ru, Rh; catalyst support: C, Al2O3, SiO2-Al2O3; temperature: 423 K. Reactant: guaiacol or 2-methoxycyclohexanol. In a specific run, 0.4 g 5wt.% catalyst was added to 40 mL 7.5 wt.% solution in the autoclave. The reactions were conducted at 473 K for 0.5 h.

In the study by Park et al., [94] the reaction path was proposed as Figure 2.11. The major difference compared with the reaction network in Figure 2.10 is that guaiacol was directly hydrogenated to 2-methoxy-cyclohexanol under 331-381 K. Then, the methoxyl group was removed by the acid site on support surface. In the last step, cyclohexane was produced by dehydration of cyclohexanol and cyclohexanone. The acid catalyst and temperature above 523 K were necessary for demethoxylation and dehydration reactions.

CHAPTER 3: PROBLEM ANALYSIS AND OBJECTIVE

3.1 Problem Statement

The effective utilization of lignin is always attractive. The literature review indicates the major obstacles in lignin application are its poor thermal stability and complex structure. Lignin tends to form tar and char during heating. Once the lignin polymer condenses, it is difficult to convert it into low molecular weight compounds. Pyrolysis is regarded as a promising approach. Part of the biomass can decompose to gas products and liquid products. Pyrolysis oil is the liquid product obtained from the process. The compounds in the pyrolysis oil are mainly dimers and trimers.

The pyrolysis process could successfully convert lignin from a solid to a liquid oil. However, the oil cannot be directly used due to several poor properties, such as thermal instability, corrosiveness, poor volatility, high coking tendency, low heating value, and its immiscibility with petroleum fuels. Hence, it is necessary to develop an upgrading process that can increase the oil quality.

3.2 Problem Analysis

The primary goal of this research is to upgrade the lignin derived pyrolysis oil into stable and gasoline compatible fuel products. There are two common approaches for oil upgrading: zeolite cracking and hydrodeoxygenation. In this study, the

hydrodeoxygenation is adopted for the lignin pyrolysis oil upgrading because the oil quality is superior.

Hydrodeoxygenation is a catalytic process; hence, the catalyst selection is critical. The complex chemical structures in the pyrolysis oil are a tough challenge to the catalyst, which should be robust and efficient throughout the upgrading process. Therefore, the first challenge is to screen a proper catalyst.

The complex structure of lignin and lignin pyrolysis oil is another challenge in the upgrading process. Without accurate product identification and structure analysis, it is hard to evaluate the performance and deduce the reaction mechanism. Therefore, the second challenge is the oil product characterization.

The reaction mechanism analysis is a necessary step in this thesis study. However, deducing reaction pathway directly from the upgrade of lignin pyrolysis oil is difficult because there are hundreds of compounds in the oil. The third challenge is the reaction mechanism deduction.

3.3 Hypothesis

1. As discussed in Chapter 2.5 and 2.6, metal catalysts are in wide use in oil upgrading. The reaction mechanisms typically come from the model compounds study. Most of the publications [80, 86, 140-143] did not compare

the reaction mechanism between the upgrade of model compounds and real oil because of the complex structure of the oil. The first hypothesis is that catalysts that are highly active and selective for model compounds, and will also be active and selective for real lignin pyrolysis oil.

2. Due to the different physical and chemical properties between the heavy and light oil, the upgrading process can be different. The heavy oil consists mainly of aromatic dimers and trimers. The large amount of aromatic structure is likely to induce the formation of tar and coke products. On the contrary, the light oil is predominantly monomers. The second hypothesis is that performing the HDO reaction of the two oils separately will increase the overall yield.

3. The poor thermal stability of lignin and lignin pyrolysis oil often leads to catalyst deactivation during the upgrading process. Therefore, one-step HDO cannot achieve complete upgrading. The hypothesis is that some lignin molecules contain more unstable groups than others. Therefore, a two-step HDO process was proposed. By raising the reaction temperature in the first HDO step, the lignin molecules with easy char formation groups will condense at this condition. By removing the char formed in the first step, the remaining stable lignin can fully upgrade even at lower temperatures.

3.4 Objectives

Objective 1:

Use model compounds to screen the proper catalyst for heavy oil upgrading. Study the catalytic behavior of the commonly used noble metal catalysts at similar conditions to understand the reaction mechanisms. Pick the proper catalyst for lignin heavy oil upgrading.

Objective 2:

Once the proper catalyst is chosen based on the model compound study, it will be applied in the lignin derived pyrolysis oil upgrading process. The analysis of the mixed products and deduction of the HDO reaction mechanism with lignin pyrolysis heavy oil need to be performed. The main goals of this step are (1) to reveal how the lignin heavy oil decomposes from dimers or trimers to monomers, and (2) investigate how the pyrolysis heavy oil upgrades to the hydrogenated products.

Objective 3:

Analyze the chemical compositions of the light oil derived from different parts of the biomass, including stem, residue, and bark. Conduct the catalytic HDO reaction under the same condition as heavy oil upgrading. The aim is to evaluate the possibility of co-processing the heavy oil with the light oil. The HDO reaction pathways of other major components in biomass are also included in this part.

CHAPTER 4: NOBLE METAL CATALYZED AQUEOUS PHASE HDO OF LIGNIN MODEL COMPOUNDS[2]

4.1 Introduction

The growth of global energy consumption positions biofuel as an attractive alternative fuel source. Lignin, as the second most abundant natural polymer, receives little attention because of its complex structure and poor thermal stability. The US paper industry produces over 50 million tons of lignin per year, and over 98% of it is burned directly [5]. Another major source of lignin is bioethanol plants. Regardless of the technology employed, almost all bioprocessing approaches result in the formation of a waste lignin process stream [6]. Different from other biomass wastes, lignin is energy-rich. Therefore, it is pragmatic and desirable to find an efficient approach to convert lignin into fuel and useful chemicals.

Pyrolysis is an economical and feasible approach for lignin conversion [144]. The slow pyrolysis process produces both heavy oil and light oil as liquid products [10]. The heavy oil consists of water-insoluble compounds, and the molecular structures in the heavy oil

---

[2] Reprinted from Mu, W., Ben, H., Du, X., Zhang, X., Hu, F., Liu, W., Ragauskas, A.J., and Deng, Y., Noble metal catalyzed aqueous phase hydrogenation and hydrodeoxygenation of lignin-derived pyrolysis oil and related model compounds. Bioresource Technology, 2014. 173(0): p. 6-10, Copyright (2014), with permission from Elsevier.

are mainly dimers and trimers. Conversely, the light oil is mostly composed of water-soluble monomers. Both oil products possess several poor properties, such as thermal instability, corrosiveness, low volatility, high coking tendency, low heating value, and immiscibility with petroleum fuels [11]. Further upgrading the pyrolysis oil via hydrodeoxygenation reaction can improve the conversion of biomass to fuels.

Hydrodeoxygenation (HDO) has been widely used in the pyrolysis bio-oil upgrading [80]. Noble metal catalysts are highly reactive in the HDO reactions. The performance of the commonly used noble metal catalysts for HDO reaction was reviewed in the previous publication. [11] The sulfur-induced noble metal catalyst deactivation does not pose a problem in this study because lignocellulosic biomass generally only consists of a small amount of sulfur. Most of the studies reported in the review paper were carried out under various conditions with different supporting materials, making the evaluation of the catalytic performance very difficult.

The purpose of this study is to compare the performance of the commonly used noble metal catalysts under similar conditions to understand the mechanistic differences between these noble metal catalysts in the HDO reaction. Four noble metals (Pd, Pt, Rh, Ru) were used with activated carbon being the support material. Compared with oxidic supports, activated carbon is a more suitable material to study the catalytic behavior of active metal because the neutral surface shows weak interaction with metals and organic compounds [140]. The leaching of the active metal is a potential cause of catalyst deactivation. According to the literature review, only a small amount of active metal is

leached with carbon support in the aqueous phase hydrogenation [145-148]. DI water with pH 7 was used as dispersant in the reaction. The neutral aqueous phase also facilitated identifying the genuine catalytic behavior.

4.2 Materials and experimental procedure

4.2.1 Lignin separation and purification.

The milled pine wood was ethanol-organosolv pretreated as previously described in the literature. [149-152] In brief, 100.0 g (dry weight) sample was treated with 65% ethanol/water solution with 1.2 w/w % sulfuric acid at 443 K for 60 min. The solid to liquid ratio used was 1:8. The pretreatments were carried out in a Parr reactor equipped with a temperature controller (Parr Instrument Company, Moline, IL). The pre-treated pine wood was washed with warm (333 K) ethanol/water (8:1, 3×50.0 mL). The washes were combined and 3 volumes of water were added to precipitate the Ethanol Organosolv Lignin (EOL), which was collected by centrifugation and air dried. The EOL was purified by Soxhlet extraction with pentane and stored at ~ 273 K prior to use.

4.2.2 Equipment and process of pyrolysis.

Pyrolysis experiments were conducted in a quartz pyrolysis tube heated with a split-tube furnace. Typically, EOL powder sample (3.00 g) was placed in a quartz sample boat that was positioned in the center of a pyrolysis tube. A K-type thermal couple was immersed in the sample powder during the pyrolysis to measure temperature of sample in-situ. The

pyrolysis tube was flushed with nitrogen gas at 500 mL/min and then inserted in the pre-heated furnace. The outflow from pyrolysis passed through two sequentially connected condensers that were immersed in liquid N_2. Upon completion of pyrolysis, the reaction tube was removed from the furnace and allowed to cool down to room temperature under constant N_2 flow. The condensers were then removed from liquid nitrogen. In general, the liquid products contained two immiscible phases: heavy oil and light oil. In this study, the heavy oil was recovered by washing the reactor with acetone followed by evaporation under reduced pressure and kept in refrigerator under 273 K for further study.

4.2.3 Hydrogenation reaction of model compounds

All catalysts used in this study were purchased from Sigma-Aldrich. The catalysts were used directly without any pretreatment. In a standard procedure, the catalyst should be reduced before the reaction, therefore, the kinetics data could be calculated from the conversion of the feedstock and total amount of the active sites. In this study, we focused more on the reaction pathway, therefore, the catalyst was used directly without reduction. HDO of both model compounds and EOL heavy oil were carried out in a 75.0 mL Parr 4590 Micro Stirred Reactor. One step HDO was used for model compounds study. In a typical run, 25 mmol model compound and 20 mL DI water were loaded in a glass liner with 50 mg catalyst. A gas entrainment impeller was used in this experiment to enhance the mass transfer. The reactor was purged 5 times with nitrogen gas to remove the air in the reaction vessel followed by another 5 times purge with hydrogen to replace nitrogen. The initial hydrogen pressure was one atmosphere. When the temperature reached the

target, it was pressurized with hydrogen to 4.0 MPa. The reaction was conducted at 523 K for 2 hours.

For EOL heavy oil, HDO reaction was examined in two steps. In the first step, 150 mg heavy oil and 20 mL DI water were loaded in a glass liner with 15 mg noble metal catalyst. The reactor was then purged 5 times with nitrogen gas to remove the air in the reaction vessel and then purged another 5 times with hydrogen to replace nitrogen. The initial hydrogen pressure was set to 10.0 MPa and the stirring rate was 300 rpm. The reactor temperature was hold at 573 K for 4 hours and the reactor pressure was 14 MPa throughout the experiment. The water solution of the products was filtered through a 0.45 μm syringe filter to remove the spent catalyst. The filtrate was further upgraded in the second-step HDO. The experiment was conducted at 523 K for 2 hours with the initial hydrogen pressure of 10.0 MPa and 10 mg of the fresh catalyst.

4.2.4 Characterization of catalyst.

(1) BET measurement

The BET surface area test of the catalyst was carried out in the Quadrasorb system from Quantachrome Instruments. About 50 mg of the catalyst was placed in a quartz cell, degassed for 24 h at 673 K. Nitrogen adsorption isotherms were measured at 77 k. Specific surface area and pore size were determined by applying BET model and BJH model, respectively. For the spent catalyst, the catalyst particles were rinsed with 5 mL acetone first, then it is degassed and measured in the same procedure as the fresh catalyst.

(2) Metal dispersion measurements

Metal dispersion measurements were conducted in AutoChem II 2920 from Micromeritics Instrument Corporation following literature methods. [153] In brief, approximately 20 mg of catalyst was placed in the U-shaped quartz tube. Both ends of the tube were connected to the instrument. The sample was dried at 473 K for 2 hours. The temperature then ramped to 673 K at 10 K/min and hold at 673 K for 2 hours. After that, the temperature was reduced to 313 K and H_2 gas was introduced to the system in pulse mode. The loss of the TCD signal area was caused by the hydrogen adsorption on the active metal surface. The metal surface area was calculated using H/M ratio of 1. According to the literature, the reduction peak of Ru on carbon support is between 373 – 383 K [154].

(3) Scanning electron microscope (SEM)

SEM images were taken by LEO 1530 Thermally-Assisted Field Emission (TFE) Scanning Electron Microscope with a 3 kV acceleration voltage.

4.2.5 Quantitative ^{1}H-NMR and ^{13}C-NMR.

All NMR spectral data reported in this study were recorded with a Bruker Avance/DMX 400 MHz NMR spectrometer. Quantitative ^{1}H-NMR was acquired with 16 transients and 1.0 s pulse delay. (Note: the longest T1 was determined to be 0.16 s). Quantitative ^{13}C

NMR employing an inverse gated decoupling pulse sequence, 90 ° pulse angle, a pulse delay of 5.0 s for heavy oils and 10.0 s for hydrogenated products (Note: the longest T1 for pyrolysis oil was determined to be 0.8 s. For the hydrogenated products after adding the relaxation reagent $Cr(acac)_3$, the T1 relaxation time reduced from 6 s to 2 s. The T1 was measured using the Inversion-Recovery method and calculated with Bruker's TopSpin software 2.1 and the number of scan is 6,000. [67, 69]

4.3 Reactivity with model compounds

Phenol, catechol and guaiacol are commonly used as model compounds to study the reaction mechanisms of lignin pyrolysis oil upgrading. As shown in Figure 4.1, there are three major reaction pathways in the HDO of guaiacol: (1) direct hydrogenation of aromatic ring, (2) demethylation reaction and (3) demethoxylation reaction. No transalkylated product was detected after the reaction because transalkylation reaction is catalysed by the acid site, [95] and the untreated carbon support processes few acid sites. [155] For phenol and catechol, all four catalysts showed similar reactivity. However, both Pt and Pd catalysts did not catalyze the HDO of guaiacol.

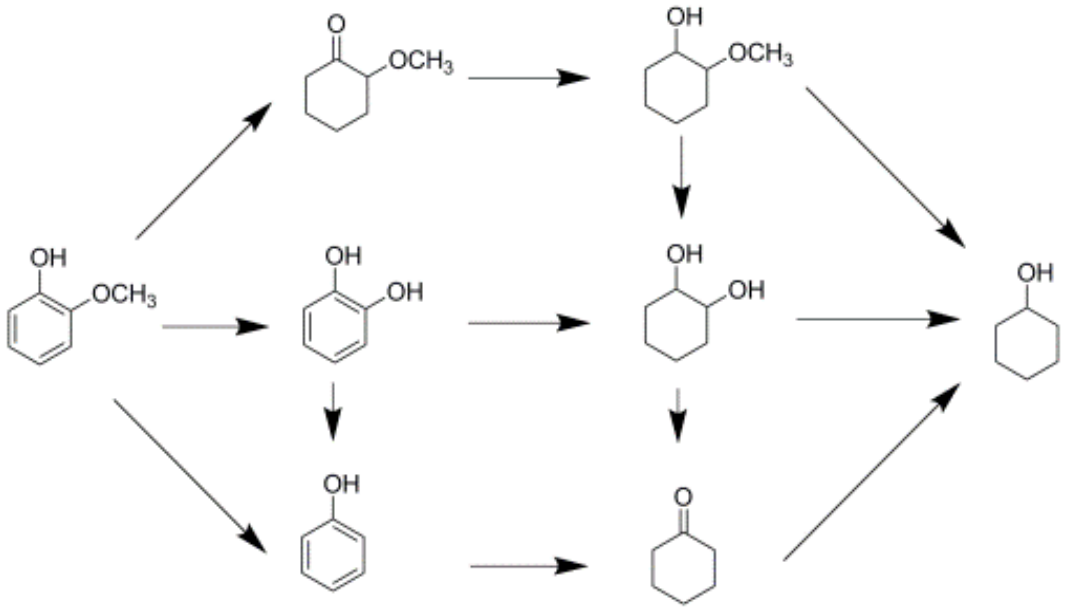

Figure 4.1 Reaction path of guaiacol HDO.

The conversions of the model compounds of all four catalysts are summarized in Figure 4.2 (a), and the experimental results with different guaiacol/catalyst weight ratios are shown in Figure 4.2 (b). The reactivity of the four catalysts with the three model compounds are different because each combination of the catalyst and model compound has various activation energy and adsorption energy. The main products from phenol hydrogenation were cyclohexanol and cyclohexanone, caused by the adsorption configuration of phenol on the catalyst. Cyclohexanone is produced if phenol is adsorbed non-planar to the surface. If the phenol is adsorbed co-planar to the surface, cyclohexanol is produced directly. [117] The selectivities of phenol to cyclohexanol were approximately 100% for all four catalysts, probably due to the further hydrogenation of cyclohexanone. The major products from catechol HDO were 1,2-cyclohexane-diol, cyclohexanone and cyclohexanol. The possible reaction pathways were shown in Figure

4.1. The selectivity of catechol to the hydrogenated products (predominantly 1,2-cyclohexane-diol) for Pd, Pt, Rh, Ru were 74%, 78%, 52%, and 48%, respectively. The selectivity towards the HDO products (cyclohexanol and cyclohexanone) were 24%, 22%, 34%, and 41%. Phenol was a minor product in all the solution.

Ru was the best catalyst at all ratios. When the weight ratio was 20, the conversion of Ru catalyzed guaiacol HDO is almost 100%. Rh was the second best catalyst. When the weight ratio of guaiacol to the catalyst was decreased, the difference in the conversion of guaiacol with Ru and Rh catalysts also decreased. Pt and Pd catalysts had approximately zero guaiacol conversion at weight ratio of 20 and 60. When the weight ratio decreased to 2, the conversions were over 80%.The majority product was 1,2-cyclohexane-diol and no 2-methoxy-cyclohexanol was detected for both Pt/C and Pd/C catalysts.

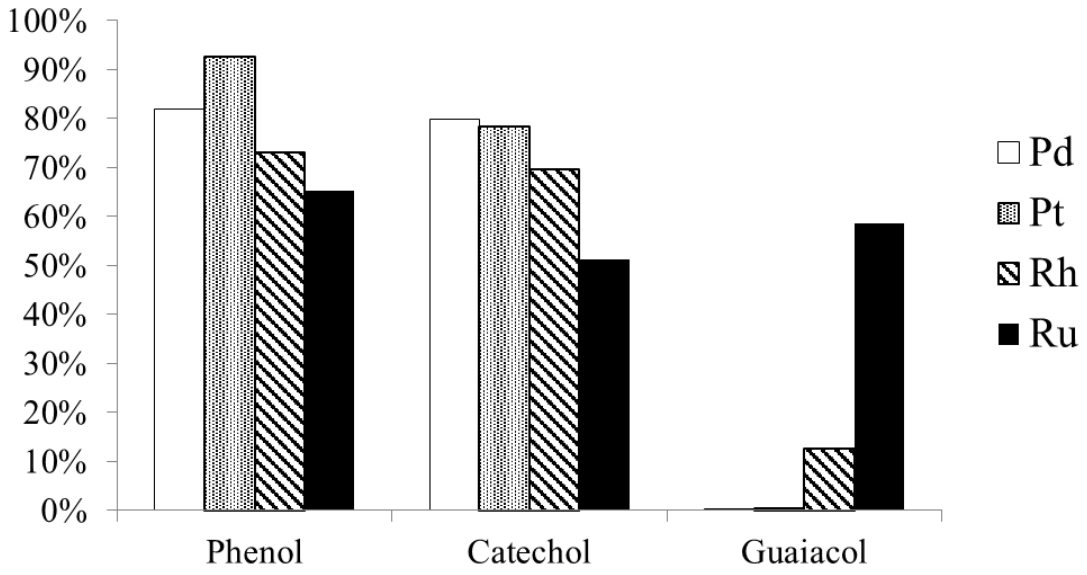

Figure 4.2 (a) Conversion of model compounds with different catalysts (top). *Reaction condition: 50 mg catalyst, 25 mmol model compounds, 523 K, 40 bar H_2, 2 hours.* (b) Conversions with different guaiacol/catalyst ratio (bottom). *Reaction condition: 25 mmol (3.1g) guaiacol, 523 K, 40 bar H_2, 2 hours*

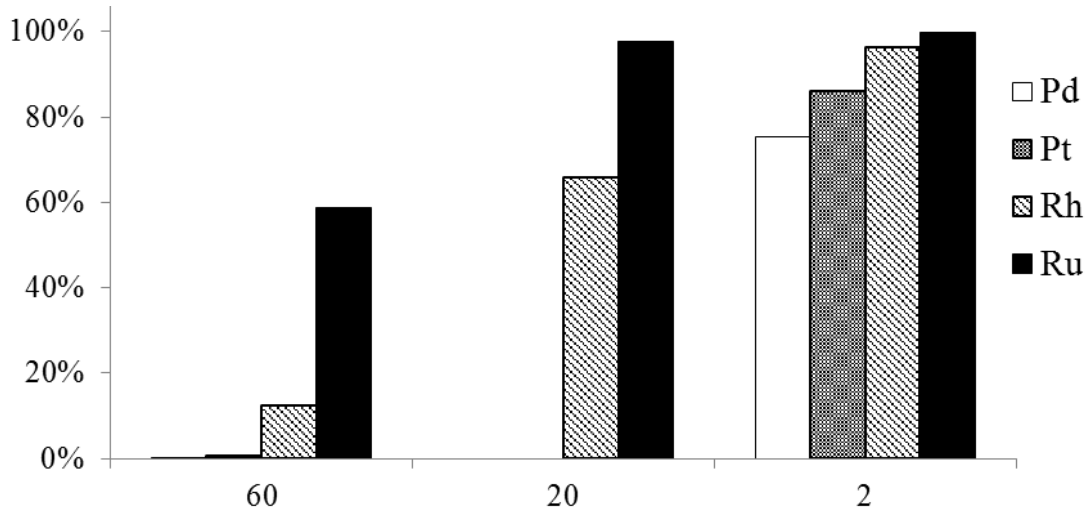

Figure 4.2 Continued

4.3.1 Platinum and palladium catalyzed guaiacol HDO

Runnebaum et al. reported that demethylation was a fast reaction step in the HDO of guaiacol using Pt catalyst, which yielded catechol [156]. Another paper demonstrated that coke was formed with the presence of guaiacol and catechol [80]. Therefore, a possible assumption is that catechol is produced from the demethylation of guaiacol first, then the produced catechol becomes a potential cause of the deactivation of Pt and Pd catalysts. Therefore, the guaiacol can deactivate Pt and Pd catalysts alone. To validate this hypothesis, three groups of control experiments were performed and the results are listed in Table 4.1.

Table 4.1 Control experiments for guaiacol HDO.

Group	Experiment Condition	Result
1	Catalyst: Ru/C Reactant: GUA + CAT Gas Phase: 40 bar H_2	No hydrogenated product obtained.
2	Catalyst: Pt/C, Pd/C Reactant: GUA + Ph Gas Phase: 40 bar H_2	No hydrogenated product obtained.
3	Catalyst: Pt/C, Pd/C Reactant: Ph Gas Phase: 10 bar CO and 30 bar H_2	The yields of hydrogenated products with both catalysts are over 55%.

** Reaction condition: 523 K, 40 bar H_2, 2 hours. For group 1 and 2, 12.5 mmol of each model compound was added. For group 3, 25.0 mmol phenol was added. Ph, CAT, GUA stand for phenol, catechol, guaiacol respectively.*

In group 1, Ru catalyst was used in the HDO reaction of both guaiacol and catechol because Ru exhibits excellent reactivity individually with guaiacol or catechol. The low guaiacol conversion indicates the deactivation of Ru catalyst in the presence of guaiacol and catechol. In group 2, Pt and Pd were used to catalyze the HDO reaction of guaiacol and phenol aqueous mixture, respectively. Both Pt and Pd catalyzed phenol hydrogenation effectively. In the presence of guaiacol, almost no phenol was hydrogenated, which meant that both catalysts were deactivated in the presence of guaiacol. In the last group, carbon monoxide was added in the gas phase. It was reported that CO was produced during the Pt catalyzed guaiacol HDO. [157] CO is known to be a

potential cause of Pt catalyst deactivation. The result showed that both Pt and Pd were still reactive in the hydrogenation of phenol with the existence of a relatively high amount of CO in the gas phase. Therefore, catalyst deactivation is mainly caused by the coke generated from guaiacol and catechol.

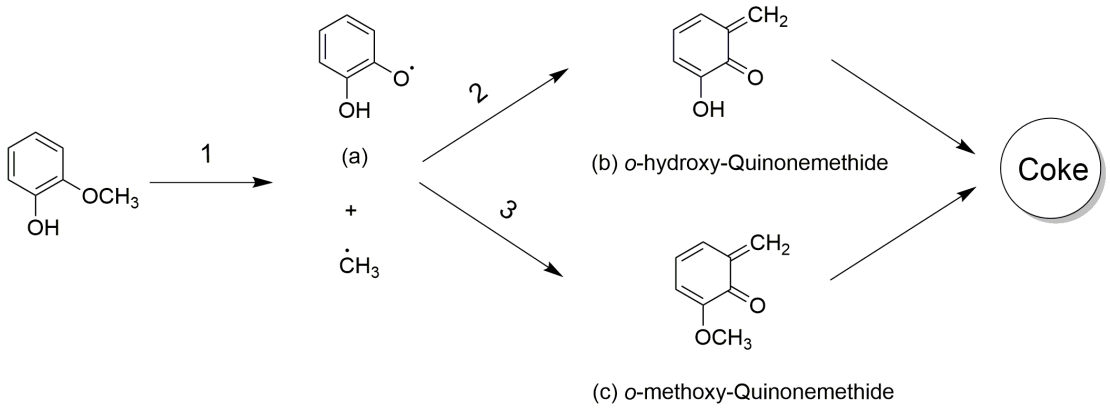

Figure 4.3 Tentative coke formation mechanism with Pt/C and Pd/C catalysts

The tentative coke formation mechanism of Pt and Pd catalyzed guaiacol HDO is shown in Figure 4.3. As discussed in section 4.3, when the weight ratio of guaiacol to Pt/C or Pd/C catalyst reduced to two, the major product was 1,2-cyclohexane-diol and no 2-methoxy-cyclohexanol was observed. The reaction energies calculation indicated that the demethlyation reaction of guaiacol was more facile compared with the demethoxylation reaction, therefore, the demethylation reaction is typically favored kinetically. [158] Prasomsri et al. [159] also did a hemolytic bond-dissociation energy analysis that the bond strengths follow an order of Ph–OH > Ph–OMe > Ph–O–Ph > PhO–Me. Therefore, catalyst preferentially cleaves PhO-Me bond. The hydrogenolysis of the O–CH_3 bond (step 1 in Figure 4.3) generated CH_3 radical and phenoxy radical (structure (a) in Figure 4.3). The two radicals further recombined and rearranged to produce *o*-hydroxy-

Quinonemethide (step 2 in Figure 4.3) and the CH_3 radical could also react with guaiacol to produce *o*-methoxy-Quinonemethide (step 3 in Figure 4.3). [160] Both *o*-Quinonemethide compounds are key intermediates for coke formation. [161] The unreacted phenoxy radical (structure (a) in Figure 4.3) produced catechol, followed by the hydrogenation reaction, which generated 1,2-cyclohexane-diol. In a summary, during the catalytic HDO of guaiacol, both Pd and Pt catalysts produced catechol as the intermediate product and the presence of catechol might lead to the coking problem.

4.3.2 Rhodium catalyzed guaiacol HDO

The products distribution of Rh catalyzed guaiacol HDO is given in Figure 4.4 (a). The overall conversion is low since only 12% guaiacol was converted after four hours. Phenol, cyclohexanone, cyclohexanol and 1,2-cyclohexane-diol were the main products. The distribution of products did not show remarkable changes after 1 hour, indicating the deactivation of Rh catalyst.

Experimental results demonstrate that Rh was able to catalyze the demethoxylation of guaiacol, which produces phenol at high selectivity. No 2-methoxy-cyclohexanol was detected in the solution, which means no direct hydrogenation reaction occurred in the reaction. 2-methoxy-cyclohexanol was also used as the model compound, and the HDO experiment was carried out under the same condition. The conversion was less than 30% after 2 hours, which confirmed that no direct hydrogenation reaction occurred during the Rh catalyzed guaiacol HDO. The existence of 1,2-cyclohexane-diol, with selectivity

around 15%, showed that catechol was the intermediate product from the guaiacol HDO. The reaction mechanism of Rh catalyzed guaiacol HDO was deduced from the results concluded above. Rh was also deactivated by the coke from guaiacol and catechol. While Pt and Pd both catalyzed demethylation reaction efficiently and deactivated rapidly, Rh catalyzed demethylation reaction, comparatively, was a relatively slow step. The reactivity decayed slowly and it was completely deactivated after two hours. The tentative reaction pathway is shown in Figure 4.4 (b).

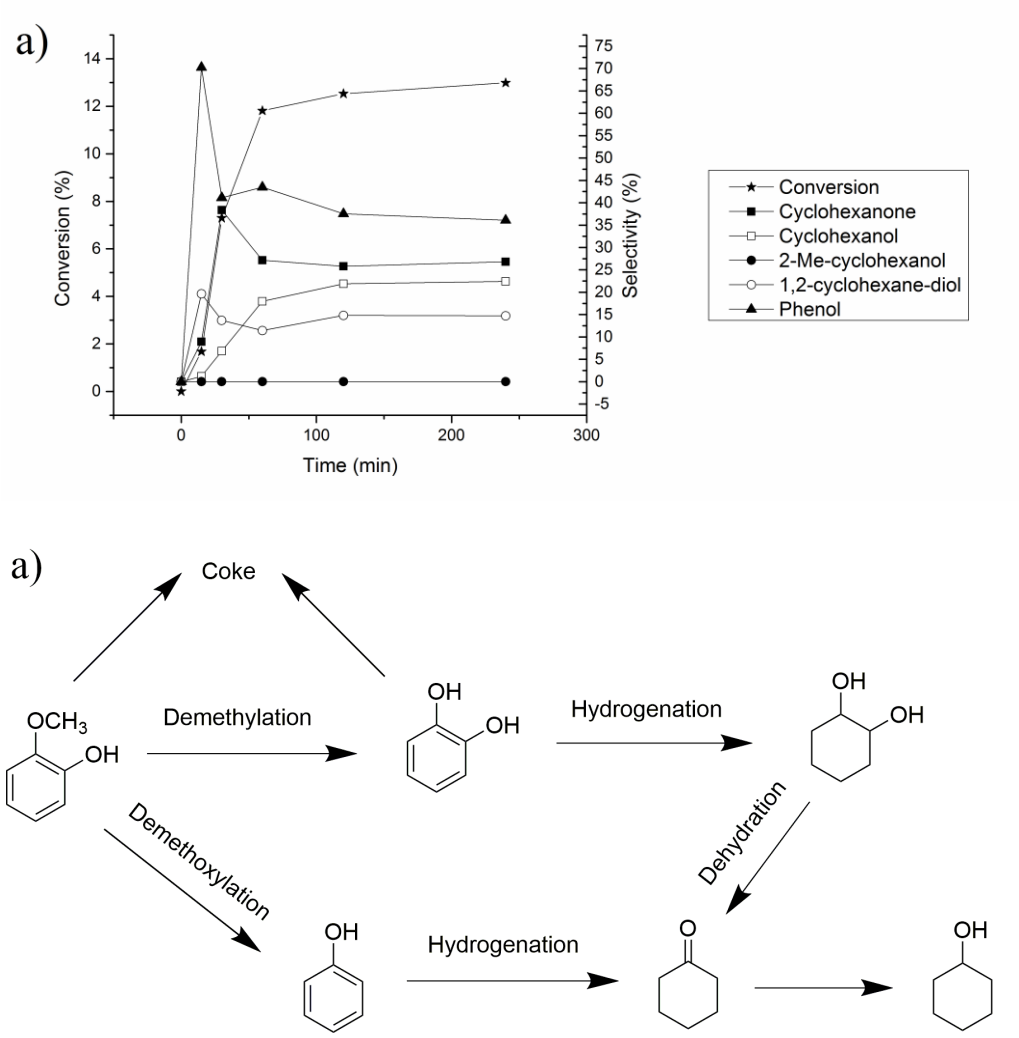

Figure 4.4 (a) Product distribution after rhodium catalyzed guaiacol HDO (top) and (b) tentative reaction mechanism of Rh catalyzed guaiacol HDO (bottom).
Reaction condition: 50 mg Rh/C, 25 mmol model compounds, 523 K, 40 bar H_2, 2 hours.

4.3.3 Ruthenium catalyzed guaiacol HDO

The products distribution in the HDO of guaiacol by Ru catalyst is shown in Figure 4.5 (a). Ruthenium reached the highest conversion among all four catalysts. Cyclohexanol and 2-methoxy-cyclohexanol were the main products, and phenol was the key intermediate product in the beginning of the reaction. The yield of phenol was around 20% after 15 minutes and gradually converted to cyclohexanol after four hours. 1,2-cyclohexanediol was a minor intermediate product. Compared to the Rh catalyst in the same reaction, which produced 1,2-cyclohexanediol at the beginning of the reaction, the ruthenium catalyst did not produce 1,2-cyclohexanediol in the first 60 minutes. After 90 minutes, only 2% of 1,2-cyclohexanediol was detected, indicating that it was not likely to be produced directly from guaiacol. One possible reaction for the generation of 1,2-cyclohexanediol is the hydrolysis of 2-methoxy cyclohexanol. The proposed reaction mechanism of the HDO of guaiacol by Ru is shown in Figure 4.5 (b). No catechol was detected throughout the reaction, which prevented the formation of coke.

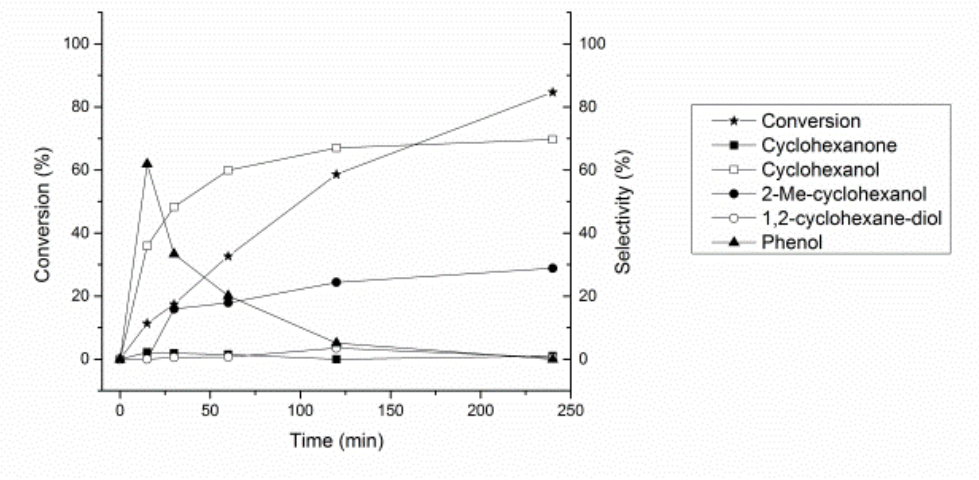

Figure 4.5 (a) Product distribution after ruthenium catalyzed guaiacol HDO (top) and (b) tentative reaction mechanism of Ru catalyzed guaiacol HDO (bottom).
Reaction condition: 50 mg Ru/C, 25 mmol model compounds, 523 K, 40 bar H_2, 2 hours.

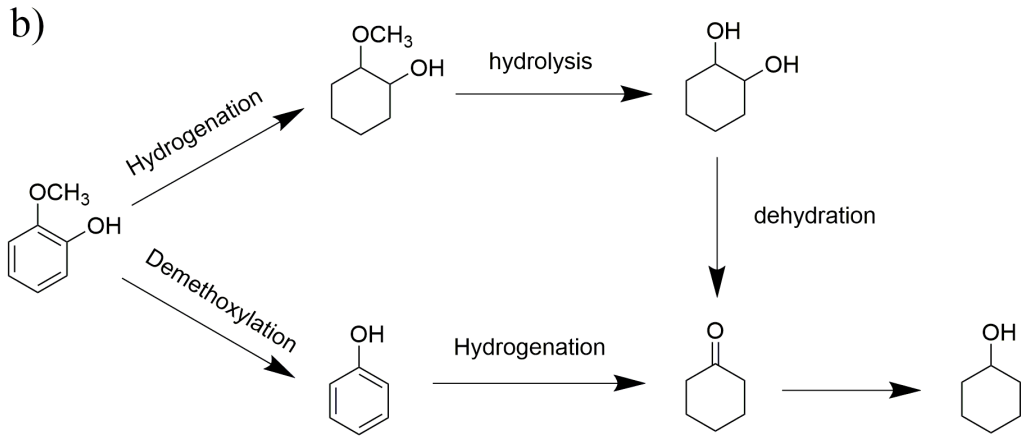

Figure 4.5 Continued.

4.4 Characterization of catalysts

The physisorption and chemisorption results of all four catalysts were characterized before reaction without any pretreatment. The results are summarized in Table 4.2. The dispersions of active metals indicates the percentage of the metallic atoms contribution for the reactant adsorption. Rh/C had the highest dispersion, followed by Ru/C, Pt/C and Pd/C. All catalysts had similar surface area and pore radius before the reaction as the support was activated carbon obtained from the same source.

Table 4.2. Physical and chemical property of all four catalysts

	Pd/C	**Pt/C**	**Rh/C**	**Ru/C**
Metal Loading	5%	5%	5%	5%
Dispersion (%)	41.1	30.7	46.8	23.7
Surface Area (m^2/g)	1000	990	928	815
Pore size (nm)	1.91	1.54	1.71	1.53
Pore Volume (cm^3/g)	0.732	0.484	0.745	0.557

BET results of the spent catalysts are shown in Figure 4.6. The experimental results from the studies of model compounds align well with the BET data in Figure 4.6 very well. The surface area of Pd and Pt catalysts decreased by 37% and 49%, respectively. The significant reductions in surface area indicate the existence of severe coke formation. For Rh, the surface area reduced by 28%, which was less than the values of Pt and Pd. There was only a 12% decrease in surface area for Ru. The pore sizes of all the catalysts were also calculated. No significant decrease in the pore size was observed due to the neutral surface area of carbon, which possessed a small number of Lewis acid sites [140].

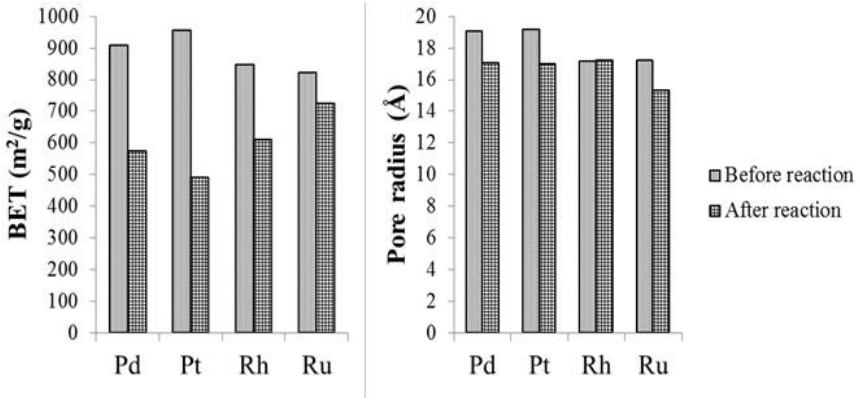

Figure 4.6 BET surface area and pore size of the catalysts before and after the HDO

4.5 Conclusion

In summary, four commonly used noble metal catalysts were evaluated with three lignin model compounds under aqueous phase reaction. The major conclusions from this study include the follwing: (1) Pd, Pt and Rh were all deactivated during the HDO of guaiacol due to the formation of catechol through the demethylation reaction. The rearrangement of the radicals from the hydrogenolysis of O-CH_3 bond produced two types of *o*-methoxy-Quinonemethide, which were reported as key intermediates for coke formation.

The difference was that Pd and Pt lost reactivity right after the reaction started and Rh was slowly deactivated in two hours. (2) Ru was the only catalyst that was able to fully convert guaiacol into hydrogenated compounds because of its unique reaction pathway. Although Ru had the lowest metal dispersion among all the catalysts, it possessed the highest reactivity in this reaction. No demethylation but mainly demethoxylation and hydrogenation reactions were observed in the Ru catalyzed guaiacol HDO. (3) The decrease in BET surface area indicated coke formation within Pt, Pd and Rh catalysts. Ru had the lowest reduction in surface area, which showed that its morphology had not changed much after the reaction.

CHAPTER 5: NOBLE METAL CATALYZED AQUEOUS PHASE HDO OF EOL PYROLYSIS HEAVY OIL[3]

5.1 Introduction

Catalytic hydrodeoxygenation is a promising approach for pyrolysis oils upgrading. [162] The hydrogenation of biomass components and pyrolysis oils has been intensively studied. Recently, several publications studied the hydrogenation of phenolic pyrolysis oil model compounds. [163, 164] In these studies, noble metals, such as Ru, Rh, Pd and Pt, were used as the catalysts for HDO reaction. Several model compounds, such as anisole, *4*-ethylphenol, 2-methoxy-4-n-propylphenol and 4-hydroxy-3-methoxyphenyl-acetone, were upgraded to the aliphatic compounds. The yields of the hydrogenated products were approximately 100%. Huber et al. reported a two-step hydrogenation process for pyrolysis bio-oil upgrading. [165] In the first step, Ru/C catalyst was used, and the reaction was carried out at 398 K with a 10 MPa H_2 gas. In the second step, a Pt/C catalyst was used, and the reaction is conducted at 523 K with a 10.0 MPa H_2 gas. The two-step hydrogenation process converted the water-soluble fraction of pinewood

[3] Reproduced from (1) Ben, H., Mu, W., Deng, Y., and Ragauskas, A.J., Production of renewable gasoline from aqueous phase hydrogenation of lignin pyrolysis oil. Fuel, 2013. 103(0): p. 1148-1153,and (2) Ben, H., Ferguson, G.A., Mu, W., Pu, Y., Huang, F., Jarvis, M., Biddy, M., Deng, Y., and Ragauskas, A.J., Hydrodeoxygenation by deuterium gas - a powerful way to provide insight into the reaction mechanisms. Physical Chemistry Chemical Physics, 2013. 15(44): p. 19138-19142. with permission from Elsevier and PCCP Owner Societies, respectively.

pyrolysis oil to the gasoline like compounds. The upgraded products had a boiling range of 338 -448 K, and the overall carbon yields for the gas, liquid and coke products were 26%, 17% and 34% respectively [165]. In another study, Ru/C was used as the catalyst of hydrogenation of whole fast pyrolysis oils produced from beech wood [166]. The operation temperature was 623 K, and hydrogen pressure was 20.0 MPa. The ^{1}H-NMR results indicated that the aliphatic/aromatic proton ratio increased from 6.4:1 to 11.2-16.4:1 after the reaction, which suggests that aromatic ring was hydrogenated during the process but the reaction is not complete. The hydrogenation process is catalyzed by Pt, Pd or Ru at 393 - 538 K with a 5.2 - 6.2 MPa H_2 gas. The carbon yield of the hydrogenation of aqueous carbohydrates derived from maple wood was around 57%.

The pyrolysis of lignin yields a large amount of water-insoluble heavy oil. The weight percentage is between 65 - 85 wt.% [167, 168]. The pyrolysis of the carbohydrates produces mostly a water-soluble light oil. The major products in light oil are methanol, levoglucosan and catechol with a high content of water (> 60 wt.%). When tannin and cellulose is used as feedstock, the pyrolysis light oil yields are 77 - 80 wt.% and 85 wt.%, respectively. [169, 170] Hence, the biomass pyrolysis heavy oil is mainly produced from the lignin. However, it does not mean the heavy oil is only produced from lignin. The carbonhydrates can also convert to aromatic structure through acid catalyzed dehydration and reforming reactions. [171, 172] The heavy oil yields from the bark and residue pyrolysis are 60 - 68 wt.% and 55 - 57 wt.%, respectively. [170] However, such a major portion has only received little attention. The major problem is that the complex aromatic structures of the heavy oil make it difficult to upgrade via the hydrogenation process.

Several studies have been conducted and the whole biomass pyrolysis oil can only be partially hydrogenated. [165, 166] In my thesis work, two-step hydrogenation of lignin pyrolysis heavy oil was carried out due to the tar formation (refer to section 5.3.5). Based on the results presented in Chapter 4, ruthenium was used as the catalyst for this reaction.

Besides directly applying the catalyst to the pyrolysis heavy oil upgrading, the fundamental reaction mechanism has also been studied in detail. As shown in Chapter 2, the reaction networks of model compounds are already very complex, not to mention the pyrolysis oil that contains hundreds to thousands of compounds. One feasible approach is to trace the hydrogen during the HDO reaction. The isotope of hydrogen, deuterium, can be used to label the hydrogenated site, and this would be a great help to provide insights to the HDO reaction mechanism. The deuterium atom is invisible in traditional ^{1}H-^{13}C Heteronuclear Single Quantum Coherence (HSQC) NMR. Therefore, a direct comparison of the NMR spectra between proton and deuteron hydrogenated products will provide intuitive and detailed information about the added hydrogen atom. The results would be direct evidence to validate the mechanism of both hydrogenation and HDO reaction, which are valuable in developing the processing for whole biomass pyrolysis oil hydrogenation.

5.2 Materials and experimental procedures

All reagents used in this study were purchased from VWR International or Sigma-Aldrich (St. Louis, MO) and used as received. Wood chips used in this study were acquired from

a 15-year old Loblolly pine trees from the southeastern U.S.A. The wood chips were refined with a Wiley mill through a 0.13 cm screen and dried under high vacuum at 323 K for 48 h. Pine wood samples were stored at ~ 273 K prior to use.

5.2.1 Lignin separation and purification

The milled pine wood was ethanol-organosolv-pretreated as previously described in the literatures. [150-152, 173] Briefly, a 100.0 g (dry weight) sample of the milled pine wood was treated with 65% ethanol/water solution with 1.2 w/w% sulfuric acid as a catalyst at 443 K for 60 min. The solid to liquid ratio used was 1:8. The pre-treatments were carried out in a Parr reactor equipped with a temperature controller (Parr Instrument Company, Moline, IL). The pre-treated pine wood was washed with warm (333 K) ethanol/water (8:1, 3×50.0 mL). The washes were combined and 3 volumes of water were added to precipitate the Ethanol Organosolv Lignin (EOL), which was collected by centrifugation and air dried. The EOL was purified by Soxhlet extraction with pentane and stored at ~ 273 K prior to use.

5.2.2 Equipment and process of pyrolysis [67, 69]

Pyrolysis experiments were conducted in a quartz pyrolysis tube heated with a split-tube furnace. Typically, a sample of lignin powder (3.00 g) was placed in a quartz sample boat that was then positioned in the center of a pyrolysis tube. A K-type thermal couple was immersed in the sample powder during the pyrolysis to measure the heating rate. The

pyrolysis tube was flushed with nitrogen gas and the flow rate was adjusted to a value of 500 mL/min and then inserted in the pre-heated furnace. The outflow from pyrolysis was passed through two condensers, which were immersed in liquid N_2. Upon completion of pyrolysis the reaction tube was removed from the furnace and allowed to cool to room temperature under constant N_2 flow. The condensers were then removed from liquid nitrogen. The pyrolysis char and pyrolysis oil were collected for subsequent chemical analysis. In general, the liquid products contained two immiscible phases referred to as a heavy oil (contains water insoluble components) and a light oil (contains water soluble components and ~80 wt.% of water). The light oil was acquired by decantation and the heavy oil was recovered by washing the reactor with acetone followed by evaporation under reduced pressure. Char yields were determined gravimetrically and gas formation was calculated by mass difference.

5.2.3 Hydrogenation process

Hydrogenation of EOL heavy oil was examined in two steps. Both experiments were carried out in a 75mL Parr 4590 Micro Stirred Reactor. In the first step, 150 mg heavy oil and 20 mL DI water were loaded in a glass liner with 15 mg 5 wt.% Ru/activated carbon catalyst (Alfa Aesar, Product No. 7440-18-8). The reactor was then purged 5 times with nitrogen gas to remove the air present in the reaction vessel. Then the reactor was purged 5 times with hydrogen to replace nitrogen. The initial hydrogen pressure was 10 MPa and the stirring rate was 200 rpm. The reactor temperature was held at 573 K for 4 hours and the reactor pressure was ~14 MPa. After the first-step hydrogenation, the EOL heavy oil

has been upgraded to water soluble components and the water solution of the products was filtered through a 0.45 μm syringe filter. The filtrate was further upgraded by the second-step HDO, which was conducted at 523 K for 2 hours with the initial hydrogen pressure of 10 MPa and 10.0 mg fresh 5 wt.% Ru/activated carbon as the catalyst.

5.2.4 Characterization of heavy oil by GPC

The weight average molecular weight (M_w) was determined by GPC analysis following literature methods. [67, 69] Prior to GPC analysis, the heavy oil and tar were dissolved in THF (1 mg/mL) and filtered through a 0.45 μm syringe filter. The samples were injected into a Polymer Standards Service (PSS) Security 1200 system featuring Agilent HPLC vacuum degasser, isocratic pump, refractive index (RI) detector and UV detector (270 nm). Separation was achieved with four Waters Styragel columns (HR0.5, HR2, HR4, HR6) using THF as the mobile phase (1.0 mL/min) with injection volumes of 30 μL. Data collection and processing were performed using PSS WinGPC Unity software. Molecular weights (M_n and M_w) were calibrated against a polystyrene calibration curve. The calibration curve was created by fitting a third order polynomial equation to the retention volumes obtained from a series of narrow molecular weight distribution polystyrene standards (i.e., 3.90×10^6, 3.64×10^6, 2.22×10^6, 1.36×10^6, 9.96×10^5, 6.68×10^5, 5.38×10^5, 1.97×10^5, 5.51×10^4, 3.14×10^4, 1.39×10^4, 7.21×10^3, 4.43×10^3, 1.39×10^3, 5.80×10^2 Da), phenol and acetone. The curve fit had an R^2 value of 0.9984.

5.2.5 Preparation of NMR samples

(1) EOL heavy oil (70.0 mg) dissolved in 450 μL DMSO-d_6.

(2) Hydrogenation products

The water solution of first or second-step hydrogenation products (20 mL) was extracted by 1.00 mL $CDCl_3$. The $CDCl_3$ phase was dried by $MgSO_4$ and filtered through a 0.45 μm syringe filter. The relaxation reagent Chromium (III) acetylacetonate (0.01 M) [174] was added to the $CDCl_3$ filtrate to provide complete relaxation of all nuclei and the $CDCl_3$ solution was used as the NMR sample for the first or second step HDO product.

(3) Tar from the catalyst of 1st step hydrogenation process

The catalyst was separated from water solution by filtration. Acetone was used to wash the catalyst and the tar was recovered by the evaporation of acetone under reduced pressure. The recovered tar (70 mg) was dissolved in 450 μL DMSO-d_6.

5.2.6 Characterization of heavy oil, hydrogenation products and tar by NMR

(1) Quantitative ^{13}C NMR

All NMR spectral data reported in this study were recorded with a Bruker Avance/DMX 400 MHz NMR spectrometer. Quantitative ^{13}C NMR employing an inverse gated decoupling pulse sequence, 90° pulse angle, a pulse delay of 5 s for heavy oils and tar and 10 s for hydrogenation products (Note: the longest T1 for pyrolysis oil was determined to be 0.8 s, and for the hydrogenation products after adding the relaxation reagent the T1 reduced from 6 s to 2 s. The T1 was measured using the Inversion-

Recovery method and calculated with Bruker's TopSpin software 2.1 and the scan number is 6000. [67, 69]

(2) ^{1}H-^{13}C HSQC-NMR

The ^{1}H-^{13}C HSQC-NMR employed a standard Bruker pulse sequence "hsqcetgpsi.2" with a 90° pulse, 0.11 s acquisition time, a 1.5 s pulse delay, a $^{1}J_{C-H}$ of 145 Hz, 48 scans and acquisition of 1024 data points (for ^{1}H) and 256 increments (for ^{13}C). The ^{1}H and ^{13}C pulse widths are p1=11.30 μs and p3=10.00 μs, respectively. The ^{1}H and ^{13}C spectral widths are 13.02 ppm and 220.00 ppm, respectively. HSQC data processing and plots were carried out using MestReNova v7.1.0 software's default processing template and automatic phase and baseline correction. [175, 176]

(3) DEPT-135 ^{13}C-NMR

DEPT-135 ^{13}C-NMR was employing a standard Bruker pulse sequence "dept135" with a 135° pulse angle, 2 s pulse delay, and 5000 scans.

(4) Quantitative ^{1}H-NMR

Quantitative ^{1}H-NMR was acquired with 16 transients and 1 s pulse delay. (Note: the longest T1 was determined to be 0.16 s)

(5) ^{2}D-NMR

Deuterium NMR was carried out with Bruker's pulse program "zg2h" by using the lock channel in a Bruker's BBO probe. A 90° C pulse, 4.5 s acquisition time and 800 scans were employed for acquiring the ^{2}D-NMR spectra.

5.2.7 Elemental analysis of EOL and EOL heavy oil and carbon content of hydrogenation products

Elemental analysis data of EOL and EOL heavy oil was obtained by Atlantic Microlab. Inc. (Norcross, GA) utilizing combustion to determine carbon, hydrogen and sulfur contents. The oxygen content was calculated by mass difference. The error is 0.3%.

The carbon contents of the first- and second-step hydrogenation products were determined by Total Organic Carbon (TOC) analyzer. (Ionics Inc 1555B)

5.2.8 SEM characterization of catalyst

The catalyst samples were imaged with a scanning electron microscope (Hitachi S-800) with 12 kV acceleration voltages.

5.2.9 GC-MS analysis of hydrogenation products

The GC-MS analysis of hydrogenation products was conducted by Agilent 5975C MSD and 7890A GC with a 7693 auto sampler. The Agilent HP-5MS, 19091S-433 column was used. The GC oven was programmed with the following temperature regime: hold at 323 K for 5 min, ramp to 473 K at 5 °C/min and hold at 473 K for 5 min.

5.3 Results and Discussion

5.3.1 Platinum and ruthenium catalyzed lignin heavy oil HDO

To examine whether the reaction mechanisms deduced in Chapter 4 are applicable to the catalytic HDO of EOL heavy oil, one inactive catalyst (Pt) and the most reactive catalyst (Ru) were chosen to catalyze the EOL heavy oil upgrading. A two-step HDO reaction was used because of the tar formation in the first HDO reaction. In the first step, the reaction was operated under a relatively high temperature (573 K) to stabilize the compounds. The spent catalyst was removed, and the fresh catalyst was replenished for the second-step HDO, which was operated under the same condition as that in the model compound study. The chemical structure and mechanism of the tar products are discussed in section 4.3.4.

The carbon yields of Ru and Pt are summarized in Table 5.1. The carbon yields in the first-step HDO were around 30% for both catalysts. There were three significant changes after the first HDO reaction. First, compounds that tended to condense were removed. Second, the molecules in the heavy oil (M_w=265 g/mol) were degraded from dimers and trimers to monomers. Third, the water-soluble compounds were obtained from the water-insoluble heavy oil.

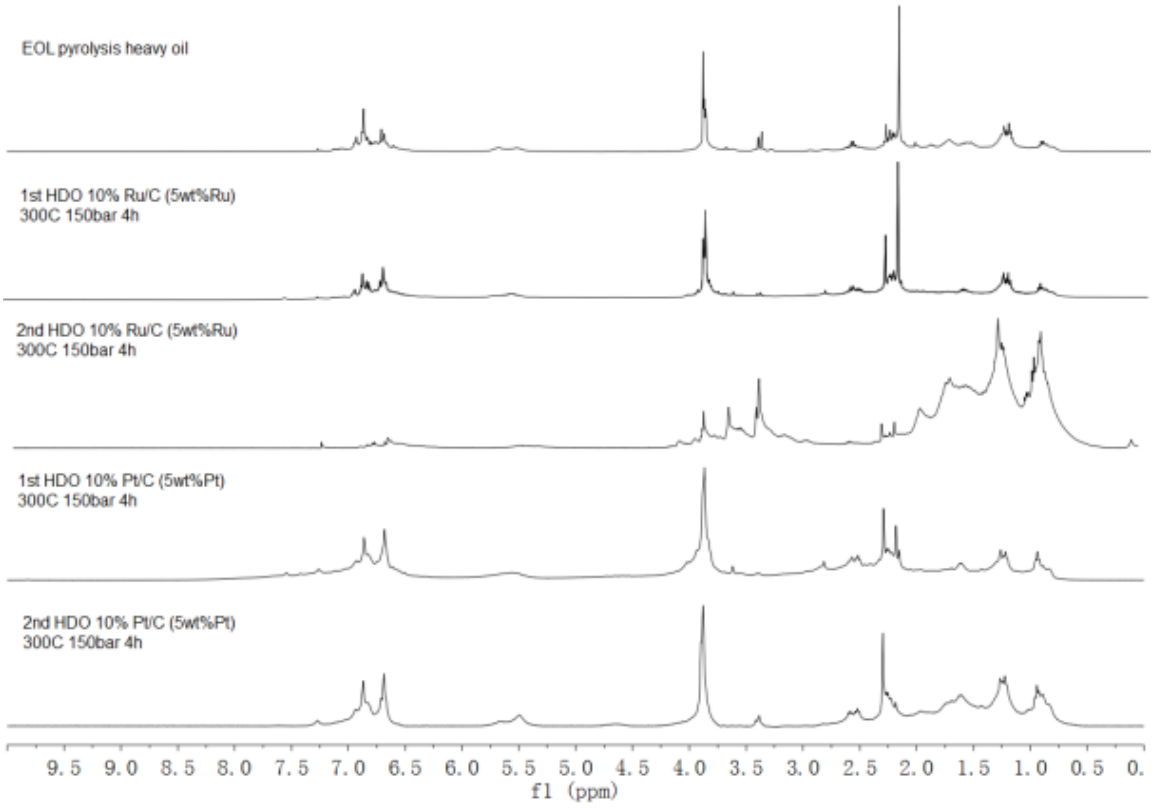

Figure 5.1 ^{1}H-NMR spectra for the Ru and Pt catalyzed EOL heavy oil, first- and second-step HDO products. (from top to bottom)

Reaction condition: First-step HDO: 15.0 mg 5 wt.% Ru/C, 150 mg heavy oil in 20 mL DI H_2O, 573 K, 10 MPa H_2, 4 hours.
Second-step HDO: 10.0 mg 5 wt.% fresh Ru/C, 523 K, 10 MPa H_2, 2 hours.

Proton NMR was used to quantify the degree of hydrogenation. The ^{1}H-NMR spectra for the EOL heavy oil and the products after the first and second-step upgrading reaction are listed in the Figure 5.1. The integration results are presented in Table 5.1. The aromatic proton peaks almost disappeared in the second HDO reaction catalyzed by Ru and 85% of the protons belonged to aliphatic protons with no oxygen atoms bonded to the α-carbon. This indicates that the second HDO reaction products contained only aliphatic carbons, and the products had relatively low oxygen content, which represents a potential resource for bio-gasoline. The major reaction mechanism of second-step upgrading are

discussed in Chapter 6. Compared to the EOL heavy oil, the first-step HDO products contained fewer aromatic protons (see Table 1) and more aliphatic protons, which meant that the hydrogenation of benzene ring also occurred during the first HDO process. On the other hand, the products from the second HDO reaction catalyzed by Pt still had 15.73% protons in the aromatic region, which was likely due to the low reactivity of the guaiacol-based compounds. Each carbon owned roughly one hydrogen atom in an aromatic ring and two hydrogen atoms in an aliphatic ring. This meant that around 30% of the carbon rings remained in the aromatic structure. Pt could not catalyze the HDO reaction of guaiacol-based compound. Compared with the NMR spectrum of the first HDO reaction products, no significant change was observed after second HDO reaction.

Table 5.1 ^{1}H-NMR and Total organic carbon (TOC) yield of EOL heavy oil and products from first and second-step upgrading catalyzed by Pt or Ru.

Type of protons	EOL heavy oil	Ru		Pt	
		First-step	Second-step	First-step	Second-step
-C**H**O, -COO**H**	0[#]	0	0	0	0
Ar**H**, **H**C=C-	31	21	0	24	14
-C**H**$_n$-O- , C**H**$_n$-O-	27	18	15	32	24
-C**H**$_3$, -C**H**$_n$-	42	61	85	44	62
TOC yield to the feedstock		36%	34%	28%	26%

[#] The results are shown as percentage of hydrogen.
* The assignment ranges are on the basis of literature reports.[168, 177]
Reaction condition: First-step HDO: 15.0 mg 5 wt.% Ru/C, 150 mg heavy oil in 20 mL DI H_2O, 573 K, 10 MPa H_2, 4 hours.
Second-step HDO: 10.0 mg 5 wt.% fresh Ru/C, 523 K, 10 MPa H_2, 2 hours.

5.3.2 Further study of ruthenium catalyzed lignin heavy oil upgrading

Figure 5.2 is the quantitative ^{13}C-NMR of the EOL heavy oil and first-step hydrogenation product. Table 5.2 summarizes the integration of the ^{13}C-NMR spectra on the basis of the chemical shift of the corresponding functional groups in the EOL heavy oil and first-step HDO products. Relatively lower amounts of the carbonyl C=O bonds, aromatic C-C bonds and C-H bonds existed after the first-step HDO. The percentage of the aliphatic C-C bonds increased after HDO reaction, which was also in accordance with the ^{1}H-NMR result. This change indicates that there were hydrogenation reactions during the first-step HDO process, and a portion of the carbonyl C=O bonds and benzene rings were hydrogenated.

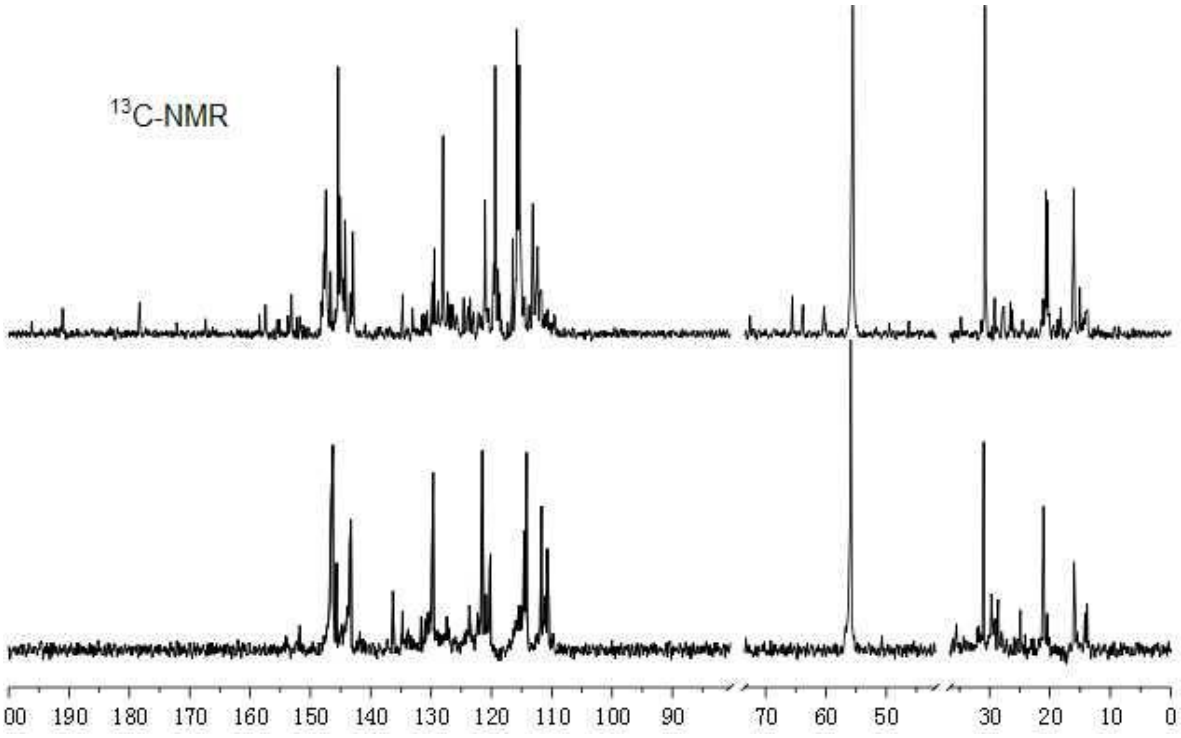

Figure 5.2 Quantitative ^{13}C-NMR for the EOL heavy oil (Top) and first-step hydrogenation product (Bottom).
Reaction condition: 15.0 mg 5 wt.% Ru/C, 150 mg heavy oil in 20 mL DI H_2O, 573 K, 10 MPa H_2, 4 hours.

Table 5.2. ^{13}C-NMR chemical shift assignment ranges and functional group contributions for the EOL heavy oil and first-step hydrogenation products.

Functionality	Range* (ppm)	EOL heavy oil	First-step HDO
Carbonyl C=O	215.0-166.5	1[#]	0
Aromatic C-O	166.5-142.0	20	20
Aromatic C-C	142.0-125.0	17	13
Aromatic C-H	125.0-95.8	40	36
Aliphatic C-O	95.8-60.8	1	1
Methoxyl	60.8-55.2	10	10
Aliphatic C-C	55.2-0.0	11	20

* The assignment ranges are on the basis of literature reports.[167, 178]
[#] The results are shown as percentage of carbon.

Reaction condition: 15.0 mg 5 wt.% Ru/C, 150 mg heavy oil in 20 mL DI H_2O, 573 K, 10 MPa H_2, 4 hours.

In order to characterize the first-step HDO products in detail, besides ^{1}H- and ^{13}C-NMR, other NMR techniques, such as DEPT-135 and ^{1}H-^{13}C HSQC-NMR, were used, and the spectra are shown in Figs. 5.3 and 5.4. ^{1}H-^{13}C HSQC-NMR spectrum of the first-step HDO products indicates that the major compounds were guaiacol, 4-methylguaiacol and catechol because the chemical shift of the signals in the HSQC spectrum was the same as the fingerprints of the two compounds. This result supports that the EOL heavy oil (M_w=265 g/mol) was decomposed to the mono-aromatic molecule after the first-step HDO reaction. The DEPT-135 NMR spectrum showed that the carbonyl C=O bonds in the EOL heavy oil were reduced after the first-step HDO reaction, which was consistent with the ^{1}H- and ^{13}C-NMR study. It was reported that Ru catalyst was capable of

converting carboxylic acid to alcohols and alkanes through the HDO reaction and cleavage of C-C bonds of carboxylic acid [179]. The experiment was also performed in aqueous phase at an elevated temperature, which supported our results. In the DEPT 135 NMR spectrum, several aliphatic CH_2 peaks (the negative peaks) showed up after the first-step HDO because of the hydrogenation of the aromatic rings. The product after first-step HDO was also characterized by GC-MS, and the major compounds are listed in Figure 5.5. The structures match well with the conclusions drawn from the NMR study. No carbonyl group was observed in the GC-MS result, and cyclohexanol was the major hydrogenated product. Over half of the predominant compounds showed a guaiacol-based structure.

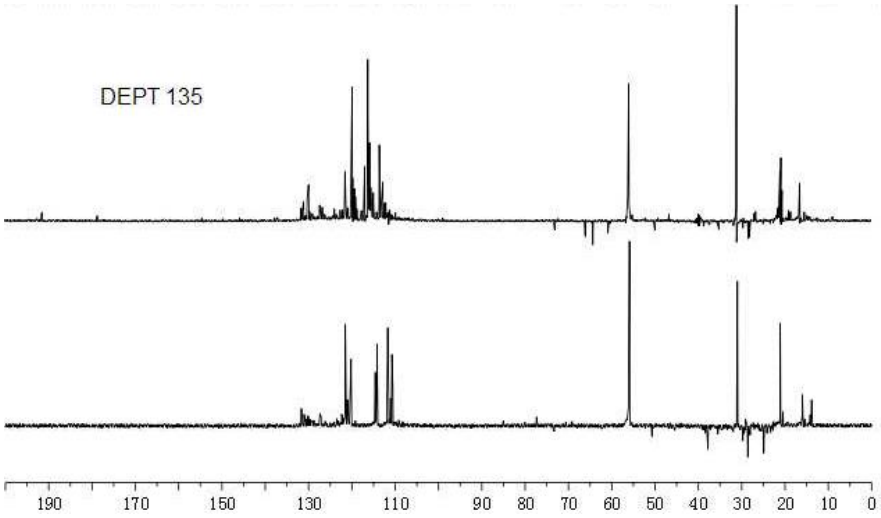

Figure 5.3 DEPT-135 NMR for the EOL heavy oil (top) and the first-step hydrogenation product. (bottom) *Reaction condition: 15.0 mg 5 wt.% Ru/C, 150 mg heavy oil in 20 mL DI H_2O, 573 K, 10 MPa H_2, 4 hours.*

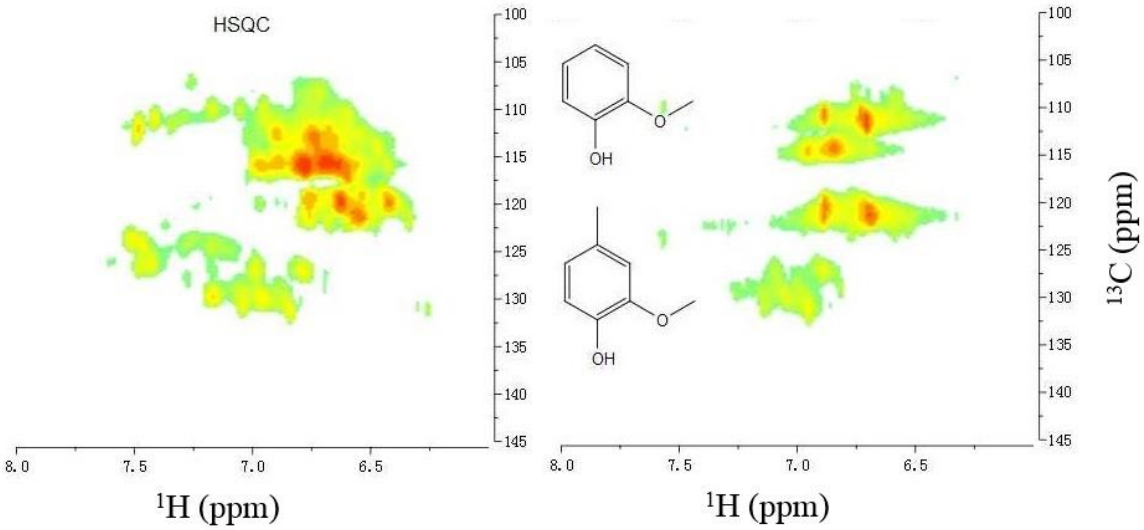

Figure 5.4 ^{1}H-^{13}C HSQC-NMR spectra for the EOL heavy oil (left) and Ru catalyzed first-step HDO product (right). *Reaction condition: 15.0 mg 5 wt.% Ru/C, 150 mg heavy oil in 20 mL DI H_2O, 573 K, 10 MPa H_2, 4 hours.*

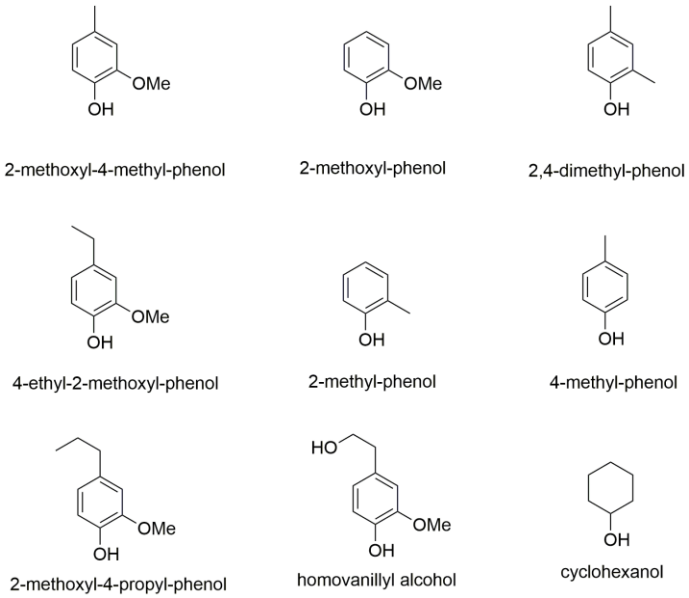

Figure 5.5 Compounds detected in GC-MS after first-step Ru catalyzed HDO. *Reaction condition: 15.0 mg 5 wt.% Ru/C, 150 mg heavy oil in 20 mL DI H_2O, 573 K, 10 MPa H_2, 4 hours.*

5.3.3 Reaction mechanism of ruthenium catalyzed lignin heavy oil upgrading

Possible pathways of the first-step Ru catalyzed heavy oil upgrading are shown in Figure 5.6. Condensation was the predominant pathway. This led to the formation of tar and coke that rapidly deactivated the catalyst. The GPC analysis showed that the EOL pyrolysis oil was degraded from dimers and trimers to monomers in the first-step HDO. This was mainly achieved by the cleavage of ether bonds and methoxyl groups in the heavy oils. The GC-MS and ^{1}H-^{13}C HSQC-NMR indicated that guaiacol and 4-methyl-guaiacol were the predominant products in the first-step HDO products. The reaction pathway in the second HDO step is discussed in Chapter 6.

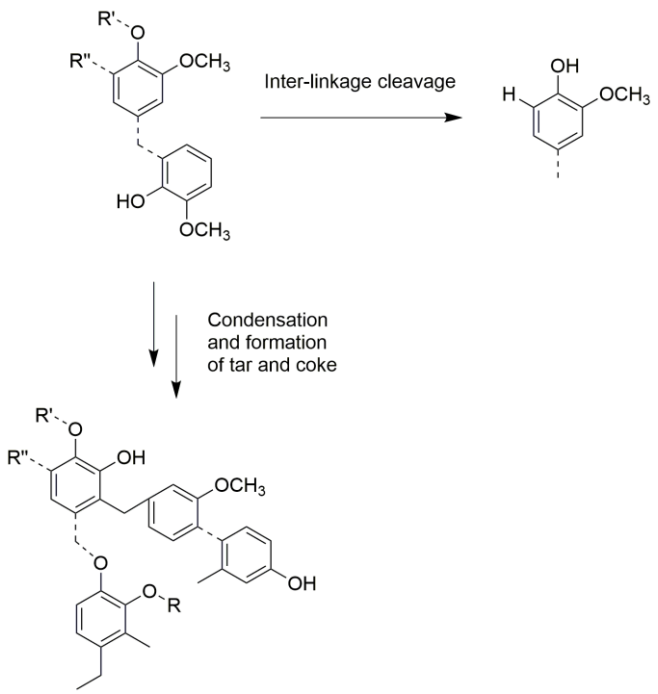

Figure 5.6 Major reaction pathway of HYD and HDO process of EOL heavy oil during first-step HDO.

5.3.4 Ruthenium catalyzed first-step deuterium HDO EOL pyrolysis heavy oil

The hydrogenation experiments using proton and deuteron were performed under the exact same process parameters. The ^{1}H-^{13}C HSQC-NMR is a two-dimensional NMR, and it can provide the distribution of C-H bonds under different chemical environments. The C-D bonds are invisible in ^{1}H-^{13}C HSQC-NMR. Therefore, the HSQC NMR peak density of the bonds in hydrogen hydrogenated products will decrease or even disappear in the spectrum. The ^{1}H-^{13}C HSQC spectra of hydrogen hydrogenated oil and deuterium hydrogenated oil are shown in Figure 5.7. There were two obvious missing peaks in the deuterium hydrogenated oil in the aromatic area. The two peaks corresponded to the ortho and para positions in a phenol/guaiacol structure, which means hydrogen atoms were mainly added in the two positions. The illustration is given in Figure 5.8.

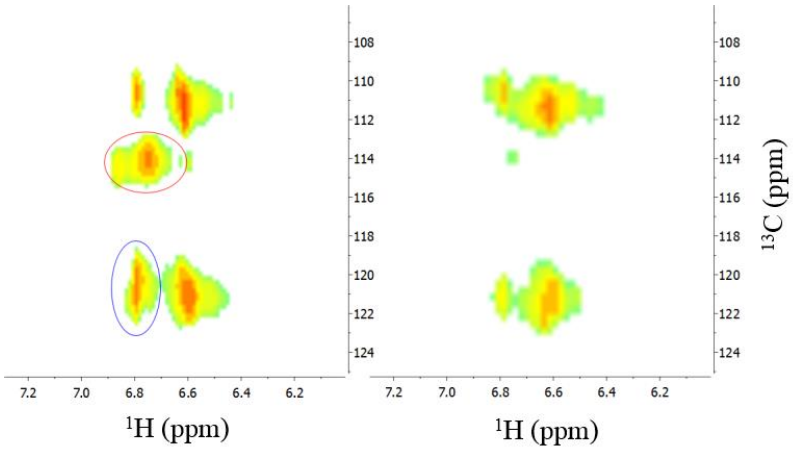

Figure 5.7 ^{1}H-^{13}C HSQC NMR for HDO products produced from H and D systems. (left to right). *Reaction condition: 15.0 mg 5 wt.% Ru/C, 150 mg heavy oil in 20 mL DI H_2O (for deuterium system used D_2O), 1.2 MPa H_2 (for deuterium system used D_2), 573 K, 4 h.*

In order to deduce the EOL heavy oil degradation in the HDO mechanism, the representative linkage within the heavy oil was desired. On the basis of quantitative ^{13}C

NMR, ^{31}P NMR, molecular weight and elemental analysis, the detailed chemical structure can be obtained [167, 169, 178, 180-184]. Table 5.3 shows the mol number of a variety of functional groups in one mol EOL pyrolysis oil.

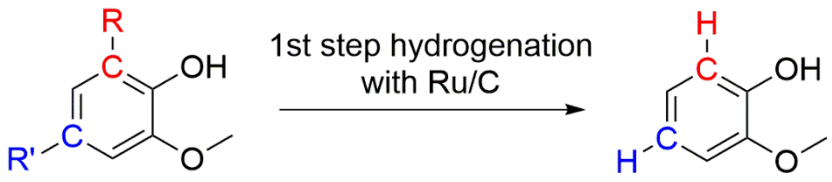

Figure 5.8 Possible decomposition position in the EOL pyrolysis oil composite structure based on ^{1}H-^{13}C HSQC-NMR results during the 1st step HDO process.

Reaction condition: 15.0 mg 5 wt.% Ru/C, 150 mg heavy oil in 20 mL DI H_2O (for deuterium system used D_2O), 1.2 MPa H_2 (for deuterium system used D_2), 573 K, 4 hours.

Table 5.3 contains a lot of information related to the chemical structure of the EOL oil. The quantitative ^{13}C NMR provided the percentage of carbon in different chemical environments. With the average molecular weight obtained from the GPC, it was calculated that the average number of the aromatic carbons in one molecule was 11.7, suggesting that the majority of the compounds has a dimer structure with two aromatic rings. The low value of the aliphatic carbon meant that the aliphatic linkage between the two aromatic monomers only contained one or two carbons. Oxygen is another possible linkage between the two aromatic monomers. Several possible molecular structures in the EOL pyrolysis oil were proposed, and these are listed in Figure 5.9. These tentative structures can represent the EOL pyrolysis oils and be used in the mechanism study. The comparison between the tentative HDO pathways shown in Figure 5.9 and the real upgraded pyrolysis oil indicated that these proposed structures were reliable in mechanism deduction.

Table 5.3 Lumped chemical structure information of whole portion EOL pyrolysis oil based on quantitative ^{13}C and ^{31}P NMR results.

Functional group (different carbons)	mol of Cs per mol pyrolysis oil based on ^{13}C NMR	Functional groups (different OHs)	mol of OHs per mol pyrolysis oil based on ^{31}P NMR
Carbonyl or Carboxyl bond	0.2	Aliphatic OH	0.1
		C_5 substituted	0.1
Aromatic C-O bond	3.1	Condensed phenolic OH	
Aromatic C-C bond	2.6	Guaiacyl phenolic OH	0.8
Aromatic C-H bond	6	Catechol type OH	0.2 (for two OHs)
Aliphatic C-O bond	0.2	*p*-hydroxy-phenyl OH	0.1
Methoxyl-Aromatic bond	1.5	Acid-OH	0.1
Aliphatic C-C bond	1.7		
Methyl – Aromatic	1		

[a] Average molecular weight and elemental analysis results for EOL pyrolysis oil have been reported in our previous work[180] and presented in supporting material.

[b] Calculated by carbon% (detected by ^{13}C NMR) * 15.3 (number of carbon based on molecular formula).

[c] For exhibition convenience all units are mol which are calculated based on weight average molecular weight.

[d] Calculated by mmol/g OH (detected by ^{31}P NMR) * 265 g/mol (average molecular weight) /1000

Reaction condition: 15.0 mg 5 wt.% Ru/C, 150 mg heavy oil in 20 mL DI H_2O (for deuterium system used D_2O), 1.2 MPa H_2 (for deuterium system used D_2), 573 K, 4 hours.

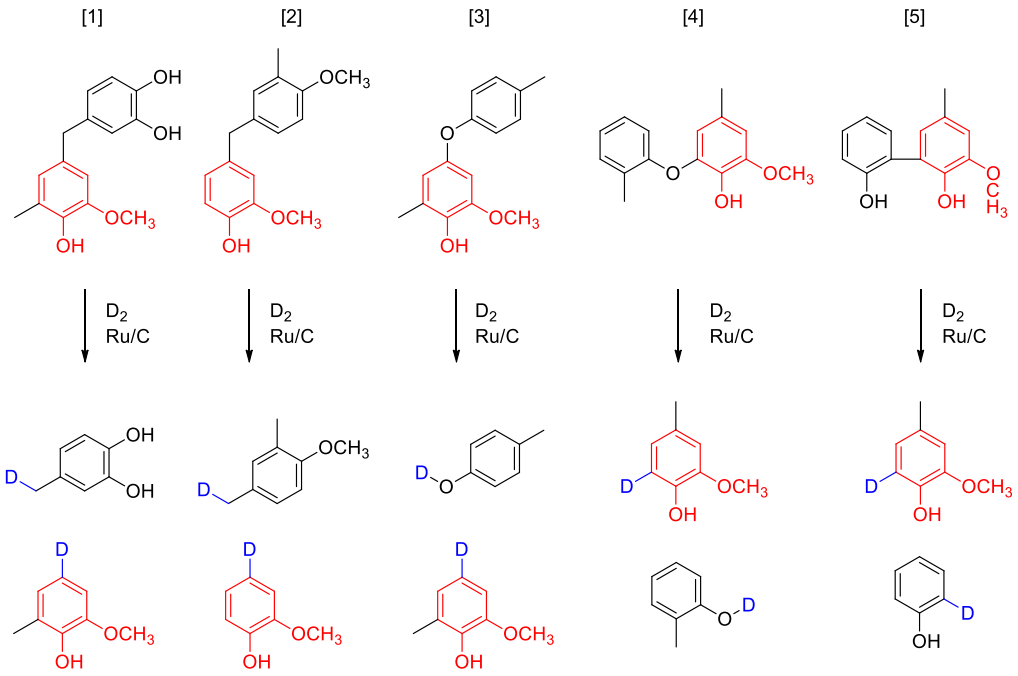

Figure 5.9 Tentative HDO pathways of major linkage of composite structures. (Used guaiacol, blue color and D atom for illumination convenience)

Reaction condition: 15.0 mg 5 wt.% Ru/C, 150 mg heavy oil in 20 mL DI H_2O (for deuterium system used D_2O), 1.2 MPa H_2 (for deuterium system used D_2), 573 K, 4 hours.

The proposed reaction pathways in Figure 5.9 were supported by the ^{1}H-^{13}C HSQC NMR spectrum that many compounds showed a guaiacol-based structure. The predominant compounds were in guaiacol-based structures, which had no functional group on the ortho-position of the phenolic-OH. The hydrogenolysis of C-O bond has been reported in previous studies [185, 186]. During the Ni catalyszed HDO of diphenyl ether, phenol and benzene are two major final products, indicating the occurrence of hydrogenolysis reaction. In another experiment, phenol was produced after the HDO of diphenyl ether, which also meant the hydrogenolysis of C-O is the major pathway. The results supported the proposed cleavage of the linkages in structure 3 and 4 in Figure 5.9.

Besides the hydrogenolysis of C-O bond, the hydrogenolysis of C-C bond was also reported during the liquefaction of lignin model compounds [187], coal [188], and HDO of model compounds [189]. During the liquefaction of lignin, the *o,o'*-biphenol was converted to single ring structure via C-C hydrogenolysis. In the study by Aubert et al., $NiO\text{-}MoO_3/\gamma\text{-}Al_2O_3$ was used to catalyze the cleavage of the aromatic dimer and the inter-linkage was methylene. The hydrogenolysis of C-C bond was observed in the reaction. The reported reaction mechanism supported the proposed cleavage of the methylene bridge in structure 1 and 2 in Figure 5.9.

The 5-5 linkage is the second most abundant inter-linkage in the lignin pyrolysis oil. The decomposition of such linkage is proposed in structure 5 in Figure 5.9. However, such kind of structure also tends to condense and form tar product. The composition of the tar product will be introduced in the next section (section 5.3.5), but there is a significant amount of aromatic structures in the tar product. Therefore, structure 5 could be a potential precursor of tar product during the first-step HDO. If some of the structures were degraded to monomers, it would be very likely to follow the reaction path 5 in Fig 5.9. The hydrogen was added to the ortho position of the guaiacyl hydroxyl group and the result was consistent with the $^{1}H\text{-}^{13}C$ HSQC NMR results.

The analysis above summarized the bond cleavage between aromatic monomers during the first-step HDO. The hydrogen atoms are most likely to be added into the ortho- and para-position of the guaiacolic hydroxyl group or phenolic hydroxyl group and produce

the aromatic C-H or phenolic –OH structure.

5.3.5 Characterization of tar product during the first-step HDO reaction

The formation of tar or coke are often observed in the hydrogenation or HDO of phenolic model compounds [190, 191] and water-soluble pyrolysis bio-oils [165, 192]. It also happened during the first-step HYD process. The M_w of the tar products was 462 g/mol, which was almost as twice much as the M_w of EOL heavy oil (265 g/mol). The quantitative ^{13}C-NMR spectrum of the tar is shown in Fig 5.10, and the result shows that much more condensed aromatic C-C bonds existed in the tar products compared to it in the EOL heavy oil. This indicated the severe condensation reactions occurring during the HDO reaction. The fresh catalyst and the spent catalyst were characterized by SEM, and the pictures are shown in Figure 5.10. After the first-step HDO, the catalyst surface became bulky so that the pores on the surface were reduced. The hydrogen gas could not penetrate the tar layer. Therefore, the reaction was stopped. Thus, only a small portion of the aromatic compounds was upgraded in the first-step HDO. The surface of catalyst looked almost intact after the second-step HDO process, which was in accordance with the high carbon yield in the reaction. Similar condensation reactions have been reported in the literature. [190, 191] The possible pathways have already been shown in Figure 5.6.

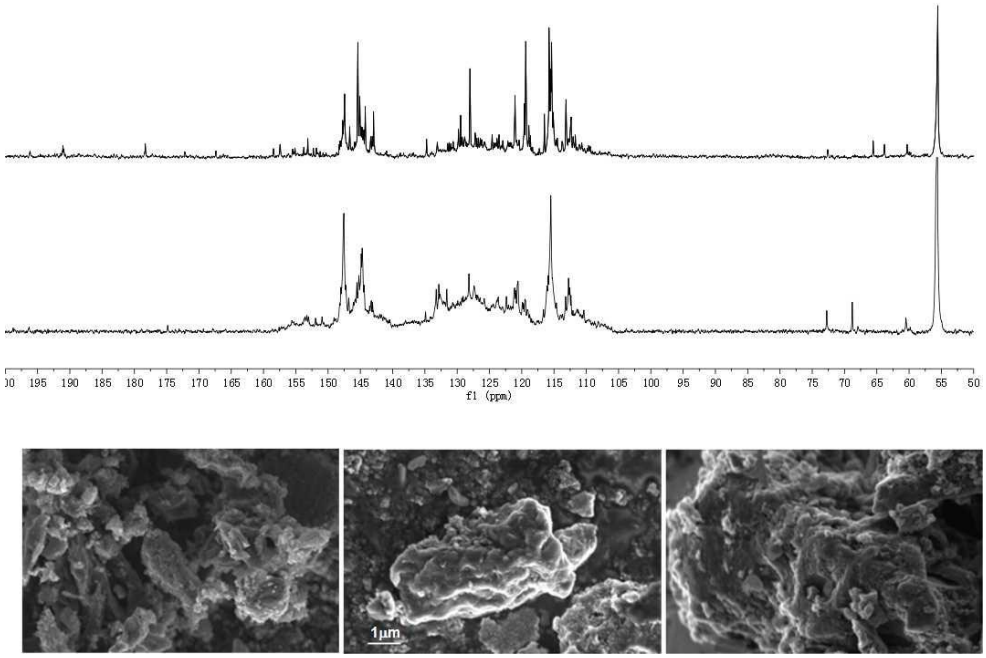

Figure 5.10 Quantitative ^{13}C-NMR for EOL heavy oil and tar from first-step HDO catalyst (from top to bottom), and SEM for the original catalyst, catalyst after first and second-step HDO process (from left to right).

Reaction condition: First-step HDO: 15.0 mg 5 wt.% Ru/C, 150 mg heavy oil in 20 mL DI H_2O, 573 K, 10 MPa H_2, 4 hours.

Second-step HDO: 10.0 mg 5 wt.% fresh Ru/C, 523 K, 10 MPa H_2, 2 hours.

5.4 Conclusion

In this chapter, the EOL pyrolysis oil was upgraded by using the Ru catalyst screened from section 4. The concept established in this work opens up a new opportunity for the conversion of lignin pyrolysis oils. The water-insoluble heavy oils were converted to water-soluble monomers with 34% carbon yield with Ru catalyst. On the contrary, Pt could not fully upgrade the EOL heavy oil.

The Ru catalyzed EOL heavy oil was studied in detail. The products obtained from first-

step HDO are monomer with aromatic structure. These compounds were produced from the cleavage of ether bonds and methoxyl groups in the heavy oils. The water insoluble heavy oils (M_w=265 g/mol) were decomposed to monomers and the carbon yield was 33 mol%. The proposed reaction mechanism agreed well with the conclusion drawn from model compound studies.

Furthermore, deuterium gas was used to reveal the insights of reaction mechanism during the first-step HDO process of pine wood EOL pyrolysis oil. The comparison between the ^{1}H-^{13}C HSQC-NMR spectra of H and D hydrogenated EOL showed which C-D bonds are formed during the HDO process. Several linkages between aromatic rings and molecular structures in the pyrolysis oil structures were proposed first and how these linkages were cleaved was deduced. In the HDO process, hydrogen atoms were mostly added to the ortho and para positions of a guaiacol or phenol and formed aromatic C-H bonds and phenolic –OH bonds.

CHAPTER 6: PRODUCTS ANALYSIS OF UPGRADED OIL AND SUPPORTING EFFECT[4]

6.1 Introduction

After the first-step HDO, the pyrolysis heavy oil is decomposed to monomers. The compounds survived from the first-step HDO (573 K) are relatively thermally stable. Although the NMR spectra look similar between the EOL pyrolysis oil and the first-step HDO product, according to the ^{1}H-^{13}C HSQC NMR and GC-MS results, the upgraded products are mainly in phenolic and guaiacolic structure, which are very close to the structure of the model compounds used in Chapter 4.

The main goal for the research was to produce gasoline-compatible fuel. Therefore, the products of first-step HDO require further hydrogenation and deoxygenation. Ruthenium is a well-known catalyst for both hydrogenation and HDO reaction. It showed excellent behavior in the model compound study. Therefore, a second-step HDO with Ru catalyst is carried out in section 6.3.1. The spent catalyst in the first-step HDO was removed and the fresh catalyst was replenished.

---

[4] Reproduced from Ben, H., Mu, W., Deng, Y., and Ragauskas, A.J., Production of renewable gasoline from aqueous phase hydrogenation of lignin pyrolysis oil. Fuel, 2013. 103(0): p. 1148-1153, with permission from Elsevier.

Besides the active noble metal, the support material was also a significant component in catalyst. The engineering of the supporting material could further improve the product quality. The modification of the supporting material was conducted, and the results are presented in section 6.3.3.

6.2 Materials and experimental procedure

The raw material used in this section is the same as it is in chapter 5. The pyrolysis reaction, first and second upgrading procedure can be found in Section 5.2.2 and 5.2.3 respectively. The solution was filtered through a 0.45 μm syringe filter. The filtrate was further upgraded by the second-step hydrogenation at 523 K for 2 hours with the initial hydrogen pressure of 10 MPa and 10.0 mg 5 wt.% Ru/activated carbon as the catalyst.

6.2.1 Characterization of the upgraded oil after second-step HDO

(1) GC-MS

The GC-MS analysis of hydrogenation products was conducted by Agilent 5975C MSD and 7890A GC with a 7693 auto sampler. The Agilent HP-5MS, 19091S-433 column was used. The GC oven was set to the following temperature regime: hold at 323 K for 5 min, ramp to 473 K at 5 K/min and hold at 473 K for 5 min.

(2) NMR (including 1H, 13C, DEPT and ^{1}H-^{13}C HSQC NMR)

The NMR sample preparation procedure and parameters used during the NMR measurement are listed in Section 5.2.6.

6.2.2 Alkali treatment of ZSM-5

The H-ZSM-5 zeolite sample was were purchased from Zeolyst, Inc (Model: CBV 8014. The Si/Al ratio is 80). Three samples were prepared for the following test. The first was the H-ZSM-5 sample as received. The second was a lightly alkali-treated H-ZSM-5 (5.0 g H-ZSM-5 into 40 mL 0.5 M NaOH solution, 343 K for 1 hour). The third was an intensively alkali-treated H-ZSM-5 (5.0 g H-ZSM-5 into 40 mL 1.0 M NaOH solution, 343 K for 1 hour). Once the reaction was finished, the zeolite particles were washed by DI water and collected by filtration. After that, the samples were dried under 373 K for 12 hours, then calcinated in the furnace under 573 K for 4 hours

6.2.3 Proton exchange of the alkali treated ZSM-5

After the treatment, the surface of the modified ZSM-5 was partially covered by the sodium ions. Therefore, the surface acidity of selected samples was regenerated via the proton exchange with 1.0 M NH_4NO_3 aqueous solution at 353 K. After the reaction, the particles were recovered by filtration, dried under 373 K for 12 hours, and calcinated at 573 K for 4 hours.

6.2.4 Impregnation of ruthenium

The Ru/modified ZSM-5 were prepared by impregnation. $RuCl_3$ aqueous solution was used as the precursor of Ru. Once the impregnation process was finished, the sample was

dried under vacuum at 323 K for 12 hours, then calcinated in air at 573 K for 4 hours. Before the reaction, the catalyst was reduced at 573 K for 2 h under hydrogen gas flow. The Ru metal loading was 5 wt.%.

6.2.5 Catalyst Characterization

The BET surface area test of the catalyst was carried out in the quadrasorb system from quantachrome instruments. About 50 mg of the catalyst was placed in a quartz cell, degassed for 24 h at 673 K. Nitrogen adsorption isotherms were measured at 77 k. Specific surface area and pore size were determined by applying BET model and BJH model to these isotherms respectively. For the spent catalyst, the catalyst particles were rinsed with 5 mL acetone first, then it was degassed and measured in the same procedure as the fresh catalyst.

NH_3 temperature programmed desorption (TPD) was measured using Micromeritics AutoChem 2920 II. In a typical run, approximately 50 mg of the sample was placed in the tube reactor. Both ends of the tube were connected to the instrument. After drying at 473 K in flowing He for 1 hour, the sample was cooled down to room temperature. The 0.2 vol % NH_3/He was introduced into the tube for 2 hours. After that, Helium gas was introduced again for 1 hour to remove the physically adsorbed NH_3. The temperature was ramped from room temperature to 1073 K at a rate of 10 K min-1. The quantity of NH_3 desorbed was monitored by a thermal conductivity detector (TCD).

6.2.6 Catalytic HDO of guaiacol by using 5% Ru/ modified ZSM-5

HDO of both model compounds was carried out in a 75.0 mL Parr 4590 Micro Stirred Reactor. One step HDO was used for model compounds study. In a typical run, 200 mg guaiacol and 20 mL DI water were loaded in a glass liner with 40 mg 5 wt.% Ru/modified ZSM-5. A gas entrainment impeller was used in this experiment to enhance the mass transfer. The reactor was then purged 5 times with nitrogen gas to remove the air in the reaction vessel followed by another 5 times purge with hydrogen to replace nitrogen. The initial hydrogen pressure was one atmosphere. When the temperature reached the target, it was pressurized with hydrogen to 4.0 MPa. The reaction was conducted under 523 K for 2 hours.

6.3 Results and Discussion

6.3.1 Characterization of the products from second-step HDO

Figure 6.1 is the ^{1}H NMR spectra of the EOL heavy oil, as well as the first- and second-step HDO products. The numerical integration results are presented in Table 6.1. The data indicated no aromatic carbon remained after the second-step HDO, which was consistent with the ^{1}H-NMR result in Table 5.1. In the products of the second-step HDO, there were fewer methoxyl groups and much more aliphatic C-O bonds compared with the products of first-step HDO due to the hydrogenated aromatic ring that transformed the original aromatic C-O bond to aliphatic C-O bond. After the two-step reaction, 85% of the protons were aliphatic protons with no oxygen atoms bonded to the α-carbon.

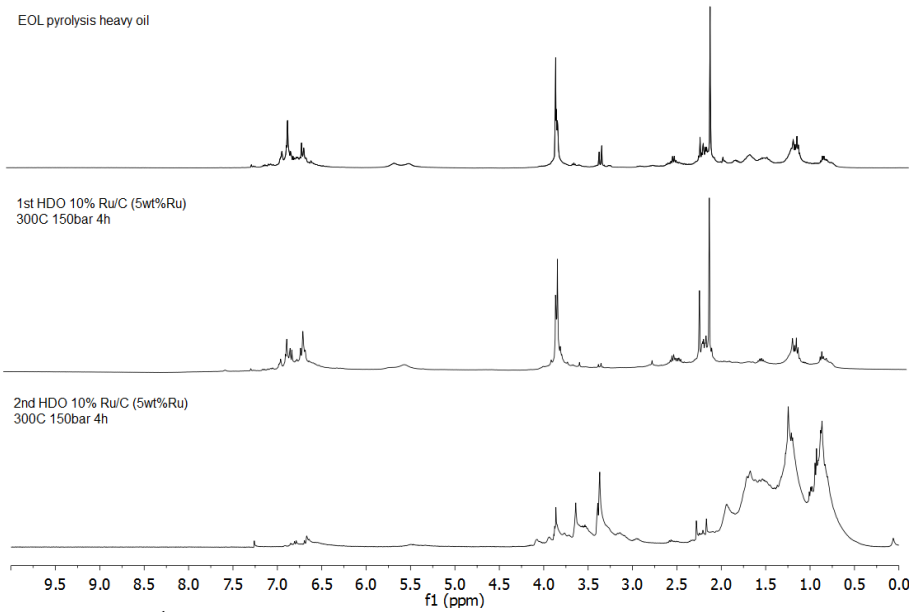

Figure 6.1 ^{1}H-NMR spectra for the Ru catalyzed EOL heavy oil, first and second-step HDO products. (from top to bottom)
Reaction condition: First-step HDO: 15.0 mg 5 wt.% Ru/C, 150 mg heavy oil in 20 mL DI H_2O, 573 K, 10 MPa H_2, 4 hours. Second-step HDO: 10.0 mg 5 wt.% fresh Ru/C, 523 K, 10 MPa H_2, 2 hours.

Table 6.1. ^{13}C-NMR chemical shift assignment ranges and functional group contributions for the second-step Ru/C catalyzed hydrogenation products.

Functionality	Range* (ppm)	EOL heavy oil	First-step HDO	Second-step HDO
Carbonyl C=O	215.0-166.5	1[#]	0	0
Aromatic C-O	166.5-142.0	20	20	0
Aromatic C-C	142.0-125.0	17	13	0
Aromatic C-H	125.0-95.8	40	36	0
Aliphatic C-O	95.8-60.8	1	1	24
Methoxyl	60.8-55.2	10	10	7
Aliphatic C-C	55.2-0.0	11	20	69

Reaction condition: First-step HDO: 15.0 mg 5 wt.% Ru/C, 150 mg heavy oil in 20 mL DI H_2O, 573 K, 10 MPa H_2, 4 hours. Second-step HDO: 10.0 mg 5 wt.% fresh Ru/C, 523 K, 10 MPa H_2, 2 hours.

In Figure 6.2, the two peaks around 10 - 15 ppm were attributed to the terminal carbon of aliphatic chains. After the second-step HDO, the aliphatic C-O bonds (from 60.8 - 95.8 ppm) contained tertiary carbons, which was produced by the hydrogenation of phenols. The carbon in the C-O bond was also represented as the α-carbon in the alcohols. The chemical shift around 30 – 40 ppm represented the secondary carbons and a significant number of peaks appeared after the second-step HDO. The carbon yield of second-step HDO was approximately 95 wt.%, which was similar to the HDO of phenolic pyrolysis oil model compounds reported in literature. [163, 164]

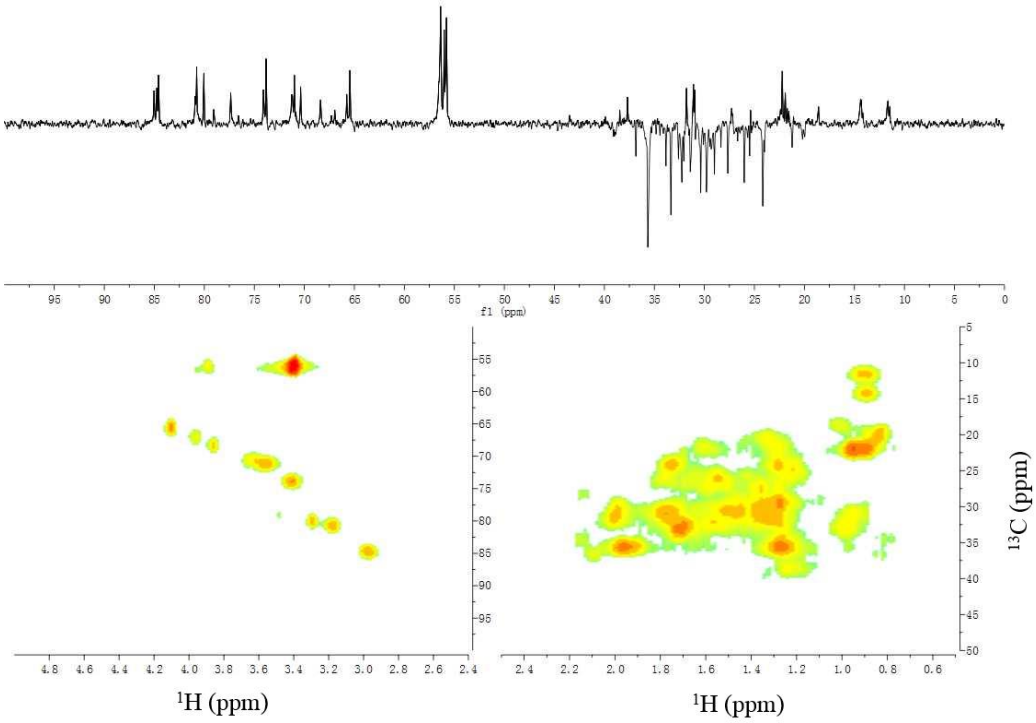

Figure 6.2 DEPT-135 and ^{1}H-^{13}C HSQC-NMR spectra for the second-step Ru/C catalyzed hydrogenation products.
Reaction condition: 10.0 mg 5 wt.% fresh Ru/C, filtrate from the first-step HDO, 523 K, 10 MPa H_2, 2 hours.

The chemical structures of the compounds after two-step HDO were identified by GC-MS. The results are summarized in Figure 6.3, and they further supported the conclusion of the NMR study. Most of the peaks in the ^{1}H-^{13}C HSQC-NMR were attributed to cyclohexanol and its derivatives. Comparing the compounds listed in Figure 5.5, which are the chemical structures after the first-step HDO, the two predominant reactions were hydrogenation and demethoxylation. This conclusion supports that the model compounds study very well.

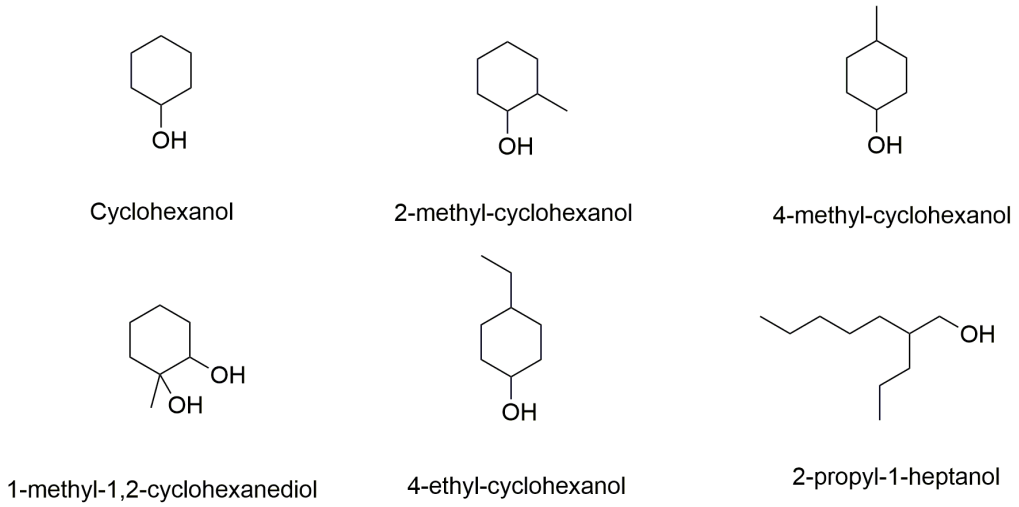

Figure 6.3. Compounds detected in GC-MS after two-step Ru catalyzed HDO.

6.3.2 Reaction mechanism of second-step HDO

The tentative reaction pathway in the second HDO step is shown in Fig 6.4 and was similar to the reaction mechanism for the model compounds. Ru catalyzed either direct hydrogenation or demethoxylation reaction, in which both reactions yielded cyclohexanol

as the final product. Both GC-MS and NMR indicated that the major compounds in the upgraded oil were cyclohexanol and 4-methyl-cyclohexanol.

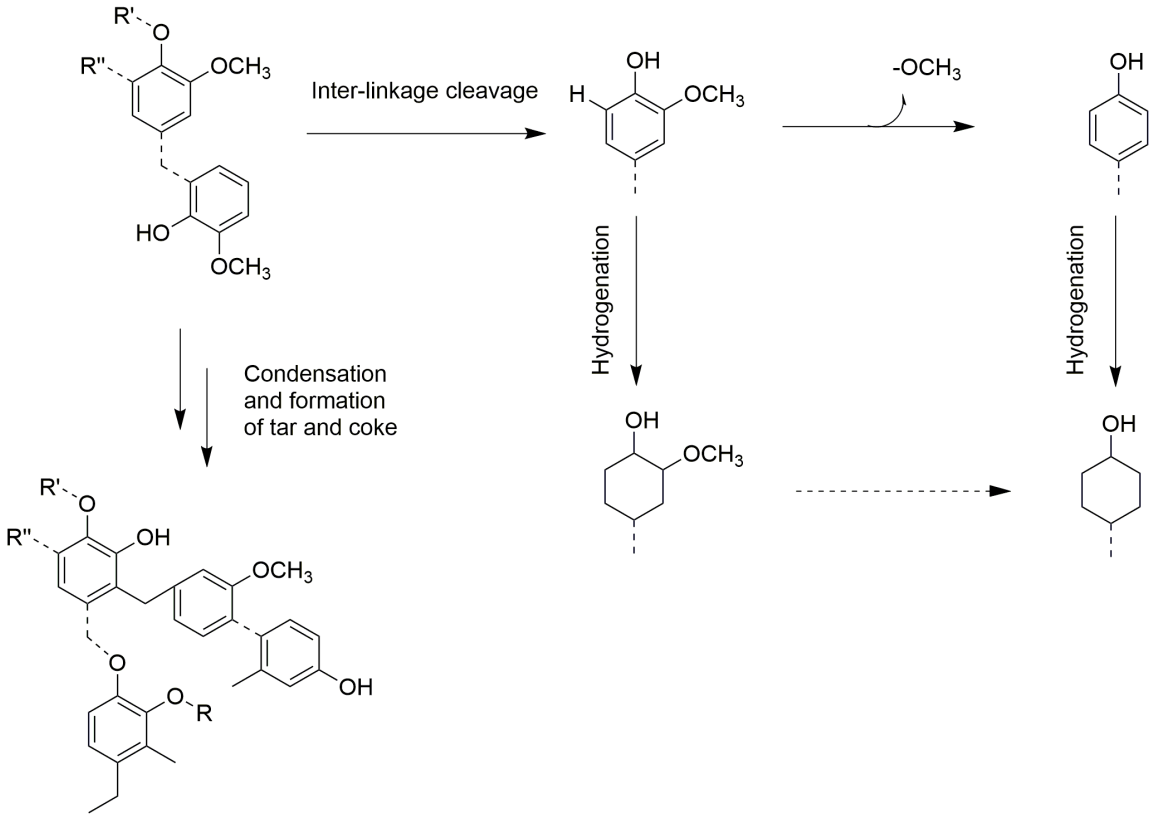

Figure 6.4 Tentative reaction pathways of HDO process of EOL heavy oil in the first-step HDO [179, 190, 191, 193, 194].

6.3.3 Alkali treatment of the ZSM-5 zeolite

After the two-step HDO, there were still hydroxyl groups remaining in the molecules, mainly in cyclohexanol molecule. Removal of the hydroxyl group could improve the miscibility of the bio-oil in gasoline fuel and further enhance the thermal stability of the fuel product.

Acid catalyzed dehydration reaction is a common method for hydroxyl group removal. It is mainly catalyzed by the Brønsted acid site [195]. Mineral acids, some metal oxides and zeolites all contain the Brønsted acid site [196]. In my study, ZSM-5 was used because of its superior hydrothermal stability [197].

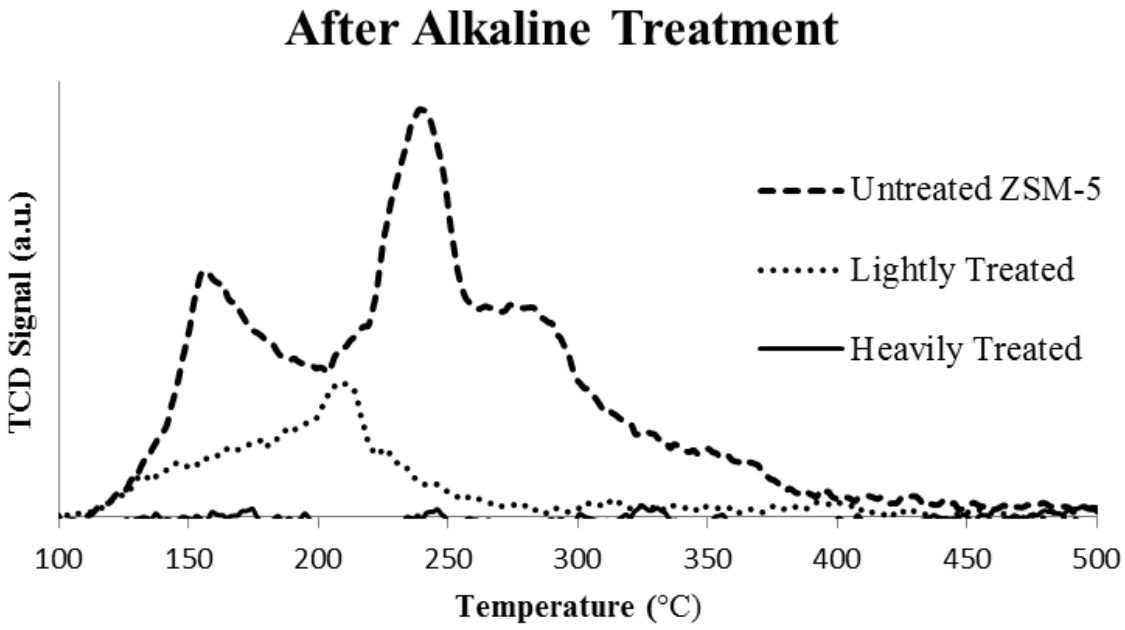

Figure 6.5 NH_3 TPD results of the alkali treated ZSM-5.
Reaction condition: 5.0 g HZSM-5 stirred in 0.5 M NaOH (for heavily treatement 1.0 M NaOH) at 343 K for 1 hour, followed by drying at 373 K for 12 hours and calcinating under 573 K for 4 hours.

The major reason for alkali treatment is to enlarge the pore opening of ZSM-5. The alkali molecules preferentially attack siliceous species in the zeolite and as a result, the pore is enlarged [198]. However, one disadvantage of this process is that it will reduce the number of Brønsted acid sites on the zeolite surface. The protons are exchanged by the sodium ion, which greatly reduced the surface acidity. The alkali-treated samples were characterized by NH_3 TPD and the results are shown in Figure 6.5. It is clear that the

more intensive treatment led to less surface acidity. For the heavily treated sample, there was almost no proton on the zeolite surface.

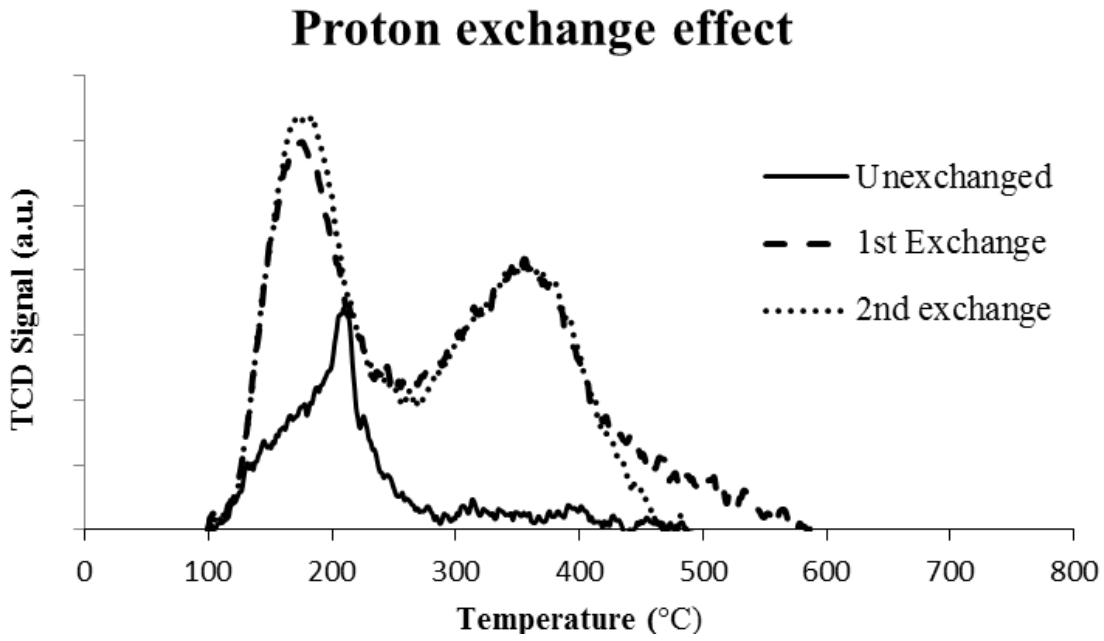

Figure 6.6 Surface acidity of the alkali treated ZSM-5 after the proton exchange. *Reaction condition: 5.0 g HZSM-5 stirred in 0.5 M NaOH (for heavily treatement 1.0 M NaOH) at 343 K for 1 hour, followed by drying at 373 K for 12 hours and calcinating under 573 K for 4 hours.*

The common way to regenerate the surface acidity is the proton exchange. The ammonium ion solution is commonly used for this process. The NH_4^+ group would substitute the sodium ion on the surface of the zeolite. The ammonium exchange was followed by calcination at 573 K. When calcinated at 723 K, the NH_4^+ was decomposed to NH_3 and proton. In this way, the surface acidity was regenerated. The NH_3 TPD result is plotted in Figure 6.6.

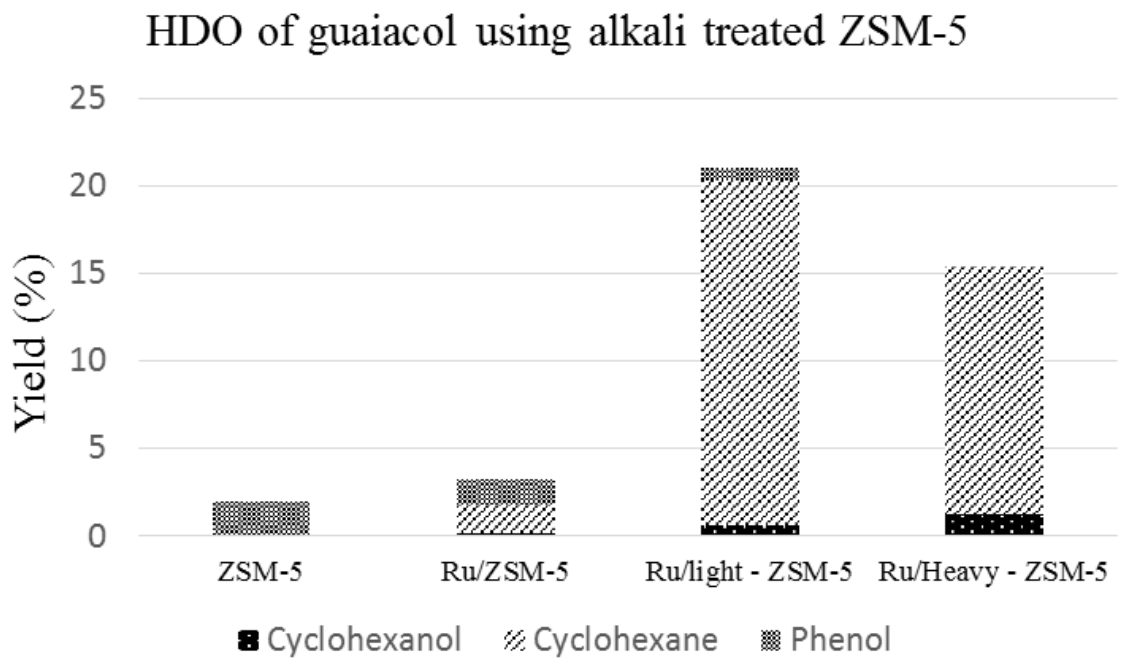

Figure 6.7 Ru/ modified ZSM-5 catalyzed HDO of guaiacol model compound
Reaction condition: 40.0 mg catalyst, 200 mg guaiacol in 20 mL DI H_2O, 523 K, 4.0 MPa H_2, 2 hours.

The untreated ZSM-5 zeolite and alkali-treated zeolite were used in the catalytic HDO of guaiacol, and the experimental results are shown in Fig 6.7. No conversion of guaiacol was observed without catalyst. In this case, the light-ZSM 5 and heavy ZSM-5 were all exchanged twice with proton, followed by ruthenium impregnation. The untreated ZSM-5 only catalyzed the hydrogenolysis reaction, and phenol was the only product. No hydrogenated product was observed. The ruthenium impregnation on the untreated ZSM-5 led to a small portion of hydrogenated products. The yield was approximately 2%. It was probably due to the low dispersion of the noble metal and small pore opening of zeolite support. However, after the alkali treatment, the conversion was greatly increased. The yield of the cyclohexane was over 15%, and almost no phenol was produced. The selectivity toward cyclohexane was 94%. The intense treatment reduced the total acid

sites [198]. Therefore, the yield was slightly lower than that of the less intensively treated catalyst. A small amount of cyclohexanol was detected in the product solution. The selectivity was retained as high as 92%.

The leaching of the active metal and non-framework elements in zeolite can induce catalyst deactivation. The mesoporous structured zeolite is more unstable and the pore tends to collapse during the reaction. [198] Therefore, a hydrothermally stable mesoporous structured ZSM-5 zeolite would be the ideal support for this application.

6.4 Conclusion

This section discussed the second-step HDO reaction of EOL heavy oil. Two support materials, activated carbon and HZSM-5, were used to catalyze the upgrading reaction. The Ru/C catalyst converted water-insoluble heavy oils to water-soluble monomers with a 34% carbon yield. The structure proposed for the NMR study matched well against the results from the GC-MS characterization. The proposed reaction mechanism agrees well with the conclusion drawn from model compound studies.

However, after the two-step upgrading, the bio-oil still contained a small portion of the hydroxyl group, which may cause solubility and stability problems when it is mixed with the gasoline fuel. Therefore, ZSM-5 was adopted as the supporting material. The experiment result showed that the modified ZSM-5 was effective in hydrogenation and hydroxyl group removal. The selectivity toward cyclohexane was over 90%. It can be

used in the second-step HDO directly instead of Ru/C. The further optimization of the zeolite is proposed in the recommendations for future work.

CHAPTER 7: RU CATALYZED AQUEOUS PHASE HDO OF BIOMASS DERIVED PYROLYSIS LIGHT OIL[5]

7.1 Introduction

As proved in chapter 3, 4 and 5, Ru/C is an effective catalyst for pyrolysis oil derived lignin. In some applications, the whole biomass might be used as starting material instead of lignin. Therefore, the reaction mechanism of catalytic HDO reaction with cellulose and hemicellulose are also valuable. Two most commonly used processes are fast and slow pyrolysis. The key difference between the two methods are heating rates, which are roughly 1273 K/s for fast pyrolysis and 0.1 - 3 K/s for slow pyrolysis. [199, 200] Both processes have been extensively studied and reviewed [10, 73, 201-203]. Fast pyrolysis produces liquid products in one phase. The liquid products from slow pyrolysis are separated into the aqueous phase (light oil) and the organic phase (heavy oil). [204] The yield of heavy oil increased by using fast pyrolysis process compare to slow pyrolysis. However, the molecular weight and the content of polyaromatic hydrocarbons also increased in the fast pyrolysis oil, which could detrimentally affect the following upgrading process. [205] Besides heating rates, pyrolysis temperature and pressure also affect the liquid product yields. The increase of pyrolysis temperature produces more

---

[5] Reprinted with permission from Mu, W., Ben, H., Newalkar, G., Ragauskas, A., Qiu, D., and Deng, Y., Structure Analysis of Pine Bark-, Residue-, and Stem-Derived Light Oil and Its Hydrodeoxygenation Products. Industrial & Engineering Chemistry Research, 2014. 53(28): p. 11269-11275. Copyright 2014 American Chemical Society

liquid and gaseous products. [69] The increase of pyrolysis pressure leads to a higher char yield. [206] However, the carrier gas flow rate has limited effect. [33] Bio-oil obtained from slow pyrolysis generally contains less oxygen than that obtained from fast pyrolysis due to secondary reactions such as dehydration, decarboxylation, and condensation involved in slow pyrolysis. [207] Lower oxygen content is desirable for the subsequent upgrading process, which will be introduced later.

As mentioned before, the major liquid products from slow pyrolysis are heavy oil and light oil. Briefly speaking, the organic compounds contained in heavy oil have higher boiling points than those in light oil. The molecular weight of heavy oil is about 300 - 1300 Da with high viscosity. Most of the compounds in heavy oil are water-insoluble. The typical yield of heavy oil is roughly 25 - 35%. [204] The molecular structures in heavy oil are very complicated, including levoglucosan, catechol-, guaiacol- phenol-based aromatic compounds etc. Extensive studies have been done on the post-treatment of the heavy oils derived either from whole biomass [142, 208, 209] or solely derived from lignin. [201, 210, 211] However, less attention has been given to the post-treatment of light oil. The yield of light oil from pyrolysis is around 15 - 35%. [204] Although a large amount of water presents in light oil (~40-80 w/w%), the overall weight of the organic compounds in light oil is still over 1/3 the weight of heavy oil. Therefore, the portion of light oil is not negligible in the slow pyrolysis process. The properties of heavy oil and light oil are significantly different. Thus, a comprehensive study of the compositions and reaction paths of both heavy oil and light oil during the upgrading process can provide a better understanding in a bio-refinery plant design.

Light oil contains mainly water-soluble organic molecules. It is known that the water-soluble products from pyrolysis include levoglucosan, acetic acid, formic acid, furfural and some aromatic-structured compounds. [212] Compared to heavy oil, light oil contains more oxygen functionalities which results in a low energy density. [213] Light oil also contains more carboxyl groups, which leads to a lower pH and can potentially cause equipment corrosion. [73] The higher amount of oxygen in the light oil causes problem such as: increase in instability, storage difficulty, [182] and immiscibility with traditional fossil fuels. [10]

The most common bio-oil upgrading methods were recently reviewed by Mortensen et al. [142] Hydrodeoxygenation (HDO) is a general routine used for upgrading. High pressure hydrogen and catalyst are required for the reaction. During the process, the unsaturated bonds are hydrogenated and the oxygen atoms are removed as water, carbon monoxide, carbon dioxide and other small compounds. [114] Related papers [142, 201, 209-211] indicate that high stability and high quality biofuel could be produced from HDO reaction. However, all these publications use either bio-oil or heavy oil as the starting material. No research has been published for light oil post-treatment. Our previous study showed that Ru is excellent in catalyzing the HDO reaction of the heavy oil from lignin pyrolysis and the products was successfully upgraded to gasoline range chemicals. [210] Among noble metals, the cost of ruthenium is relatively low. The weight-based cost of ruthenium is approximately 1/10 compared with palladium and rhodium, and 1/16 the

platinum and gold. It has shown superior performance compared to other noble metal catalysts in bio-oil upgrading. [214]

In this study, pyrolysis oils derived from loblolly pine stem, residue and bark were used as starting material. Loblolly pine grows fast and is predominantly used to produce high quality wood fibers in the United States. However, large amount of residues (non-merchantable part of the tree, such as stumps, bark and stem, limbs, tops, dead trees) are produced in the pulp production process. The quantity of these residues represents about 20% of potential biomass nationally [215]. The chemical compositions of all three components are remarkably different. For example, the lignin and tannin contents in the bark are much higher than it is in the other parts of trees. The varied chemical compositions of these feedstock make the reactions in pyrolysis/upgrading process and the distribution of final products very different. Therefore, this paper focuses on: 1) examining the chemical composition of light oil derived from pine wood stem, residue and bark; and 2) studying the major reactions involved in the light oil upgrading process.

7.2 Materials and experimental procedure

All reagents used in this study were purchased from VWR International and used as received. All the biomass materials used in the study were collected from a University of Georgia plantation research plot in Macon, GA. More detailed information about the biomass and pre-treatment procedures has been described in previous publication [216]. The stem wood was debarked and chipped from raw wood. The residue and bark were

obtained from several trees collected adjacent to stem wood. These trees have no significant difference in their component. All three biomasses were milled and passed through a Wiley mill and passed through a 2 mm screen as per the TAPPI method T257cm-02.

6.2.1. Equipment and procedure for pyrolysis.

Pyrolysis was done in a tube furnace employing a quartz tube. In a typical experiment, dried biomass (4.00 g) was placed in a quartz sample boat and the boat was placed in the center of the pyrolysis tube. The heating rate of the biomass sample powder was measured using a K-type thermocouple which was immersed in biomass bed during pyrolysis. The quartz tube was flushed with nitrogen at 500 mL/min. The tube was then inserted into the preheated furnace. The heating rate was about 2.7 K/s and the target temperature was 873 K. The light oil was collected from two condensers connected to the outlet of the pyrolysis tube. Both condensers were immersed in liquid nitrogen. Based on the heating rate, the pyrolysis samples reached the target temperature in 5 min. No vapor was observed after 10 min. Upon the completion of pyrolysis, the liquids in both condensers were collected and stored in freezer for analysis and upgrading.

6.2.2. HDO upgrading of light oil or levoglucosan as model compound.

Hydrogenation of the light oil (or levoglucosan) was carried out in a 75 mL Parr batch reactor. About 200 mg of light oil (or levoglucosan) was added to 20 mL DI water. 1.00

mL solution was withdrawn for total organic carbon test. The remaining solution was loaded in the reactor with 4.0 mg of 5 wt.% Ru/C (dry basis, from Alfa Aesar). The reactor was sealed and purged with nitrogen for 5 times to remove the residual air. The pressure in the reactor was reduced to normal atmosphere and then purged with hydrogen for 3 times to replace nitrogen. The target hydrogen pressure was 8 MPa at room temperature. The reactor was then heated up to 573 K at a heating rate of about 23 K/min. The pressure during the reaction was held at 110 MPa. After 2 hours, the vessel was quenched using cool water and the temperature reduced to 323 K within 1 min. The reactor was opened when the temperature was below 303 K and the solution was filtrated using a 0.2 μm syringe filter. 1.00 mL solution was withdrawn for total organic carbon test. The remaining solution (18 mL) solution was separated into two parts with equal volumes. One part was extracted with 2.00 mL chloroform for GC-MS analysis. Another part was extracted with 2 mL deuterium chloroform for ^{1}H NMR test.

6.2.3. Characterization of pyrolysis oil and upgraded products by NMR (Quantitative 1H NMR, 13C NMR and ^{1}H-^{13}C HSQC-NMR).

All NMR spectral data reported in this study was recorded using a Bruker Avance/DMX 400 MHz NMR spectrometer. Light oil (100 mg) from each component was dissolved in 450 μL DMSO-d_6 for analysis. Quantitative ^{13}C NMR was acquired by employing an inverse gated decoupling pulse sequence, 90 ºpulse angle, a pulse delay of 5 s and 6000 scans. Quantitative ^{1}H NMR was acquired with 16 transients and 1s pulse delay. The ^{1}H-^{13}C HSQC-NMR employed a standard Bruker pulse sequence “hsqcetgpsi.2” (90˚ pulse,

0.11 s acquisition time, 1.5 s pulse day, $^{1}J_{C-H}$ of 145Hz). The scan number was 48 and the acquisition of data points were 1024 for ^{1}H and 256 increments for ^{13}C. The spectral widths are 13.02 ppm for ^{1}H and 220.00 ppm for ^{13}C. HSQC-NMR data was processed using MestReNova v7.1.0 under default template and automatic phase and baseline correction.

6.2.4. Aqueous phase product processing

(1) Total Organic Carbon:

The carbon contents of the liquid solution collected before and after the reaction were measured by Ionics Inc. 1555B total organic carbon (TOC) analyzer. The carrier gas used was air (ultra zero grade) from AirGas and the flow rate was set to 100 mL/min. All samples were diluted to achieve a carbon concentration below 200 ppm. The volume of each injection was 100 μm^3. The temperature set point was 1173 K and the catalyst was CuO. The calibration curve was based on isopropanol.

(2) Gas Chromatography-Mass Spectroscopy:

The GC-MS analysis of hydrogenation products was run on a Micromass AutoSpec mass spectrometer. The GC was an Agilent 6890 and the column was an Agilent DB-5MS. The GC oven was programmed with the following temperature regime: held at 303 K for 1 min, ramp to 573 K at 15 K/min and held at 573 K for 6 min. 1 μL of the sample was injected in splitless mode to inject the analyte into the column.

7.3 Results and discussion

7.3.1 Chemical composition of light oil using GC-MS.

The light oil yield from pyrolysis was calculated on the basis of the weight of starting biomass. The yields follow the order: stem 44% > residue 38% > bark 20%. These differences are attributed to different amounts of lignin and holocellulose in each starting material. Biomass with more holocellulose generates more light oil. The holocellulose contents in the stem, residue, bark are 69%, 65%, bark 51%, respectively. On the contrary, the presence of lignin reduces the yield of light oil. The lignin contents in the stem, residue, bark are 28%, 27% and 34%, respectively.[216].

The major compounds in bio-oil from wood pyrolysis have been reviewed by Wang et al.[217]. Except for levoglucosan, which has a boiling point of 657 K, most other water-soluble compounds in light oil are detectable by GC-MS. On the basis of the peak area integration of GC-MS spectra, the ten most abundant compounds in light oil are ranked from high to low in the Table 7.1. Because levoglucosan has a high boiling temperature, it could not fully vaporize under the temperature used in GC-MS measurement. As a result, the signal of levoglucosan is very weak in the GC-MS spectra. Furanic compounds are the major constituents in the light oil derived from stem pyrolysis. In the ten most abundant compounds from stem pyrolysis, there are four with a furanic structure. Only two furan-structured compounds are observed in the bark-derived light oil, and none is found in the residue-derived light oil. The furan-structured chemicals in the stem were found mainly because of the high amount of xylan and cellulose in the stem [216, 218].

Table 7.1 Ten most abundant compounds in light oil from GC-MS study. (Highest at top and lowest at bottom) The number next to the compounds is the peak intensity in the GC-MS spectrum. 4-methyl-guaiacol is used as standard (100.0 peak intensity) for comparison.

Light Oil from Stem		Light Oil from Residue		Light Oil from Bark	
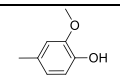	100.0	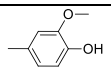	100.0	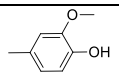	100.0
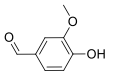	71.6	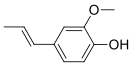	90.1		55.8
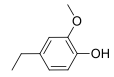	51.8	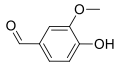	67.8	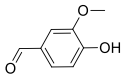	42.7
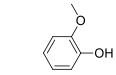	47.1	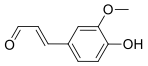	62.5	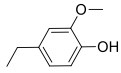	39.9
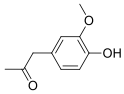	43.6	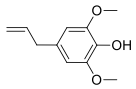	58.4		29.2
	40.8		56.2		28.1
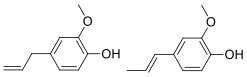	29.3	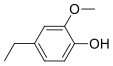	55.7	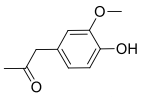	26.5
	27.5	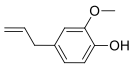	52.8	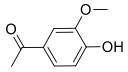	26.0
	20.4	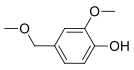	51.4	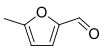	20.3
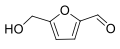	18.5	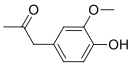	49.3	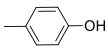	18.6

Reaction condition: 4.0 mg 5 wt.% Ru/C, 200.0 mg light oil in 20 mL DI H_2O, 573 K, 8.0 MPa H_2, 2 hours.

7.3.2 Light Oil Structural Analysis Using Quantitative ^{1}H, ^{13}C and ^{1}H-^{13}C HSQC NMR.

The ^{13}C NMR spectra of these biomass feedstock was published elsewhere.[216] The ^{1}H NMR and ^{13}C NMR spectra for all three components are included in Figure 7.2. The peak areas of the spectra are integrated and listed in Table 7.2 and 7.3. Over 60% of the protons are -CH_n-O- protons in the ^{1}H NMR spectrum. Figure 7.1 is the CH_n-O region of the ^{1}H-^{13}C HSQC-NMR spectrum. The chemical shifts of levoglucosan are marked on the spectra. Obviously the light oil from the stem has the most intense peak area because of the abundant cellulose in the stem. The peaks of residue and bark derived oil are not as strong as those in the stem's spectrum. All three spectra clearly show the existence of levoglucosan. With the information obtained from GC-MS and NMR, levoglucosan is found to be the predominant compound in the -CH_n-O- region.

As shown in Table 7.2, the aromatic region of bark-derived light oil is twice that of light oils derived from stem and residue because the bark contains much more lignin and tannin and less holocellulose compared with residue and stem. For the same reason, the aliphatic proton area in the bark's NMR spectrum is less than half the area of the aliphatic region in the spectra of light oils derived from residue and stem. The -CH_x-O- regions of the spectra from all three components are very close to each other. It is mainly contributed by levoglucosan. Bark-derived light oil has a relatively higher value in the -CH_x-O- region because aromatic compounds in lignin and tannin tend to form condensed structures [204]. The char produced from lignin and tannin pyrolysis is 50 wt.% more than that from the residue.

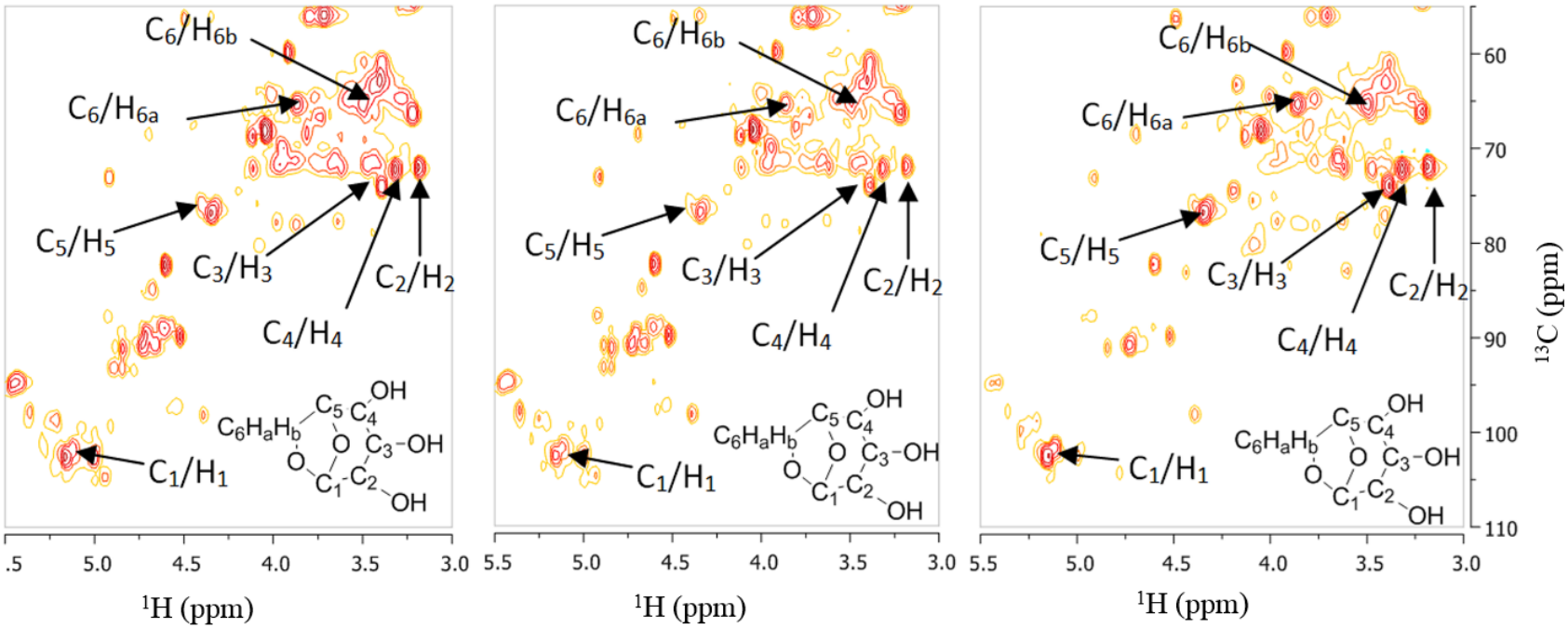

Figure 7.1 ^{1}H-^{13}C HSQC-NMR spectra in aliphatic ranges and the assignment of levoglucosan in the light oil derived from stem, residue and bark (ordered from left to right)

Reaction condition: 4.0 mg 5 wt.% Ru/C, 200.0 mg light oil in 20 mL DI H_2O, 573 K, 8.0 MPa H_2, 2 hours.

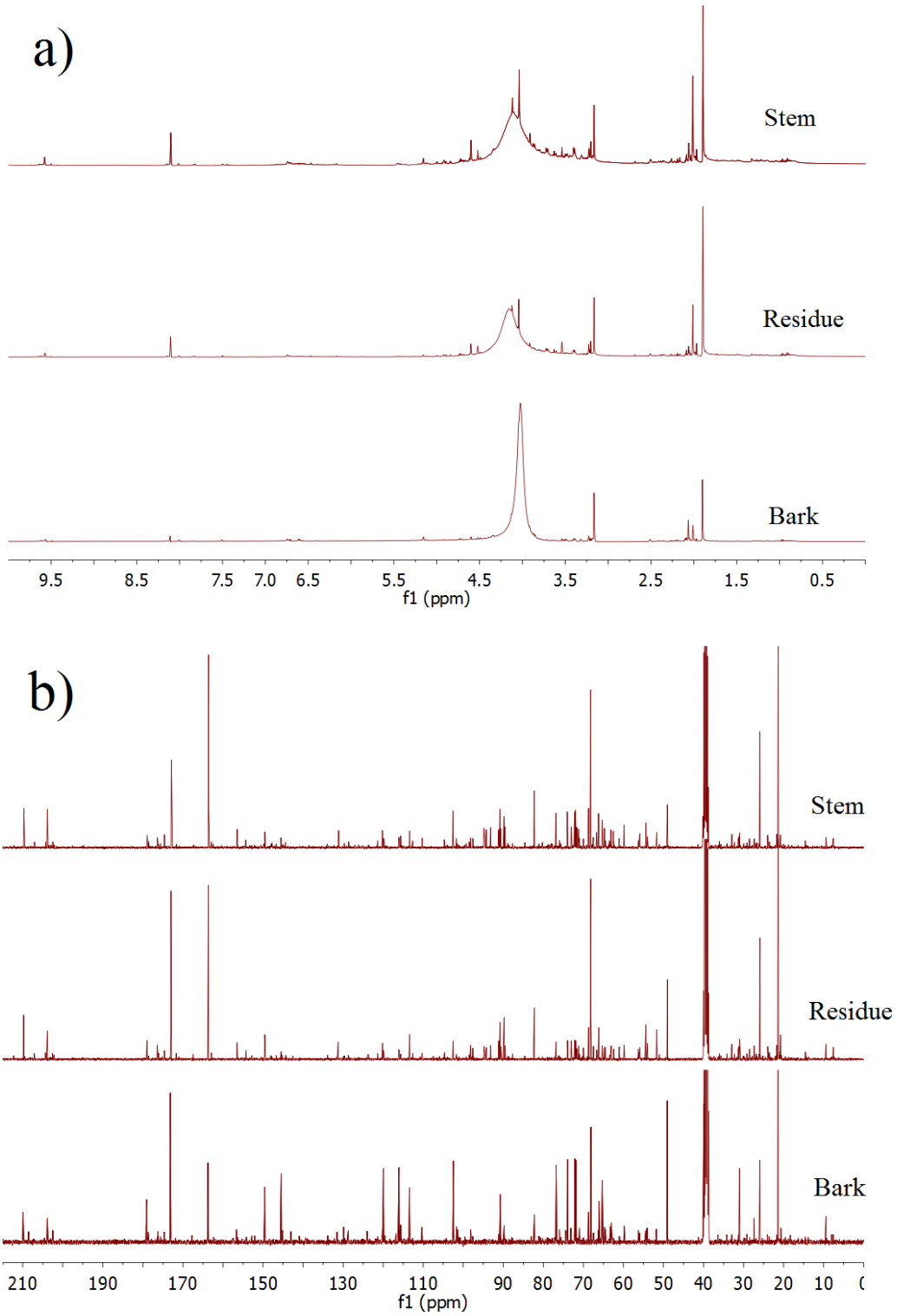

Figure 7.2 ^{1}H NMR (a) and ^{13}C NMR (b) for stem, residue and bark before HDO

Reaction condition: 4.0 mg 5 wt.% Ru/C, 200.0 mg light oil in 20 mL DI H_2O, 573 K, 8.0 MPa H_2, 2 hours.

Table 7.2 ^{1}H-NMR chemical shift assignment ranges and functional group contributions for the light oil.

Type of protons	Range (ppm)	Stem	Residue	Bark
-C**H**O, -COO**H**	10-9.6	0.4	0.4	1.3
Ar**H**, **H**C=C-	8.2-6.0	4.1	3.4	8.8
-C**H**$_n$-O-	6.0-3.0	68.4	73.1	78.9
-C**H**$_3$, -C**H**$_n$-	0.5-3.0	27.0	23.2	11.0

Reaction condition: 4.0 mg 5 wt.% Ru/C, 200.0 mg light oil in 20 mL DI H_2O, 573 K, 8.0 MPa H_2, 2 hours.

More information can be extracted using the data from the proton and carbon NMR together. From the ^{1}H NMR, the -CH_n-O- amounts in light oil are close value. The ^{13}C NMR spectral data further indicate that the ratios between aliphatic C-O and aromatic C-O for stem, residue, and bark are approximately 3.5:1, 2.7:1 and 3.5:1 respectively. Overall, the residue derived light oil has the highest amount of aromatic C-O, probably because of the relatively lower amount of lignin in residue than in the bark which leads to less aromatic condensation. For the same reason, the bark has the highest amount of lignin but the light oil derived from bark has relatively lower amount of aromatic C-O because large amount of aromatic rings condense in pyrolysis and form char product[204]. The light oil from bark also has the lowest amount of aromatic methoxyl groups. The ^{1}H-^{13}C HSQC-NMR spectra shown in Figure 7.3 show that most aromatic methoxyl groups in light oil from bark are substituted at the ortho position.

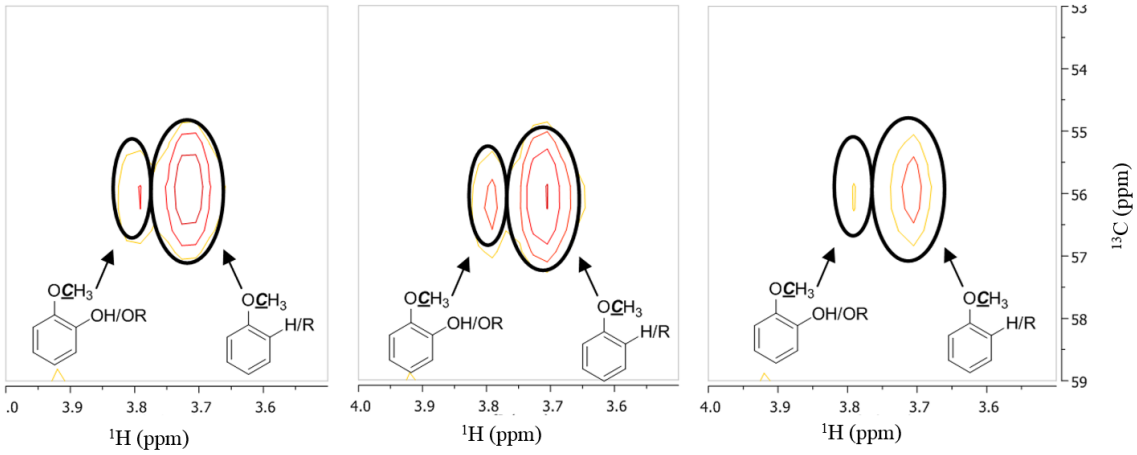

Figure 7.3 ^{1}H-^{13}C HSQC-NMR spectra of the light oil derived from stem, residue and bark (ordered from left to right) in methoxyl group ranges.

Reaction condition: 4.0 mg 5 wt.% Ru/C, 200.0 mg light oil in 20 mL DI H_2O, 573 K, 8.0 MPa H_2, 2 hours.

Another key feature in the NMR spectra is the aromatic C-H (proton directly attached to the aromatic ring). The aromatic regions of the ^{1}H-^{13}C HSQC-NMR spectra are presented in Figure 7.4. The major components in light oil are phenol and guaiacol types of aromatic C-H bond, which agrees well with the result from GC-MS analysis. The quantitative data from ^{13}C NMR in Table 7.3 indicates low amount of aromatic C-C bond in all three light oils. Bark derived light oil has highest aromatic C-H ratio and lowest aromatic C-O ratio. This supports the argument that the aromatic compounds are more likely to condense with the more aromatic C-O bond. The furan structured compounds were also shown in the dashed circle in Figure 7.4.

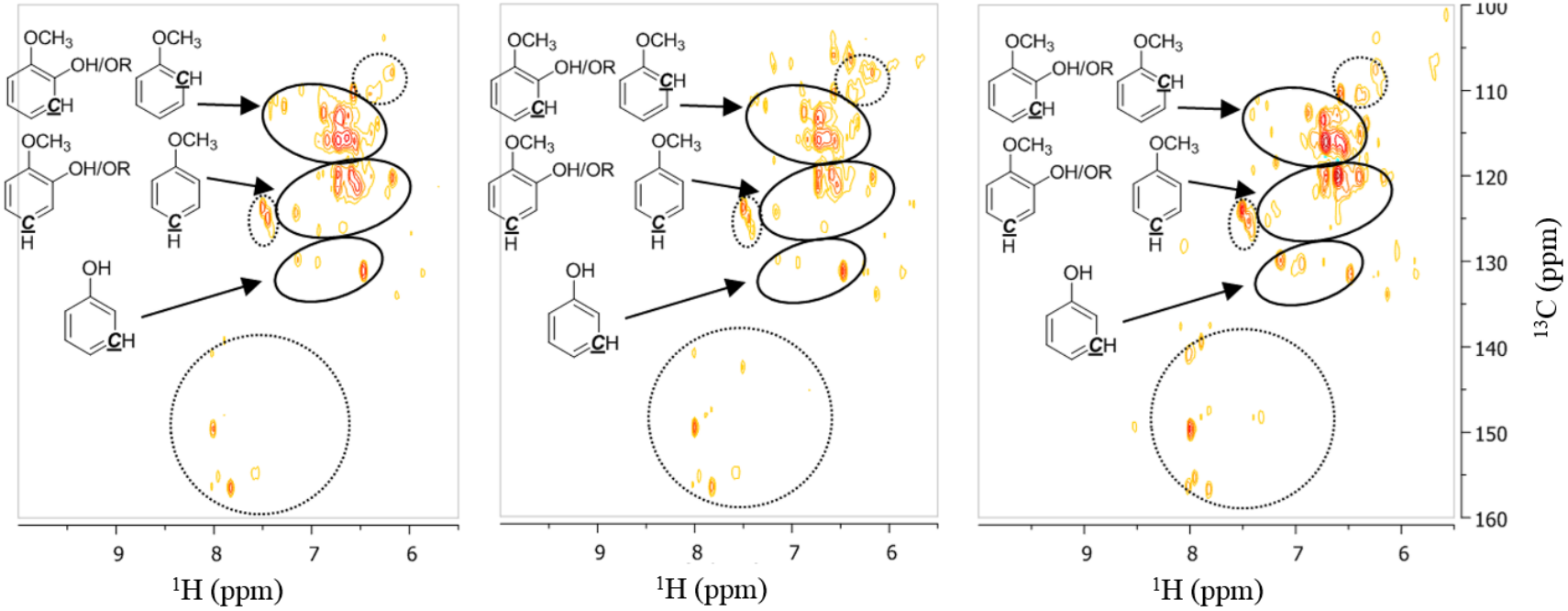

Figure 7.4. ^{1}H-^{13}C HSQC-NMR spectra of the light oil derived from stem, residue and bark (ordered from left to right) in aromatic C-H ranges (dashed circles are the range of furan based compounds.

Reaction condition: 4.0 mg 5 wt.% Ru/C, 200.0 mg light oil in 20 mL DI H_2O, 573 K, 8.0 MPa H_2, 2 hours.

Table 7.3. ^{13}C NMR chemical shift assignment ranges and functional group contributions for the light oil

Functional Group	Integration Region	Stem	Residue	Bark
Carbonyl or Carboxyl	215.0 – 166.5	8.9	12.3	10.8
Aromatic C-O	166.5 – 142.0	11.4	10.3	8.6
Aromatic C-C	142.0 – 125.0	1.7	1.0	2.3
Aromatic C-H	125.0 – 95.8	10.0	8.8	18.6
Aliphatic C-O	95.8 – 60.8	39.4	28.3	31.1
Aromatic methoxy	60.8 – 55.2	3.3	3.2	1.7
Aliphatic C-C	55.2-0.0	25.4	36.1	27.0

Reaction condition: 4.0 mg 5 wt.% Ru/C, 200.0 mg light oil in 20 mL DI H_2O, 573 K, 8.0 MPa H_2, 2 hours.

7.3.3 Analysis of Upgraded light oil.

No obvious carbon loss is observed in stem and residue derived light oil upgrading. The total carbon yield of bark derived light oil is 83% possibly due to the tar formed from tannin binding on catalyst surface[219]. ^1H NMR was used to study the change in the structure of compounds in light oil after upgrading. The spectra of all three upgraded components are listed in Figure 7.5 and the integrated results were shown in Table 7.4. All the peaks in aromatic region are absent (the sharp peak to the left around 7.2 ppm is $CDCl_3$ solvent). The $-CH_nO-$ groups in the upgraded product also decrease substantially.

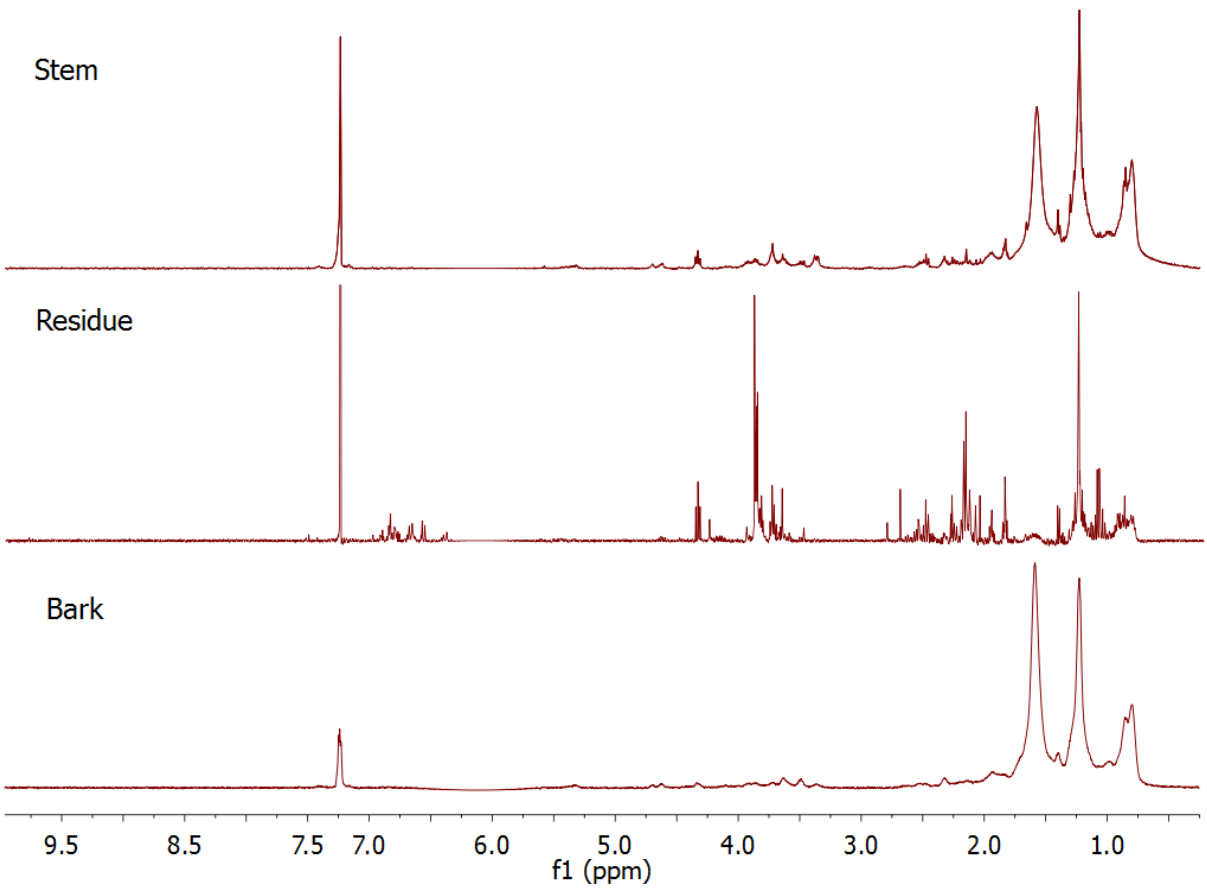

Figure 7.5 ^{1}H NMR for stem, residue and bark after upgrading

Reaction condition: 4.0 mg 5 wt.% Ru/C, 200.0 mg light oil in 20 mL DI H_2O, 573 K, 8.0 MPa H_2, 2 hours.

Levoglucosan is the predominant compound in all three light oils. Therefore, the reaction of levoglucosan with Ru/C was tested alone. GC-MS results indicate that under the same reaction conditions the same as that of light oil upgrading, the major product is 2-methyltetrahydropyran. The proposed reaction paths are shown in Figure 7.6. In the beginning, levoglucosan is converted into glucose through hydrolysis. Ru/C is unable to catalyze ring opening reaction by cleavage of the ether bond. The –OH group is removed by hydrodeoxygenation. The chemical shift of 2-methyltetrahydropyran in the ^{1}H NMR

spectrum was determined from the Scifinder database (calculated using Advanced Chemistry Development, Inc. ACD/Labs Software V11.01). The chemical shifts are around 1.15, 1.30 and 1.55 ppm in the aliphatic region and 3.22 - 3.66 ppm in -CH_n-O- region, which matches the NMR spectrum well.

Table 7.4. ^{1}H NMR chemical shift assignment ranges and functional group contributions for the upgraded light oil

Type of protons	Range (ppm)	Stem	Residue	Bark
-C**H**O, -COO**H**	10-9.6	0.0	0.0	0.0
Ar**H**, **H**C=C-	8.2-6.0	0.2	0.2	0.2
-C**H**$_n$-O-	6.0-3.0	6.7	16.2	4.0
-C**H**$_3$, -C**H**$_n$-	0.5-3.0	93.1	83.5	95.9

Reaction condition: 4.0 mg 5 wt.% Ru/C, 200.0 mg light oil in 20 mL DI H_2O, 573 K, 8.0 MPa H_2, 2 hours.

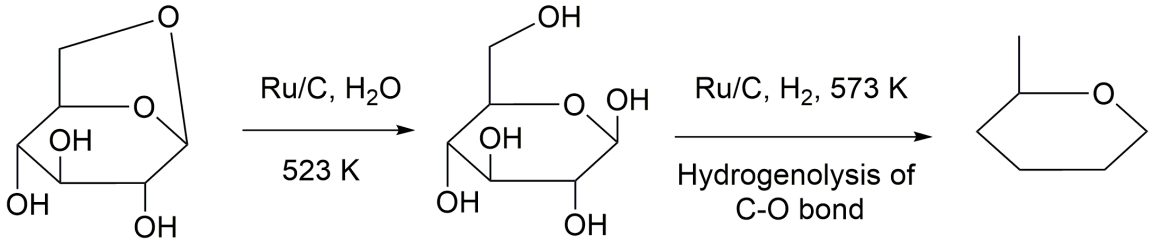

Figure 7.6. Proposed reaction mechanism of Ru catalyzed levoglucosan HDO

Reaction condition: 4.0 mg 5 wt.% Ru/C, 200.0 mg levoglucosan in 20 mL DI H_2O, 573 K, 8.0 MPa H_2, 2 hours.

The second large group in light oils is furan structured compounds. The furan-based components are very similar in the light oil from all three part of the biomass. The molecule structures obtained from GC-MS were listed in Table 7.5 and all of these

compounds matched the structures in the previous publication [68]. The reactions during the upgrading are also categorized in Table 7.5. Two major types of reaction are observed for furan based compounds. For compounds that have no carbonyl group, only the five-membered rings are hydrogenated. Ruthenium is incapable of hydrogenating the C=O bond in ester group. This phenomenon was also observed in Vispute and Huber's study [212]. For compounds with carbonyl group, ruthenium is able to cleave the C=O bond. Elliott and Hart performed furfural HDO with Ru catalyst under 523 K[220]. Hydroxymethyl-THF was the predominant product initially and gradually converted to methyl-THF, which indicates that Ru can catalyze the hydrogenation of the furan ring, C=O bond. Therefore, the most probable reaction path is hydrogenation of the C=O group at first, followed by the hydrogenolysis of hydroxyl group. All products retain the five-membered ring, which indicates that Ru cannot cleave either the ether or the ester bonds.

Table 7.7 Reaction in hydrogenation of furan-based compounds during upgrading. R stands for H or CH_3

Reactant	Product	Type of reaction
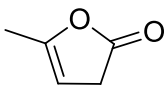	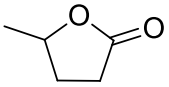	Hydrogenation
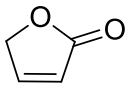	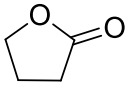	Hydrogenation
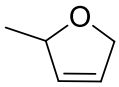	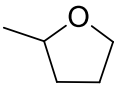	Hydrogenation
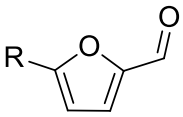	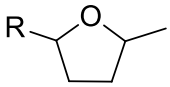	Hydrogenation Hydrodeoxygenation
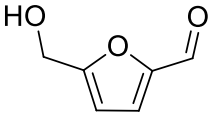	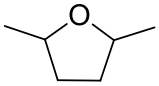	Hydrogenation Hydrodeoxygenation

Reaction condition: 4.0 mg 5 wt.% Ru/C, 200.0 mg light oil in 20 mL DI H_2O, 573 K, 8.0 MPa H_2, 2 hours.

For aromatic compounds, the reaction path (Figure 7.7) is very similar to that previously described for heavy oil upgrading [210]. The chemical structures of the upgraded products obtained from GC-MS are very similar, which supports this tentative reaction path. Cyclohexanol is the major product for light oil derived from stem and residue. The chemical shifts of the major protons (8 out of 10) on cyclohexanol are in the range of 1.47-1.53, which matches the NMR spectrum.

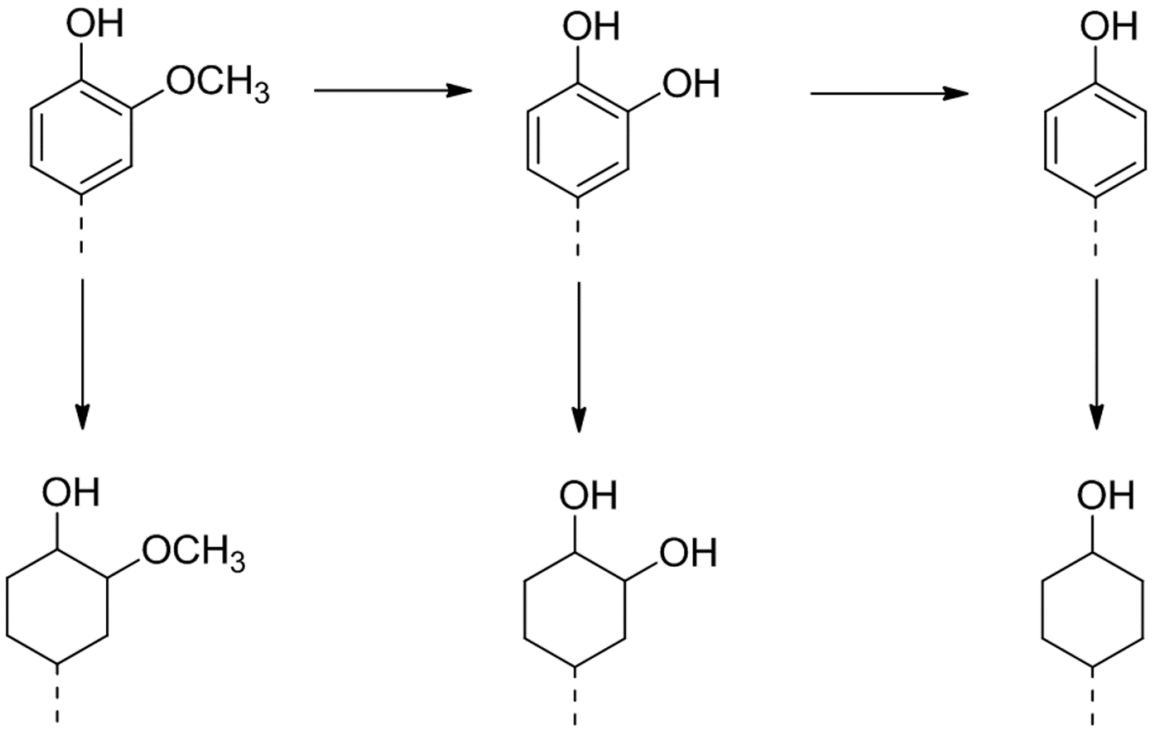

Figure 7.7 Tentative reaction pathways of HDO process of aromatic compounds in the light oil upgrading

Reaction condition: 4.0 mg 5 wt.% Ru/C, 200.0 mg light oil in 20 mL DI H_2O, 573 K, 8.0 MPa H_2, 2 hours.

The C-O regions in the NMR spectra of the upgraded products are also different. The decrease in the amount of C-O in the light oil after the HDO reaction is 90%, 78% and 95% for stem, residue, and bark respectively. According to the mechanism of levoglucosan and ketone hydrodeoxygenation, the light oil from stem is most intensively deoxygenated because of the highest amount of levoglucosan and lowest amount of aromatic structure. Light oil from the residue has more oxygen removed than the light oil from the bark because the light oil from the residue has more guaiacol type compounds while the light oil from the bark has more phenolic aromatic compounds. In the ^{1}H NMR spectra, compared to that of the light oil from the stem and the bark, light oil from the residue shows more peaks between 2.0 and 3.0, which is in the carbonyl range. In the

light oil ^{13}C NMR, the carbonyl group in light oil from the residue is about 100% more than the oil from wood and 50% more than the light oil from the bark. It also shows prominent peaks between 3.0 and 4.0, which is the chemical shift range of the ether group. As mentioned in the upgrading of furan-based compounds, Ru/C has low reactivity with ester and ether groups, which gives the light oil from residue an NMR spectrum more complex NMR spectrum than the light oil from the other two components.

7.4 Conclusion

In this paper, the chemical structures of light oils derived from the stem, residue, and the bark of the loblolly pine were analyzed by several techniques: GC-MS, ^{1}H NMR, ^{13}C NMR, and ^{1}H-^{13}C HSQC-NMR. For all the three components, levoglucosan is the most predominant. Light oil derived from the stem has the highest amount of aliphatic protons and aliphatic C-O, which are mainly contributed by levoglucosan and furanic compounds. Both structures are produced by the abundant amount of cellulose in the stem. Residue derived light oil has large amount of aliphatic protons and lowest amount of aromatic C-O, possibly caused by the lower condensation of lignin during the pyrolysis of the residue. Bark derived light oil has the highest amount of aromatic protons and extremely low amount of aromatic methoxyl groups. The weak ^{1}H NMR signal from the ortho-position in the substituted phenol indicates the severe condensation from lignin pyrolysis.

Ru/C catalyst was adopted for the process of light oil upgrading and it generated fully hydrogenated and extensively deoxygenated products. According to ^{1}H NMR, the percentage of the -CH_n-O- peak area for the stem, residue, and the bark decreases 90%, 78%, 95%, respectively, compared to that for the pre-HDO light oil. Both light oils from the stem and the residue achieve approximately 100% carbon yields. Due to the presence of tannin, the yield of light oil from the bark is 83%. Isopropoxypropane and 1-thoxybutane are the major products from levoglucosan upgrading. The furan-structured compounds mainly go through two types of reactions: hydrogenation and hydrogenolysis. However, Ru/C did not cleave either the ether or the ester bonds through hydrogenolysis. The aromatic compounds are completely hydrogenated. Cyclohexanol is the main product from the aromatic compounds.

CHAPTER 8 OVERALL CONCLUSIONS AND RECOMMENDATIONS

8.1 Overall Conclusions

The dissertation accomplished the conversions of the pyrolysis oil derived from lignin and biomass to chemicals and aliphatic gasoline-compatible fuel. It mainly includes three parts.

In the first part of the work, four commonly used noble metal catalysts underwent evaluation evaluated with three lignin model compounds under the aqueous phase reaction. Pd, Pt, and Rh catalysts are capable of hydrogenating the phenol and catechol. However, they all deactivated during the HDO of guaiacol due to the formation of catechol through the demethylation reaction. The rearrangement of the radicals from the hydrogenolysis of O-CH_3 bond produced two types of *o*-methoxy-Quinonemethide, which were reported as key intermediates for coke formation. The difference among the three catalysts is that Pd and Pt lost their reactivity right after the reaction started and Rh was slowly deactivated within two hours. Ru is the only catalyst that can convert guaiacol into hydrogenated compounds. Although in this study, the Ru/C catalyst had the lowest metal dispersions among all the catalysts, it still showed the highest reactivity. No demethylation but mainly demethoxylation and hydrogenation reactions, were observed

in the Ru catalyzed guaiacol process. The decrease in BET surface area indicates coke formation within Pt, Pd, and Rh catalysts. Ru has the lowest reduction in surface area.

In the second part, the two-step HDO processes were adopted to upgrade the heavy oil produced from pyrolysis of pinewood EOL. Ru and Pt were used in the study. The products of first-step HDO are similar for both catalysts, which are mainly simple aromatic molecules produced from the cleavage of ether bonds and methoxyl groups in the heavy oils. In the second-step HDO reaction, Pt cannot upgrade the EOL heavy oil. Around 30% carbon rings are still in aromatic structure. Ru catalyzed second-step HDO converts water insoluble heavy oils (M_w=265 g/mol) to the alkanes and aliphatic alcohols with a 33 mol% carbon yield. The upgraded pyrolysis oils could be used as green gasoline. The concept established in this work opens up a new opportunity for the conversion of lignin pyrolysis oils (which are the major parts of water insoluble product of pyrolysis of whole biomass) to the renewable gasoline.

Deuterium gas was used in the HDO process to provide insights into the reaction mechanism during the upgrade of pine wood EOL pyrolysis oil. The direct comparison between the ^{1}H-^{13}C HSQC NMR spectra of the proton hydrogenated products and the deuteron hydrogenated products provide the intuitive understanding of the HDO process. During the first-step HDO reaction, the linkages cleavage between two aromatic monomers is validated by both HSQC NMR spectra. During the linkage cleavage, the majority of the hydrogen atoms are added to the ortho and para positions of the guaiacol and phenol. Some of the hydrogen atoms generate new phenolic hydroxyl group. The

conclusions provide the understanding from the perspective of chemistry that the ortho- and para-position are more likely to break during the upgrading. This information is useful for the design of bio-refinery, because a large amount of guaiacol-based compounds generate during the degradation. Guaiacol is commonly used to produce various flavors, such as eugenol and vanillin.

In the last part, the chemical structures of light oils derived from the stem, residue, and the bark of the loblolly pine were analyzed by GC-MS, ^{1}H NMR, ^{13}C NMR, and ^{1}H-^{13}C HSQC-NMR. For all three components, levoglucosan is the most abundant. Light oil derived from the stem has the highest amount of aliphatic protons and aliphatic C−O, which are mainly contributed by levoglucosan and furanic compounds. Residue-derived light oil has a large amount of aliphatic protons and the lowest amount of aromatic C−O possibly caused by the lower condensation of lignin during the pyrolysis of the residue. Bark-derived light oil has the highest amount of aromatic protons and an extremely low amount of aromatic methoxyl groups. The weak HSQC NMR signal from the ortho-position of aromatic methoxyl indicates almost complete condensation of the lignin aromatic hydroxyl group during the pyrolysis. Ru/C catalyst was adopted in the process of light oil upgrading, and it generated fully hydrogenated and extensively deoxygenated products. According to ^{1}H NMR, the percentage of the CH_nO peak area of the stem, residue, and bark decreases 90%, 78%, and 95%, respectively, compared to that for the pre-HDO light oil. Both light oils from the stem and the residue achieve approximately 100% carbon yields. Due to the presence of tannin, the yield of light oil from the bark is 83%. 1-Isopropoxypropane and 1-ethoxybutane are the major products from

levoglucosan upgrading. The furan-structured compounds mainly go through two types of reactions: hydrogenation and hydrogenolysis. However, Ru/C did not cleave either the ether or the ester bonds through hydrogenolysis. The aromatic compounds are completely hydrogenated. Cyclohexanol is the main product of the aromatic compounds.

Overall, the main objectives of this thesis work were accomplished. The proper catalyst was screened from the model compound study, and the reaction mechanism was deduced. The best catalyst was used in lignin heavy oil upgrading, and the upgraded pyrolysis oils could be used as green gasoline. Various techniques were used for product characterization, and the fundamental reaction mechanism was studied in detail. The whole biomass was also upgraded under the same condition.

8.2 Recommendations

1. Regeneration of Catalysts

   During the heavy oil upgrading, the catalyst deactivated due to the tar formation. The chemical structures of tar products were analyzed and part of the product is soluble in organic solvent, such as chloroform. Therefore, whether the catalyst can regenerate through direct organic solvent wash would be interesting. [221] If the catalyst regeneration is complicated and costly, other cheap metal catalysts should be evaluated in the first-step HDO reaction to see if they are able to achieve a similar performance.

2. Supporting material, ZSM-5

   In Chapter 6, the modified ZSM-5 proved to be an effective supporting material for the deoxygenation reaction that produced cyclohexane as a major product. In the future, more detailed characterizations of the alkali treated ZSM-5 should be performed. The supporting material, with better tuned pore size and surface acidity, can greatly improve the application of the lignin derived heavy oil upgrading.

3. Co-process the light oil and the products obtained from first-step heavy oil upgrading

   The catalyst deactivation is only observed in the first-step HDO of the EOL pyrolysis heavy oil. There is no sign of catalyst deactivation in the second-step HDO of heavy oil and upgrading of the light oil. Therefore, it is economically favorable to co-process the two types of oils together. These results will be valuable when developing bio-fuel production through the hydrodeoxygenation of whole biomass pyrolysis oils.

APPENDIX A – REPORTED LIQUID PRODUCTS OF PYROLYSIS OF LIGNIN

GC-MS detected components in lignin pyrolysis oil		
Phenol [30, 39, 44-48] 2-Methylphenol [30, 39, 44-48] o-Cresol 4-Methylphenol [30, 39, 44, 45, 47] p-Cresol 2-Methoxyphenol [30, 39, 44-48] Guaiacol 2,6-Dimethylphenol [30, 39, 46] 2,6-Xylenol	4'-Hydroxy-3'-methoxyacetophenone [30, 39, 44-46, 48] Acetovanillone Acetoguaiacone 5-Tert-butylpyrogallol [39] 1-(4-Hydroxy-3-methoxyphenyl)-2-propanone [30, 39, 48] Guaiacylacetone 2-(3,4-Dimethoxyphenyl)-6-methyl-3,4-chromanediol [39] 3,4-Dimethylbenzoic acid [39, 46]	4-Allyl-dimethoxyphenol [45] Dimethoxypropylphenol [45] Coniferylaldehyde [45, 48] Sinapaldehyde [45, 48] 2,6-Dimethoxy-4-methylphenol [44, 48] 4-Methylsyringol

4-Ethylphenol [30, 39, 44, 47] p-Ethylphenol	3-Methoxy-4-hydroxybenzoic acid [39]	1-(4-Hydroxy-3-methoxyphenyl) propyne [44]
3-Methylbenzaldehyde [39] m-Tolualdehyde	4-Ethyl-1,2-dimethoxybenzene [39]	4-Ethyl-2,6-dimethoxyphenol [44, 48] 4-Ethylsyringol
2-Hydroxy-6-methylbenzaldehyde [39]	4-Propenylsyringol [39, 44, 48] 4-Propenyl-2,6-dimethoxyphenol	4-Vinyl-2,6-dimethoxyphenol [44, 48] Vinylsyringol
2-Ethylphenol [30, 39, 47]	Ferulic acid [39] 3-Hydroxy-4-methoxycinnamic acid	4-Propyl-2,6-dimethoxyphenol [44]
4-Methoxy-3-methylphenol [39]	4-Hydroxy-3,5-dimethoxybenzaldehyde [30, 39, 44, 45, 48] Syringaldehyde	Syringylacetone [44, 48]
2-Methoxy-4-methylphenol [30, 39, 44-48] 4-Methylguaiacol	Acetosyringone [30, 39, 44, 45] 4'-Hydroxy-3',5'-dimethoxyacetophenone	m-Cresol [46, 47]
Catechol [30, 39, 45-47] 1,2-Benzenediol	1-(2,6-Dihydroxy-4-methoxyphenyl)-1-	p-Propylphenol [47]

	butanone [39] Desaspidinol	
Benzofuran [39]	Syringic acid [39] 4-Hydroxy-3,5-dimethoxybenzoic acid	6-Ethylguaiacol [47]
p-Isopropylphenol [39] p-Cumenol	2,3,5-Trimethyl phenol [30]	2-Methoxy-4-propylphenol [46-48] 4-Propylguaiacol
2-Ethyl-4-methylphenol [39]	3-Ethyl phenol [30, 46, 47]	4-Methyl-1,2-benzenediol [46, 47] 4-Methylcatechol
3-Methoxy-1,2-benzenediol [30, 39, 47] 3-Methoxycatechol	1,2,3-Trimethoxybenzene [30]	6-Ethylcatechol [47]
3-Methyl-1,2-benzenediol [30, 39, 45-47] 3-Methylpyrocatechol 3-Methylcatechol	Coniferyl alcohol [30, 46, 47]	3-Methylguaiacol [48]
2-Methoxy-4-ethylphenol [30, 39, 44-48]	Methoxyeugenol [30, 44] 4-Hydroxy-3,5-dimethoxyallylbenzene 4-Allyl-2,6-dimethoxyphenol	3-Ethylguaiacol [48]

4-(2-Propenyl)phenol [39]	1-Methoxy-3-methylbenzene [45]	Propioguaiacone [48] 1-(4-Hydroxy-3-methoxy-phenyl)-propan-1-one
p-Isopropenylphenol [39]	Indene [45]	6-Hydroxy-5,7-dimethoxy-indene [48]
2-Methoxy-4-vinylphenol [30, 39, 44, 45, 48] 4-Vinylguaiacol	1,2,3-Trimethylbenzene [45]	Dihydroconiferylalcohol [48]
3-Methyl-5-methoxyphenol [39]	1,2,4-Trimethylbenzene [45]	Propiosyringone [48]
4-Ethyl-1,3-benzenediol [46] 4-Ethylresorcinol	Mesitylene [45]	Dihydrosinapylalcohol [48]
2,6-Dimethoxyphenol [30, 39, 44, 45, 48] Syringol	4-Ethenylphenol [44, 45] Vinylphenol	Sinapylalcohol [48]
2,5-Dimethyl-1,4-benzenediol [39]	m-Dimethoxybenzene [45]	2,3-dimethylphenol [46] 2,3-xylenol
2,4-Dimethoxyphenol [39]	Veratrole [45]	Naphthalene [45, 46]
2',4'-Dimethylacetophenone [39]	p-Dimethoxybenzene [45]	Benzene [30]
4-Ethyl-1,2-benzenediol [39, 47]	Dimethylcatechol [45]	Styrene [30]

4-Ethylpyrocatechol		
Eugenol [30, 39, 44-46, 48]	Vinylcatechol [45]	p-Xylene [30]
3-Hydroxy-4-methoxybenzaldehyde [30, 39, 45] Isovanillin	Vanillin [44-46, 48]	Ethylbenzene [30]
2,5-Dimethoxybenzylalcohol [39]	3',5'-Dimethoxyacetophenone [45]	Toluene [30]
2-Methoxy-4-(1-propenyl)phenol [30, 39, 44-46, 48] Isoeugenol	4-Methyl 2,5-dimethoxy benzaldehyde [45]	
4'-Hydroxy-3'-methoxyacetophenone [30, 39, 44-46, 48] Acetovanillone Acetoguaiacone	Fluorene [45]	

[a] The pyrolysis temperatures are from 673-1073 K.

APPENDIX B – COPYRIGHT PERMISSIONS

1. Permission from BioEnergy Research

Zimbra **wmu3@mail.gatech.edu**

Thank you for your RightsLink / Springer transaction

From : Copyright Clearance Center <rightslink@marketing.copyright.com> Thu, Nov 13, 2014 03:35 PM
Subject : Thank you for your RightsLink / Springer transaction
To : muw0@gatech.edu
Reply To : Copyright Clearance Center <reply-fe4e10777062037e7c1c-14153369_HTML-823383695-114453-81791@info.copyright.com>

To view this email as a web page, go here.

Do Not Reply Directly to This Email

To ensure that you continue to receive our emails,
please add rightslink@marketing.copyright.com to your address book.

RightsLink | Copyright Clearance Center

Thank You For Your Order!

Dear Mr. Wei Mu,

Thank you for placing your order through Copyright Clearance Center's RightsLink service. Springer has partnered with RightsLink to license its content. This notice is a confirmation that your order was successful.

Your order details and publisher terms and conditions are available by clicking the link below:
http://s100.copyright.com/CustomerAdmin/PLF.jsp?ref=38b4890d-7b68-4df5-b883-c14640be158a

Order Details
Licensee: Wei Mu
License Date: Nov 13, 2014
License Number: 3507250246247
Publication: BioEnergy Research
Title: Lignin Pyrolysis Components and Upgrading-Technology Review
Type Of Use: Thesis/Dissertation
Total: 0.00 USD

To access your account, please visit https://myaccount.copyright.com.

Please note: Online payments are charged immediately after order confirmation; invoices are issued daily and are payable immediately upon receipt.

To ensure that we are continuously improving our services, please take a moment to complete our customer satisfaction survey.

B.1:v4.2

+1-855-239-3415 / Tel: +1-978-646-2777
customercare@copyright.com
http://www.copyright.com

2. Permission from Bioresource Technology

Zimbra **wmu3@mail.gatech.edu**

Thank you for your RightsLink / Elsevier transaction

From : Copyright Clearance Center <rightslink@marketing.copyright.com> Thu, Oct 30, 2014 10:36 PM
Subject : Thank you for your RightsLink / Elsevier transaction
To : muw0@gatech.edu
Reply To : Copyright Clearance Center <reply-fe4e10777062037e7c1c-14153369_HTML-823383695-114453-71464@info.copyright.com>

To view this email as a web page, go here.

Do Not Reply Directly to This Email

To ensure that you continue to receive our emails,
please add rightslink@marketing.copyright.com to your address book.

RightsLink | Copyright Clearance Center

Thank You For Your Order!

Dear Mr. Wei Mu,

Thank you for placing your order through Copyright Clearance Center's RightsLink service. Elsevier has partnered with RightsLink to license its content. This notice is a confirmation that your order was successful.

Your order details and publisher terms and conditions are available by clicking the link below:
http://s100.copyright.com/CustomerAdmin/PLF.jsp?ref=1c4fc925-78ec-4ab4-a988-38cbf3d7e6f8

Order Details
Licensee: Wei Mu
License Date: Oct 30, 2014
License Number: 3499101384626
Publication: Bioresource Technology
Title: Noble metal catalyzed aqueous phase hydrogenation and hydrodeoxygenation of lignin-derived pyrolysis oil and related model compounds
Type Of Use: reuse in a thesis/dissertation
Total: 0.00 USD

To access your account, please visit https://myaccount.copyright.com.

Please note: Online payments are charged immediately after order confirmation; invoices are issued daily and are payable immediately upon receipt.

To ensure that we are continuously improving our services, please take a moment to complete our customer satisfaction survey.

B.1:v4.2

+1-855-239-3415 / Tel: +1-978-646-2777
customercare@copyright.com
http://www.copyright.com

This email was sent to: **muw0@gatech.edu**

Please visit Copyright Clearance Center for more information.

3. Permission from Fuel

Zimbra **wmu3@mail.gatech.edu**

Thank you for your RightsLink / Elsevier transaction

From : Copyright Clearance Center <rightslink@marketing.copyright.com> Thu, Nov 13, 2014 03:45 PM
Subject : Thank you for your RightsLink / Elsevier transaction
To : muw0@gatech.edu
Reply To : Copyright Clearance Center <reply-fe4e10777062037e7c1c-14153369_HTML-823383695-114453-81798@info.copyright.com>

To view this email as a web page, go here.

Do Not Reply Directly to This Email

To ensure that you continue to receive our emails,
please add rightslink@marketing.copyright.com to your address book.

RightsLink | Copyright Clearance Center

Thank You For Your Order!

Dear Mr. Wei Mu,

Thank you for placing your order through Copyright Clearance Center's RightsLink service. Elsevier has partnered with RightsLink to license its content. This notice is a confirmation that your order was successful.

Your order details and publisher terms and conditions are available by clicking the link below:
http://s100.copyright.com/CustomerAdmin/PLF.jsp?ref=b6271de8-ce59-401b-b645-cd25d888fa02

Order Details
Licensee: Wei Mu
License Date: Nov 13, 2014
License Number: 3507250909472
Publication: Fuel
Title: Production of renewable gasoline from aqueous phase hydrogenation of lignin pyrolysis oil
Type Of Use: reuse in a thesis/dissertation
Total: 0.00 USD

To access your account, please visit https://myaccount.copyright.com.

Please note: Online payments are charged immediately after order confirmation; invoices are issued daily and are payable immediately upon receipt.

To ensure that we are continuously improving our services, please take a moment to complete our customer satisfaction survey.

B.1:v4.2

+1-855-239-3415 / Tel: +1-978-646-2777
customercare@copyright.com
http://www.copyright.com

This email was sent to: **muw0@gatech.edu**

Please visit Copyright Clearance Center for more information.

4. Permission from PCCP

Hydrodeoxygenation by deuterium gas – a powerful way to provide insight into the reaction mechanisms

H. Ben, G. A. Ferguson, W. Mu, Y. Pu, F. Huang, M. Jarvis, M. Biddy, Y. Deng and A. J. Ragauskas, *Phys. Chem. Chem. Phys.*, 2013, **15**, 19138
DOI: 10.1039/C3CP53409J

5. Permission from I&EC

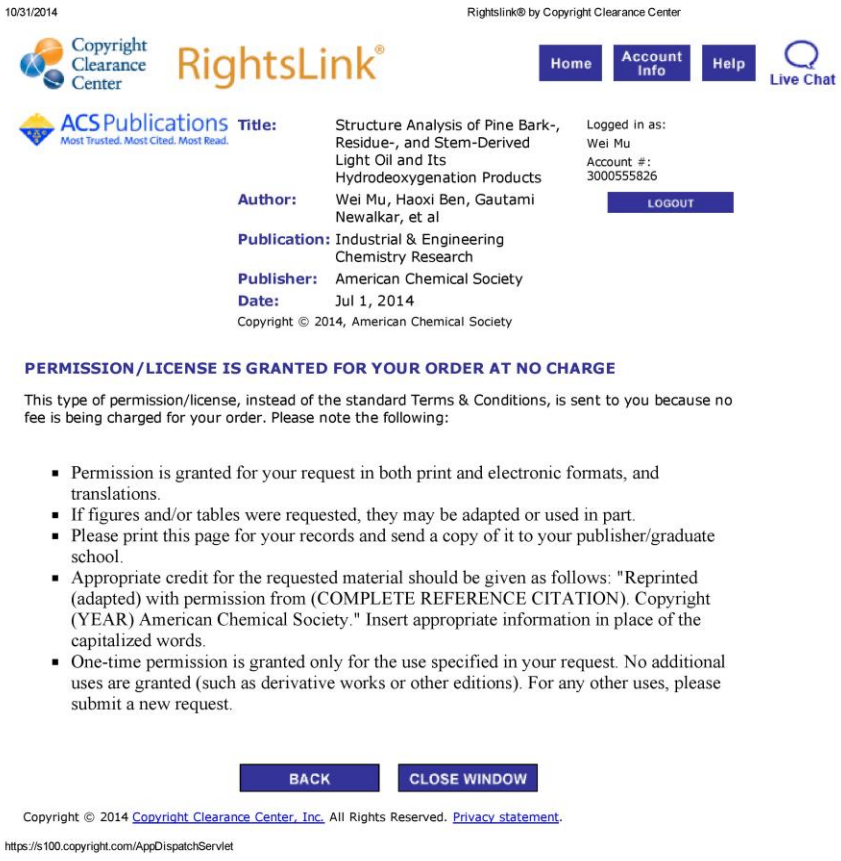

10/31/2014 Rightslink® by Copyright Clearance Center

Copyright Clearance Center RightsLink® Home Account Info Help Live Chat

ACS Publications Most Trusted. Most Cited. Most Read.

Title:	Structure Analysis of Pine Bark-, Residue-, and Stem-Derived Light Oil and Its Hydrodeoxygenation Products	Logged in as: Wei Mu Account #: 3000555826 LOGOUT
Author:	Wei Mu, Haoxi Ben, Gautami Newalkar, et al	
Publication:	Industrial & Engineering Chemistry Research	
Publisher:	American Chemical Society	
Date:	Jul 1, 2014	

Copyright © 2014, American Chemical Society

PERMISSION/LICENSE IS GRANTED FOR YOUR ORDER AT NO CHARGE

This type of permission/license, instead of the standard Terms & Conditions, is sent to you because no fee is being charged for your order. Please note the following:

- Permission is granted for your request in both print and electronic formats, and translations.
- If figures and/or tables were requested, they may be adapted or used in part.
- Please print this page for your records and send a copy of it to your publisher/graduate school.
- Appropriate credit for the requested material should be given as follows: "Reprinted (adapted) with permission from (COMPLETE REFERENCE CITATION). Copyright (YEAR) American Chemical Society." Insert appropriate information in place of the capitalized words.
- One-time permission is granted only for the use specified in your request. No additional uses are granted (such as derivative works or other editions). For any other uses, please submit a new request.

BACK CLOSE WINDOW

Copyright © 2014 Copyright Clearance Center, Inc. All Rights Reserved. Privacy statement.

https://s100.copyright.com/AppDispatchServlet 1/2

REFERENCES

1. Demirbas, A., *Progress and recent trends in biofuels.* Progress in Energy and Combustion Science, 2007. **33**(1): p. 1-18.
2. Ragauskas, A.J., Williams, C.K., Davison, B.H., Britovsek, G., Cairney, J., Eckert, C.A., Frederick, W.J., Hallett, J.P., Leak, D.J., Liotta, C.L., Mielenz, J.R., Murphy, R., Templer, R., and Tschaplinski, T., *The Path Forward for Biofuels and Biomaterials.* Science, 2006. **311**(5760): p. 484-489.
3. Administration, U.S.E.I. *PETROLEUM & OTHER LIQUIDS*. 2014.
4. Perlack, R.D., Wright, L.L., Turhollow, A.F., Graham, R.L., Stokes, B.J., and Erbach, D.C., *Biomass as feedstock for a bioenergy and bioproducts industry: the technical feasibility of a billion-ton annual supply*. 2005, DTIC Document.
5. Calvo-Flores, F.G. and Dobado, J.A., *Lignin as Renewable Raw Material.* ChemSusChem, 2010. **3**(11): p. 1227-1235.
6. Wyman, C.E., *What is (and is not) vital to advancing cellulosic ethanol.* Trends in Biotechnology, 2007. **25**(4): p. 153-157.
7. Jahangiri, H., Bennett, J., Mahjoubi, P., Wilson, K., and Gu, S., *A review of advanced catalyst development for Fischer-Tropsch synthesis of hydrocarbons from biomass derived syn-gas.* Catalysis Science & Technology, 2014. **4**(8): p. 2210-2229.
8. Bridgwater, A.V., *Review of fast pyrolysis of biomass and product upgrading.* Biomass and Bioenergy, 2012. **38**(0): p. 68-94.

9. Brethauer, S. and Wyman, C.E., *Review: Continuous hydrolysis and fermentation for cellulosic ethanol production.* Bioresource Technology, 2010. **101**(13): p. 4862-4874.

10. Mohan, D., Pittman, C.U., and Steele, P.H., *Pyrolysis of Wood/Biomass for Bio-oil: A Critical Review.* Energy & Fuels, 2006. **20**(3): p. 848-889.

11. Mu, W., Ben, H., Ragauskas, A., and Deng, Y., *Lignin Pyrolysis Components and Upgrading—Technology Review.* BioEnergy Research, 2013. **6**(4): p. 1183-1204.

12. Administration, E.I., *Monthly Energy Review*. June 2012, US Department of Energy.

13. Administration-0384, E.I., *Annual Energy Review 2010*. 2011, Department of Energy.

14. Franks, J.R. and Hadingham, B., *Reducing greenhouse gas emissions from agriculture: Avoiding trivial solutions to a global problem.* Land Use Policy, 2012. **29**(4): p. 727-736.

15. Iribarren, D., Peters, J.F., and Dufour, J., *Life cycle assessment of transportation fuels from biomass pyrolysis.* Fuel, 2012. **97**(0): p. 812-821.

16. van Oort, P.A.J., Timmermans, B.G.H., and van Swaaij, A.C.P.M., *Why farmers' sowing dates hardly change when temperature rises.* European Journal of Agronomy, 2012. **40**(0): p. 102-111.

17. Lenzen, M. and Schaeffer, R., *Historical and potential future contributions of power technologies to global warming.* Climatic Change, 2012. **112**(3): p. 601-632.

18. Biasutti, M., Sobel, A., Camargo, S., and Creyts, T., *Projected changes in the physical climate of the Gulf Coast and Caribbean.* Climatic Change, 2012. **112**(3): p. 819-845.

19. Jitaru, M., *Electrochemical carbon dioxide reduction-fundamental and applied topics.* Journal of the University of chemical Technology and Metallurgy, 2007. **42**(4): p. 333-344.

20. Zakzeski, J., Bruijnincx, P.C.A., Jongerius, A.L., and Weckhuysen, B.M., *The Catalytic Valorization of Lignin for the Production of Renewable Chemicals.* Chemical Reviews, 2010. **110**(6): p. 3552-3599.

21. Parikka, M., *Global biomass fuel resources.* Biomass and Bioenergy, 2004. **27**(6): p. 613-620.

22. Klass, D.L., *Biomass for renewable energy, fuels, and chemicals*. 1998: Academic press.

23. Sjöström, E., *Wood chemistry: fundamentals and applications*. 1993: Gulf Professional Publishing.

24. David, K. and Ragauskas, A.J., *Switchgrass as an energy crop for biofuel production: A review of its ligno-cellulosic chemical properties.* Energy & Environmental Science, 2010. **3**(9): p. 1182-1190.

25. Ragauskas, A., *Chemical Overview of Wood*. Institute of Paper Science and Technology.

26. Weng, J.-K. and Chapple, C., *The origin and evolution of lignin biosynthesis.* New Phytologist, 2010. **187**(2): p. 273-285.

27. Ralph, J., Brunow, G., and Boerjan, W., *Lignins*, in *eLS*. 2001, John Wiley & Sons, Ltd.

28. Ragauskas, A.J., *Typical H:G:S Ratio for Lignin from Biomass* in *Technical Review*. Institute of Paper Science and Technology.

29. Guerra, A., Lucia, L.A., and Argyropoulos, D.S., *Isolation and characterization of lignins from Eucalyptus grandis Hill ex Maiden and Eucalyptus globulus Labill. by enzymatic mild acidolysis (EMAL).* Holzforschung, 2008. **62**(1): p. 24-30.

30. Nowakowski, D.J., Bridgwater, A.V., Elliott, D.C., Meier, D., and de Wild, P., *Lignin fast pyrolysis: Results from an international collaboration.* Journal of Analytical and Applied Pyrolysis, 2010. **88**(1): p. 53-72.

31. Beis, S.H., Mukkamala, S., Hill, N., Joseph, J., Baker, C., Jensen, B., Stemmler, E.A., Wheeler, M.C., Frederick, B.G., Heiningen, A.v., Berg, A.G., and DeSisto, W.J., *Fast pyrolysis of lignins.* BioRes., 2010. **5**: p. 17.

32. Ferdous, D., Dalai, A.K., Bej, S.K., and Thring, R.W., *Pyrolysis of Lignins: Experimental and Kinetics Studies.* Energy & Fuels, 2002. **16**(6): p. 1405-1412.

33. Ferdous, D., Dalai, A.K., Bej, S.K., Thring, R.W., and Bakhshi, N.N., *Production of H2 and medium Btu gas via pyrolysis of lignins in a fixed-bed reactor.* Fuel Processing Technology, 2001. **70**(1): p. 9-26.

34. Caballero, J.A., Font, R., Marcilla, A., and Garc á, A.N., *Flash pyrolysis of Klason lignin in a Pyroprobe 1000.* Journal of Analytical and Applied Pyrolysis, 1993. **27**(2): p. 221-244.

35. Asmadi, M., Kawamoto, H., and Saka, S., *Gas- and solid/liquid-phase reactions during pyrolysis of softwood and hardwood lignins.* Journal of Analytical and Applied Pyrolysis, 2011. **92**(2): p. 417-425.

36. Chen, H.-W., Song, Q.-H., Liao, B., and Guo, Q.-X., *Further Separation, Characterization, and Upgrading for Upper and Bottom Layers from Phase Separation of Biomass Pyrolysis Oils.* Energy & Fuels, 2011. **25**(10): p. 4655-4661.

37. Hosoya, T., Kawamoto, H., and Saka, S., *Solid/liquid- and vapor-phase interactions between cellulose- and lignin-derived pyrolysis products.* Journal of Analytical and Applied Pyrolysis, 2009. **85**(1–2): p. 237-246.

38. Hyder, M. and Jönsson, J.Å., *Hollow-fiber liquid phase microextraction for lignin pyrolysis acids in aerosol samples and gas chromatography–mass spectrometry analysis.* Journal of Chromatography A, 2012. **1249**(0): p. 48-53.

39. Jiang, G., Nowakowski, D.J., and Bridgwater, A.V., *Effect of the Temperature on the Composition of Lignin Pyrolysis Products.* Energy & Fuels, 2010. **24**(8): p. 4470-4475.

40. Lou, R., Wu, S.-b., and Lv, G.-j., *Effect of conditions on fast pyrolysis of bamboo lignin.* Journal of Analytical and Applied Pyrolysis, 2010. **89**(2): p. 191-196.

41. Lou, R., Wu, S.-B., Lv, G.-J., and Guo, D.-L., *pyrolytic products from rice straw and enzymatic/mild acidolysis lignin.* BioRes., 2010. **5**(4): p. 2184-2194.

42. Mullen, C.A. and Boateng, A.A., *Catalytic pyrolysis-GC/MS of lignin from several sources.* Fuel Processing Technology, 2010. **91**(11): p. 1446-1458.

43. Patwardhan, P.R., Brown, R.C., and Shanks, B.H., *Understanding the Fast Pyrolysis of Lignin.* ChemSusChem, 2011. **4**(11): p. 1629-1636.

44. Bocchini, P., Galletti, G.C., Camarero, S., and Martinez, A.T., *Absolute quantitation of lignin pyrolysis products using an internal standard.* Journal of Chromatography A, 1997. **773**(1–2): p. 227-232.

45. Greenwood, P.F., van Heemst, J.D.H., Guthrie, E.A., and Hatcher, P.G., *Laser micropyrolysis GC–MS of lignin.* Journal of Analytical and Applied Pyrolysis, 2002. **62**(2): p. 365-373.

46. Ingram, L., Mohan, D., Bricka, M., Steele, P., Strobel, D., Crocker, D., Mitchell, B., Mohammad, J., Cantrell, K., and Pittman, C.U., *Pyrolysis of Wood and Bark in an Auger Reactor: Physical Properties and Chemical Analysis of the Produced Bio-oils.* Energy & Fuels, 2007. **22**(1): p. 614-625.

47. Jegers, H.E. and Klein, M.T., *Primary and secondary lignin pyrolysis reaction pathways.* Industrial & Engineering Chemistry Process Design and Development, 1985. **24**(1): p. 173-183.

48. Scholze, B. and Meier, D., *Characterization of the water-insoluble fraction from pyrolysis oil (pyrolytic lignin). Part I. PY–GC/MS, FTIR, and functional groups.* Journal of Analytical and Applied Pyrolysis, 2001. **60**(1): p. 41-54.

49. Saiz-Jimenez, C. and De Leeuw, J.W., *Lignin pyrolysis products: Their structures and their significance as biomarkers.* Organic Geochemistry, 1986. **10**(4–6): p. 869-876.

50. Britt, P.F., Buchanan, A.C., Cooney, M.J., and Martineau, D.R., *Flash Vacuum Pyrolysis of Methoxy-Substituted Lignin Model Compounds.* The Journal of Organic Chemistry, 2000. **65**(5): p. 1376-1389.

51. Britt, P.F., Buchanan, A.C., and Malcolm, E.A., *Impact of Restricted Mass Transport on Pyrolysis Pathways for Aryl Ether Containing Lignin Model Compounds.* Energy & Fuels, 2000. **14**(6): p. 1314-1322.

52. Britt, P.F., Kidder, M.K., and Buchanan, A.C., *Oxygen Substituent Effects in the Pyrolysis of Phenethyl Phenyl Ethers.* Energy & Fuels, 2007. **21**(6): p. 3102-3108.

53. Kawamoto, H., Nakamura, T., and Saka, S., *Pyrolytic cleavage mechanisms of lignin-ether linkages: A study on p-substituted dimers and trimers*, in *Holzforschung*. 2008. p. 50.

54. Kawamoto, H., Ryoritani, M., and Saka, S., *Different pyrolytic cleavage mechanisms of β-ether bond depending on the side-chain structure of lignin dimers.* Journal of Analytical and Applied Pyrolysis, 2008. **81**(1): p. 88-94.

55. Kawamoto, H. and Saka, S., *Role of Side‐Chain Hydroxyl Groups in Pyrolytic Reaction of Phenolic β‐Ether Type of Lignin Dimer.* Journal of Wood Chemistry and Technology, 2007. **27**(2): p. 113-120.

56. Kawamoto, H., Horigoshi, S., and Saka, S., *Pyrolysis reactions of various lignin model dimers.* Journal of Wood Science, 2007. **53**(2): p. 168-174.

57. Chu, S., Subrahmanyam, A.V., and Huber, G.W., *The pyrolysis chemistry of a [small beta]-O-4 type oligomeric lignin model compound.* Green Chemistry, 2013. **15**(1): p. 125-136.

58. Mullen, C.A., Strahan, G.D., and Boateng, A.A., *Characterization of Various Fast-Pyrolysis Bio-Oils by NMR Spectroscopy†.* Energy & Fuels, 2009. **23**(5): p. 2707-2718.

59. Luo, Z., Wang, S., and Guo, X., *Selective pyrolysis of Organosolv lignin over zeolites with product analysis by TG-FTIR.* Journal of Analytical and Applied Pyrolysis, 2012. **95**(0): p. 112-117.

60. Kosa, M., Ben, H., Theliander, H., and Ragauskas, A.J., *Pyrolysis oils from CO2 precipitated Kraft lignin.* Green Chemistry, 2011. **13**(11): p. 3196-3202.

61. Joseph, J., Baker, C., Mukkamala, S., Beis, S.H., Wheeler, M.C., DeSisto, W.J., Jensen, B.L., and Frederick, B.G., *Chemical Shifts and Lifetimes for Nuclear Magnetic Resonance (NMR) Analysis of Biofuels.* Energy & Fuels, 2010. **24**(9): p. 5153-5162.

62. Gellerstedt, G.r., Li, J., Eide, I., Kleinert, M., and Barth, T., *Chemical Structures Present in Biofuel Obtained from Lignin.* Energy & Fuels, 2008. **22**(6): p. 4240-4244.

63. DeSisto, W.J., Hill, N., Beis, S.H., Mukkamala, S., Joseph, J., Baker, C., Ong, T.-H., Stemmler, E.A., Wheeler, M.C., Frederick, B.G., and van Heiningen, A., *Fast Pyrolysis of Pine Sawdust in a Fluidized-Bed Reactor.* Energy & Fuels, 2010. **24**(4): p. 2642-2651.

64. David, K., Kosa, M., Williams, A., Mayor, R., Realff, M., Muzzy, J., and Ragauskas, A., *31P-NMR analysis of bio-oils obtained from the pyrolysis of biomass.* Biofuels, 2010. **1**(6): p. 839-845.

65. David, K., Ben, H., Muzzy, J., Feik, C., Iisa, K., and Ragauskas, A., *Chemical characterization and water content determination of bio-oils obtained from various biomass species using 31P NMR spectroscopy.* Biofuels, 2012. **3**(2): p. 123-128.

66. Ben, H. and Ragauskas, A.J., *Torrefaction of Loblolly pine.* Green Chemistry, 2012. **14**(1): p. 72.

67. Ben, H. and Ragauskas, A.J., *Pyrolysis of Kraft Lignin with Additives.* Energy & Fuels, 2011. **25**(10): p. 4662-4668.

68. Ben, H. and Ragauskas, A.J., *Heteronuclear Single-Quantum Correlation–Nuclear Magnetic Resonance (HSQC–NMR) Fingerprint Analysis of Pyrolysis Oils.* Energy & Fuels, 2011. **25**(12): p. 5791-5801.

69. Ben, H. and Ragauskas, A.J., *NMR Characterization of Pyrolysis Oils from Kraft Lignin.* Energy & Fuels, 2011. **25**(5): p. 2322-2332.

70. Beis, S.H., Mukkamala, S., Hill, N., Joseph, J., Baker, C., Jensen, B., Stemmler, E.A., Wheeler, M.C., Frederick, B.G., van Heiningen, A., Berg, A.G., and DeSisto, W.J., *Fast pyrolysis of lignins.* BioRes., 2010. **5**(3): p. 1408-1424.

71. Runnebaum, R.C., Nimmanwudipong, T., Block, D.E., and Gates, B.C., *Catalytic conversion of compounds representative of lignin-derived bio-oils: a reaction network for guaiacol, anisole, 4-methylanisole, and cyclohexanone conversion catalysed by Pt/γ-Al2O3.* Catalysis Science & Technology, 2012. **2**(1): p. 113.

72. Mortensen, P.M., Grunwaldt, J.D., Jensen, P.A., Knudsen, K.G., and Jensen, A.D., *A review of catalytic upgrading of bio-oil to engine fuels.* Applied Catalysis A: General, 2011. **407**(1-2): p. 1-19.

73. Huber, G.W., Iborra, S., and Corma, A., *Synthesis of Transportation Fuels from Biomass: Chemistry, Catalysts, and Engineering.* Chemical Reviews, 2006. **106**(9): p. 4044-4098.

74. Wang, Y., Fang, Y., He, T., Hu, H., and Wu, J., *Hydrodeoxygenation of dibenzofuran over noble metal supported on mesoporous zeolite.* Catalysis Communications, 2011. **12**(13): p. 1201-1205.

75. Chantal, P.D., Kaliaguine, S., and Grandmaison, J.L., *Reactions of phenolic compounds over HZSM-5.* Applied Catalysis, 1985. **18**(1): p. 133-145.

76. Gayubo, A.G., Aguayo, A.T., Atutxa, A., Aguado, R., and Bilbao, J., *Transformation of Oxygenate Components of Biomass Pyrolysis Oil on a HZSM-5 Zeolite. I. Alcohols and Phenols.* Industrial & Engineering Chemistry Research, 2004. **43**(11): p. 2610-2618.

77. Zhu, X., Mallinson, R.G., and Resasco, D.E., *Role of transalkylation reactions in the conversion of anisole over HZSM-5.* Applied Catalysis A: General, 2010. **379**(1–2): p. 172-181.

78. Gutierrez, A., Kaila, R.K., Honkela, M.L., Slioor, R., and Krause, A.O.I., *Hydrodeoxygenation of guaiacol on noble metal catalysts.* Catalysis Today, 2009. **147**(3–4): p. 239-246.

79. Elliott, D.C., *Historical Developments in Hydroprocessing Bio-oils.* Energy & Fuels, 2007. **21**(3): p. 1792-1815.

80. Furimsky, E., *Catalytic hydrodeoxygenation.* Applied Catalysis A: General, 2000. **199**(2): p. 147-190.

81. Odebunmi, E.O. and Ollis, D.F., *Catalytic hydrodeoxygenation: I. Conversions of o-, p-, and m-cresols.* Journal of Catalysis, 1983. **80**(1): p. 56-64.

82. Odebunmi, E.O. and Ollis, D.F., *Catalytic hydrodeoxygenation: II. Interactions between catalytic hydrodeoxygenation of m-cresol and hydrodesulfurization of benzothiophene and dibenzothiophene.* Journal of Catalysis, 1983. **80**(1): p. 65-75.

83. Gevert, B.S., Otterstedt, J.E., and Massoth, F.E., *Kinetics of the HDO of methyl-substituted phenols.* Applied Catalysis, 1987. **31**(1): p. 119-131.

84. Elliott, D.C., Beckman, D., Bridgwater, A.V., Diebold, J.P., Gevert, S.B., and Solantausta, Y., *Developments in direct thermochemical liquefaction of biomass: 1983-1990.* Energy & Fuels, 1991. **5**(3): p. 399-410.

85. Viljava, T.R., Komulainen, R.S., and Krause, A.O.I., *Effect of H2S on the stability of CoMo/Al2O3 catalysts during hydrodeoxygenation.* Catalysis Today, 2000. **60**(1–2): p. 83-92.

86. Furimsky, E. and Massoth, F.E., *Deactivation of hydroprocessing catalysts.* Catalysis Today, 1999. **52**(4): p. 381-495.

87. Laurent, E. and Delmon, B., *Influence of water in the deactivation of a sulfided NiMoγ-Al2O3 catalyst during hydrodeoxygenation.* Journal of Catalysis, 1994. **146**(1): p. 281-291.

88. Centeno, A., Laurent, E., and Delmon, B., *Influence of the Support of CoMo Sulfide Catalysts and of the Addition of Potassium and Platinum on the Catalytic Performances for the Hydrodeoxygenation of Carbonyl, Carboxyl, and Guaiacol-Type Molecules.* Journal of Catalysis, 1995. **154**(2): p. 288-298.

89. Honkela, M.L., Björk, J., and Persson, M., *Computational study of the adsorption and dissociation of phenol on Pt and Rh surfaces.* Physical Chemistry Chemical Physics, 2012. **14**(16): p. 5849.

90. Niquille-Röthlisberger, A. and Prins, R., *Hydrodesulfurization of 4,6-dimethyldibenzothiophene and dibenzothiophene over alumina-supported Pt, Pd, and Pt-Pd catalysts.* Journal of Catalysis, 2006. **242**(1): p. 207-216.

91. Tang, T., Yin, C., Wang, L., Ji, Y., and Xiao, F.-S., *Superior performance in deep saturation of bulky aromatic pyrene over acidic mesoporous Beta zeolite-supported palladium catalyst.* Journal of Catalysis, 2007. **249**(1): p. 111-115.

92. Do, P.T.M., Foster, A.J., Chen, J., and Lobo, R.F., *Bimetallic effects in the hydrodeoxygenation of meta-cresol on γ-Al2O3 supported Pt–Ni and Pt–Co catalysts.* Green Chemistry, 2012. **14**(5): p. 1388.

93. Hong, D.-Y., Miller, S.J., Agrawal, P.K., and Jones, C.W., *Hydrodeoxygenation and coupling of aqueous phenolics over bifunctional zeolite-supported metal catalysts.* Chemical Communications, 2010. **46**(7): p. 1038.

94. Lee, C.R., Yoon, J.S., Suh, Y.-W., Choi, J.-W., Ha, J.-M., Suh, D.J., and Park, Y.-K., *Catalytic roles of metals and supports on hydrodeoxygenation of lignin monomer guaiacol.* Catalysis Communications, 2012. **17**: p. 54-58.

95. Zhu, X., Lobban, L.L., Mallinson, R.G., and Resasco, D.E., *Bifunctional transalkylation and hydrodeoxygenation of anisole over a Pt/HBeta catalyst.* Journal of Catalysis, 2011. **281**(1): p. 21-29.

96. Pham, T.T., Lobban, L.L., Resasco, D.E., and Mallinson, R.G., *Hydrogenation and Hydrodeoxygenation of 2-methyl-2-pentenal on supported metal catalysts.* Journal of Catalysis, 2009. **266**(1): p. 9-14.

97. Ohta, H., Kobayashi, H., Hara, K., and Fukuoka, A., *Hydrodeoxygenation of phenols as lignin models under acid-free conditions with carbon-supported platinum catalysts.* Chemical Communications, 2011. **47**(44): p. 12209-12211.

98. Li, N., Tompsett, G.A., Zhang, T., Shi, J., Wyman, C.E., and Huber, G.W., *Renewable gasoline from aqueous phase hydrodeoxygenation of aqueous sugar solutions prepared by hydrolysis of maple wood.* Green Chemistry, 2011. **13**(1): p. 91.

99. Liu, C., Shao, Z., Xiao, Z., Williams, C.T., and Liang, C., *Hydrodeoxygenation of Benzofuran over Silica–Alumina-Supported Pt, Pd, and Pt–Pd Catalysts.* Energy & Fuels, 2012. **26**(7): p. 4205-4211.

100. Beccat, P., Bertolini, J.C., Gauthier, Y., Massardier, J., and Ruiz, P., *Crotonaldehyde and methylcrotonaldehyde hydrogenation over Pt(111) and Pt80Fe20(111) single crystals.* Journal of Catalysis, 1990. **126**(2): p. 451-456.

101. Birchem, T., Pradier, C.M., Berthier, Y., and Cordier, G., *Reactivity of 3-Methyl-Crotonaldehyde on Pt(111).* Journal of Catalysis, 1994. **146**(2): p. 503-510.

102. Huang, Y., Wei, Z., Qiu, Z., Yin, X., and Wu, C., *Study on structure and pyrolysis behavior of lignin derived from corncob acid hydrolysis residue.* Journal of Analytical and Applied Pyrolysis, 2012. **93**: p. 153-159.

103. Pan, C., Chen, A., Liu, Z., Chen, P., Lou, H., and Zheng, X., *Aqueous-phase reforming of the low-boiling fraction of rice husk pyrolyzed bio-oil in the*

presence of platinum catalyst for hydrogen production. Bioresource Technology, 2012. **125**(0): p. 335-339.

104. Wright, M.M., Román‐Leshkov, Y., and Green, W.H., *Investigating the techno‐economic trade‐offs of hydrogen source using a response surface model of drop‐in biofuel production via bio‐oil upgrading.* Biofuels, Bioproducts and Biorefining, 2012. **6**(5): p. 503-520.

105. Wright, M.M., Daugaard, D.E., Satrio, J.A., and Brown, R.C., *Techno-economic analysis of biomass fast pyrolysis to transportation fuels.* Fuel, 2010. **89**: p. S2-S10.

106. Jones, S.B., Valkenburg, C., Walton, C.W., Elliott, D.C., Holladay, J.E., Stevens, D.J., Kinchin, C., and Czernik, S., *Production of gasoline and diesel from biomass via fast pyrolysis, hydrotreating and hydrocracking: a design case*. 2009: Pacific Northwest National Laboratory Richland, WA.

107. Gevert, B., Otterstedt, J., and Massoth, F., *Kinetics of the HDO of methyl-substituted phenols.* Applied catalysis, 1987. **31**(1): p. 119-131.

108. Whiffen, V.M. and Smith, K.J., *Hydrodeoxygenation of 4-Methylphenol over Unsupported MoP, MoS2, and MoO x Catalysts†.* Energy & Fuels, 2010. **24**(9): p. 4728-4737.

109. Jiang, H., Yang, H., Hawkins, R., and Ring, Z., *Effect of palladium on sulfur resistance in Pt–Pd bimetallic catalysts.* Catalysis Today, 2007. **125**(3–4): p. 282-290.

110. Bonalumi, N., Vargas, A., Ferri, D., and Baiker, A., *Theoretical and Spectroscopic Study of the Effect of Ring Substitution on the Adsorption of*

Anisole on Platinum. The Journal of Physical Chemistry B, 2006. **110**(20): p. 9956-9965.

111. Lu, S., Lonergan, W.W., Bosco, J.P., Wang, S., Zhu, Y., Xie, Y., and Chen, J.G., *Low temperature hydrogenation of benzene and cyclohexene: A comparative study between γ-Al2O3 supported PtCo and PtNi bimetallic catalysts.* Journal of Catalysis, 2008. **259**(2): p. 260-268.

112. Lu, S., Menning, C.A., Zhu, Y., and Chen, J.G., *Correlating Benzene Hydrogenation Activity with Binding Energies of Hydrogen and Benzene on Co-Based Bimetallic Catalysts.* ChemPhysChem, 2009. **10**(11): p. 1763-1765.

113. Lonergan, W.W., Vlachos, D.G., and Chen, J.G., *Correlating extent of Pt–Ni bond formation with low-temperature hydrogenation of benzene and 1,3-butadiene over supported Pt/Ni bimetallic catalysts.* Journal of Catalysis, 2010. **271**(2): p. 239-250.

114. Zhao, C., He, J., Lemonidou, A.A., Li, X., and Lercher, J.A., *Aqueous-phase hydrodeoxygenation of bio-derived phenols to cycloalkanes.* Journal of Catalysis, 2011. **280**(1): p. 8-16.

115. Zhao, C., Kou, Y., Lemonidou, A.A., Li, X., and Lercher, J.A., *Highly Selective Catalytic Conversion of Phenolic Bio-Oil to Alkanes.* Angewandte Chemie International Edition, 2009. **48**(22): p. 3987-3990.

116. Zhao, C. and Lercher, J.A., *Selective Hydrodeoxygenation of Lignin-Derived Phenolic Monomers and Dimers to Cycloalkanes on Pd/C and HZSM-5 Catalysts.* ChemCatChem, 2012. **4**(1): p. 64-68.

117. Velu, S., Kapoor, M.P., Inagaki, S., and Suzuki, K., *Vapor phase hydrogenation of phenol over palladium supported on mesoporous CeO2 and ZrO2.* Applied Catalysis A: General, 2003. **245**(2): p. 317-331.

118. Chen, Y.Z., Liaw, C.W., and Lee, L.I., *Selective hydrogenation of phenol to cyclohexanone over palladium supported on calcined Mg/Al hydrotalcite.* Applied Catalysis A: General, 1999. **177**(1): p. 1-8.

119. Neri, G., Visco, A.M., Donato, A., Milone, C., Malentacchi, M., and Gubitosa, G., *Hydrogenation of phenol to cyclohexanone over palladium and alkali-doped palladium catalysts.* Applied Catalysis A: General, 1994. **110**(1): p. 49-59.

120. Talukdar, A.K., Bhattacharyya, K.G., and Sivasanker, S., *Hydrogenation of phenol over supported platinum and palladium catalysts.* Applied Catalysis A: General, 1993. **96**(2): p. 229-239.

121. Orita, H. and Itoh, N., *Simulation of phenol formation from benzene with a Pd membrane reactor: ab initio periodic density functional study.* Applied Catalysis A: General, 2004. **258**(1): p. 17-23.

122. Lin, Y.-C., Li, C.-L., Wan, H.-P., Lee, H.-T., and Liu, C.-F., *Catalytic Hydrodeoxygenation of Guaiacol on Rh-Based and Sulfided CoMo and NiMo Catalysts.* Energy & Fuels, 2011. **25**(3): p. 890-896.

123. Ihm, H. and White, J.M., *Stepwise Dissociation of Thermally Activated Phenol on Pt(111).* The Journal of Physical Chemistry B, 2000. **104**(26): p. 6202-6211.

124. Xu, X. and Friend, C.M., *The role of coverage in determining adsorbate stability: phenol reactivity on rhodium(111).* The Journal of Physical Chemistry, 1989. **93**(24): p. 8072-8080.

125. Kluson, P. and Cerveny, L., *Hydrogenation of substituted aromatic compounds over a ruthenium catalyst.* Journal of Molecular Catalysis A: Chemical, 1996. **108**(2): p. 107-112.

126. Guo, J., Ruan, R., and Zhang, Y., *Hydrotreating of Phenolic Compounds Separated from Bio-oil to Alcohols.* Industrial & Engineering Chemistry Research, 2012. **51**(19): p. 6599-6604.

127. Greenfield, H., *STUDIES IN NUCLEAR HYDROGENATION.* Annals of the New York Academy of Sciences, 1973. **214**(1): p. 233-242.

128. Wildschut, J., Iqbal, M., Mahfud, F.H., Cabrera, I.M., Venderbosch, R.H., and Heeres, H.J., *Insights in the hydrotreatment of fast pyrolysis oil using a ruthenium on carbon catalyst.* Energy & Environmental Science, 2010. **3**(7): p. 962.

129. Nimmanwudipong, T., Runnebaum, R., Block, D., and Gates, B., *Catalytic Reactions of Guaiacol: Reaction Network and Evidence of Oxygen Removal in Reactions with Hydrogen.* Catalysis Letters, 2011. **141**(6): p. 779-783.

130. Runnebaum, R., Nimmanwudipong, T., Block, D., and Gates, B., *Catalytic Conversion of Anisole: Evidence of Oxygen Removal in Reactions with Hydrogen.* Catalysis Letters, 2011. **141**(6): p. 817-820.

131. Bui, V.N., Laurenti, D., Afanasiev, P., and Geantet, C., *Hydrodeoxygenation of guaiacol with CoMo catalysts. Part I: Promoting effect of cobalt on HDO selectivity and activity.* Applied Catalysis B: Environmental, 2011. **101**(3-4): p. 239-245.

132. Sato, S., Takahashi, R., Sodesawa, T., Matsumoto, K., and Kamimura, Y., *Ortho-Selective Alkylation of Phenol with 1-Propanol Catalyzed by CeO2–MgO.* Journal of Catalysis, 1999. **184**(1): p. 180-188.

133. Auroux, A., Artizzu, P., Ferino, I., Solinas, V., Leofanti, G., Padovan, M., Messina, G., and Mansani, R., *Dehydration of 4-methylpentan-2-ol over zirconia catalysts.* Journal of the Chemical Society, Faraday Transactions, 1995. **91**(18): p. 3263-3267.

134. Mahata, N., Raghavan, K.V., Vishwanathan, V., Park, C., and Keane, M.A., *Phenol hydrogenation over palladium supported on magnesia: Relationship between catalyst structure and performance.* Physical Chemistry Chemical Physics, 2001. **3**(13): p. 2712-2719.

135. Shin, E.-J. and Keane, M.A., *Gas-Phase Hydrogenation/Hydrogenolysis of Phenol over Supported Nickel Catalysts.* Industrial & Engineering Chemistry Research, 2000. **39**(4): p. 883-892.

136. Aprile, C., Abad, A., Garcia, H., and Corma, A., *Synthesis and catalytic activity of periodic mesoporous materials incorporating gold nanoparticles.* Journal of Materials Chemistry, 2005. **15**(41): p. 4408-4413.

137. Fournier, R.O. and Rowe, J.J., *The solubility of amorphous silica in water at high temperatures and high pressures.* American Mineralogist, 1977. **62**: p. 1052-1056.

138. Lefèvre, G., Duc, M., Lepeut, P., Caplain, R., and Fédoroff, M., *Hydration of γ-Alumina in Water and Its Effects on Surface Reactivity.* Langmuir, 2002. **18**(20): p. 7530-7537.

139. Jongerius, A.L., Jastrzebski, R., Bruijnincx, P.C.A., and Weckhuysen, B.M., *CoMo sulfide-catalyzed hydrodeoxygenation of lignin model compounds: An extended reaction network for the conversion of monomeric and dimeric substrates.* Journal of Catalysis, 2012. **285**(1): p. 315-323.

140. Furimsky, E., *Carbons and Carbon Supported Catalysts in Hydroprocessing*. RSC Catalysis Series, ed. J.J. Spivey. 2008: The Royal Society of Chemistry.

141. Girgis, M.J. and Gates, B.C., *Reactivities, reaction networks, and kinetics in high-pressure catalytic hydroprocessing.* Industrial & Engineering Chemistry Research, 1991. **30**(9): p. 2021-2058.

142. Mortensen, P.M., Grunwaldt, J.D., Jensen, P.A., Knudsen, K.G., and Jensen, A.D., *A review of catalytic upgrading of bio-oil to engine fuels.* Applied Catalysis A: General, 2011. **407**(1–2): p. 1-19.

143. Rana, M.S., Sámano, V., Ancheyta, J., and Diaz, J.A.I., *A review of recent advances on process technologies for upgrading of heavy oils and residua.* Fuel, 2007. **86**(9): p. 1216-1231.

144. Maschio, G., Koufopanos, C., and Lucchesi, A., *Pyrolysis, a promising route for biomass utilization.* Bioresource Technology, 1992. **42**(3): p. 219-231.

145. de Vlieger, D.J.M., Mojet, B.L., Lefferts, L., and Seshan, K., *Aqueous Phase Reforming of ethylene glycol – Role of intermediates in catalyst performance.* Journal of Catalysis, 2012. **292**(0): p. 239-245.

146. Gottardo, M., *Green Procedures for the Selective Aqueous-Phase Hydrogenation of Biomass-Derived Levulinic Acid to Gamma-Valerolactone. Innovative Design for Catalytic Recycle and Regeneration.* 2013.

147. Maegawa, T., Kitamura, Y., Sako, S., Udzu, T., Sakurai, A., Tanaka, A., Kobayashi, Y., Endo, K., Bora, U., Kurita, T., Kozaki, A., Monguchi, Y., and Sajiki, H., *Heterogeneous Pd/C-Catalyzed Ligand-Free, Room-Temperature Suzuki–Miyaura Coupling Reactions in Aqueous Media.* Chemistry – A European Journal, 2007. **13**(20): p. 5937-5943.

148. Op de Beeck, B., Dusselier, M., Geboers, J., Holsbeek, J., Morre, E., Oswald, S., Giebeler, L., and Sels, B.F., *Direct catalytic conversion of cellulose to liquid straight-chain alkanes.* Energy & Environmental Science, 2015.

149. Pan, X., Xie, D., Yu, R.W., Lam, D., and Saddler, J.N., *Pretreatment of Lodgepole Pine Killed by Mountain Pine Beetle Using the Ethanol Organosolv Process Fractionation and Process Optimization.* Ind. Eng. Chem. Res., 2007. **46**: p. 2609-2617.

150. Hallac, B.B., Pu, Y., and Ragauskas, A.J., *Chemical Transformations of Buddleja davidii Lignin during Ethanol Organosolv Pretreatment.* Energy & Fuels, 2010. **24**(4): p. 2723-2732.

151. El Hage, R., Brosse, N., Chrusciel, L., Sanchez, C., Sannigrahi, P., and Ragauskas, A., *Characterization of milled wood lignin and ethanol organosolv lignin from miscanthus.* Polymer Degradation and Stability, 2009. **94**(10): p. 1632-1638.

152. El Hage, R., Brosse, N., Sannigrahi, P., and Ragauskas, A., *Effects of process severity on the chemical structure of Miscanthus ethanol organosolv lignin.* Polymer Degradation and Stability, 2010. **95**(6): p. 997-1003.

153. Ewbank, J.L., Kovarik, L., Kenvin, C.C., and Sievers, C., *Effect of preparation methods on the performance of Co/Al2O3 catalysts for dry reforming of methane.* Green Chemistry, 2014. **16**(2): p. 885-896.

154. Peng, G., Steib, M., Gramm, F., Ludwig, C., and Vogel, F., *Synthesis factors affecting the catalytic performance and stability of Ru/C catalysts for supercritical water gasification.* Catalysis Science & Technology, 2014. **4**(9): p. 3329-3339.

155. Edwin Vasu, A., *Surface Modification of Activated Carbon for enhancement of Nickel (II) adsorption.* Journal of Chemistry, 2008. **5**(4): p. 814-819.

156. Runnebaum, R.C., Nimmanwudipong, T., Block, D.E., and Gates, B.C., *Catalytic conversion of compounds representative of lignin-derived bio-oils: a reaction network for guaiacol, anisole, 4-methylanisole, and cyclohexanone conversion catalysed by Pt/[gamma]-Al2O3.* Catalysis Science & Technology, 2012. **2**(1): p. 113-118.

157. Nimmanwudipong, T., Aydin, C., Lu, J., Runnebaum, R., Brodwater, K., Browning, N., Block, D., and Gates, B., *Selective Hydrodeoxygenation of Guaiacol Catalyzed by Platinum Supported on Magnesium Oxide.* Catalysis Letters, 2012. **142**(10): p. 1190-1196.

158. Ben, H., Ferguson, G.A., Mu, W., Pu, Y., Huang, F., Jarvis, M., Biddy, M., Deng, Y., and Ragauskas, A.J., *Hydrodeoxygenation by deuterium gas - a powerful way to provide insight into the reaction mechanisms.* Physical Chemistry Chemical Physics, 2013. **15**(44): p. 19138-19142.

159. Prasomsri, T., Shetty, M., Murugappan, K., and Roman-Leshkov, Y., *Insights into the catalytic activity and surface modification of MoO3 during the hydrodeoxygenation of lignin-derived model compounds into aromatic hydrocarbons under low hydrogen pressures.* Energy & Environmental Science, 2014. **7**(8): p. 2660-2669.

160. Asmadi, M., Kawamoto, H., and Saka, S., *Pyrolysis and Secondary Reaction Mechanisms of Softwood and Hardwood Lignins at the Molecular Level*, in *Zero-Carbon Energy Kyoto 2010*, T. Yao, Editor. 2011, Springer Japan. p. 129-135.

161. Hosoya, T., Kawamoto, H., and Saka, S., *Role of methoxyl group in char formation from lignin-related compounds.* Journal of Analytical and Applied Pyrolysis, 2009. **84**(1): p. 79-83.

162. Huber, G.W., Iborra, S., and Corma, A., *Synthesis of Transportation Fuels from Biomass: Chemistry, Catalysts, and Engineering.* Chem. Rev., 2006. **106**: p. 4044-4098.

163. Yan, N., Yuan, Y., Dykeman, R., Kou, Y., and Dyson, P.J., *Hydrodeoxygenation of lignin-derived phenols into alkanes by using nanoparticle catalysts combined with Bronsted acidic ionic liquids.* Angew. Chem. Int. Ed. Engl., 2010. **49**(32): p. 5549-53.

164. Zhao, C., Kou, Y., Lemonidou, A.A., Li, X., and Lercher, J.A., *Highly selective catalytic conversion of phenolic bio-oil to alkanes.* Angew. Chem. Int. Ed. Engl., 2009. **48**(22): p. 3987-90.

165. Vispute, T.P., Zhang, H., Sanna, A., Xiao, R., and Huber, G.W., *Renewable Chemical Commodity Feedstocks from Integrated Catalytic Processing of Pyrolysis Oils.* Science, 2010. **330**(6008): p. 1222-1227.

166. Wildschut, J., Iqbal, M., Mahfud, F.H., Cabrera, I.M., Venderbosch, R.H., and Heeres, H.J., *Insights in the hydrotreatment of fast pyrolysis oil using a ruthenium on carbon catalyst.* Energy Environ. Sci., 2010. **3**(7): p. 962.

167. Ben, H. and Ragauskas, A.J., *NMR Characterization of Pyrolysis Oils from Kraft Lignin.* Energy Fuels, 2011. **25**(5): p. 2322-2332.

168. Kosa, M., Ben, H., Theliander, H., and Ragauskas, A.J., *Pyrolysis oils from CO2 precipitated Kraft lignin.* Green Chem., 2011. **13**(11): p. 3196-3202.

169. Ben, H. and Ragauskas, A.J., *Heteronuclear Single-Quantum Correlation–Nuclear Magnetic Resonance (HSQC–NMR) Fingerprint Analysis of Pyrolysis Oils.* Energy Fuels, 2011. **25**(12): p. 5791-5801.

170. Ben, H., Pan, S., Berg, A., and Ragauskas, A.J., *HSQC-NMR fingerprint analysis of pyrolysis oils produced from tannin, pine bark and residue.* 2012: p. will submit.

171. Hu, F. and Ragauskas, A., *Suppression of pseudo-lignin formation under dilute acid pretreatment conditions.* RSC Advances, 2014. **4**(9): p. 4317-4323.

172. Sannigrahi, P., Kim, D.H., Jung, S., and Ragauskas, A., *Pseudo-lignin and pretreatment chemistry.* Energy & Environmental Science, 2011. **4**(4): p. 1306-1310.

173. Pan, X., Xie, D., Yu, R.W., Lam, D., and Saddler, J.N., *<Pretreatment of Lodgepole Pine Killed by Mountain Pine Beetle Using the Ethanol Organosolv*

Process Fractionation and Process Optimization.pdf>. Ind. Eng. Chem. Res., 2007. **46**: p. 2609-2617.

174. Capanema, E.A., Balakshin, M.Y., and Kadla, J.F., *A Comprehensive Approach for Quantitative Lignin Characterization by NMR Spectroscopy.* J. Agric. Food Chem., 2004. **52**: p. 1850-1860.

175. Ben, H. and Ragauskas, A.J., *Heteronuclear Single-Quantum Correlation–Nuclear Magnetic Resonance (HSQC–NMR) Fingerprint Analysis of Pyrolysis Oils.* Energy & Fuels, 2011: p. 10.1021/ef201376w.

176. Ben, H., Pan, S., Berg, A., and Ragauskas, A.J., *HSQC-NMR fingerprint analysis of pyrolysis oils produced from tannin, pine bark and residue.* Fuel, 2011: p. Submitted.

177. Mullen, C.A., Strahan, G.D., and Boateng, A.A., *Characterization of Various Fast-Pyrolysis Bio-Oils by NMR Spectroscopy.* Energy Fuels, 2009. **23**: p. 2707-2718.

178. Ben, H. and Ragauskas, A.J., *Pyrolysis of Kraft Lignin with Additives.* Energy Fuels, 2011. **25**(10): p. 4662-4668.

179. Chen, L., Zhu, Y., Zheng, H., Zhang, C., Zhang, B., and Li, Y., *Aqueous-phase hydrodeoxygenation of carboxylic acids to alcohols or alkanes over supported Ru catalysts.* J. Mol. Catal. A: Chem., 2011. **351**: p. 217-227.

180. Ben, H., Mu, W., Deng, Y., and Ragauskas, A.J., *Production of renewable gasoline from aqueous phase hydrogenation of lignin pyrolysis oil.* Fuel, 2013. **103**: p. 1148-1153.

181. Ben, H. and Ragauskas, A.J., *Torrefaction of Loblolly pine.* Green Chemistry, 2012. **14**(1): p. 72-76.

182. Ben, H. and Ragauskas, A.J., *In Situ NMR Characterization of Pyrolysis Oil during Accelerated Aging.* ChemSusChem, 2012. **5**(9): p. 1687-1693.

183. Ben, H. and Ragauskas, A.J., *Influence of Si/Al Ratio of ZSM-5 Zeolite on the Properties of Lignin Pyrolysis Products.* ACS Sustainable Chemistry & Engineering, 2013. **1**(3): p. 316-324.

184. Ben, H. and Ragauskas, A.J., *One step thermal conversion of lignin to the gasoline range liquid products by using zeolites as additives.* RSC Advances, 2012. **2**(33): p. 12892-12898.

185. Wang, X. and Rinaldi, R., *Solvent Effects on the Hydrogenolysis of Diphenyl Ether with Raney Nickel and their Implications for the Conversion of Lignin.* ChemSusChem, 2012. **5**(8): p. 1455-1466.

186. He, J., Zhao, C., and Lercher, J.A., *Ni-Catalyzed Cleavage of Aryl Ethers in the Aqueous Phase.* Journal of the American Chemical Society, 2012. **134**(51): p. 20768-20775.

187. Petrocelli, F.P. and Klein, M.T., *Chemical modeling analysis of the yields of single-ring phenolics from lignin liquefaction.* Industrial & Engineering Chemistry Product Research and Development, 1985. **24**(4): p. 635-641.

188. Malhotra, R. and McMillen, D.F., *Relevance of cleavage of strong bonds in coal liquefaction.* Energy & Fuels, 1993. **7**: p. 227-233.

189. Aubert, C., Durand, R., Geneste, P., and Moreau, C., *Factors affecting the hydrogenation of substituted benzenes and phenols over a sulfided NiO MoO3 γ-Al2O3 catalyst.* Journal of Catalysis, 1988. **112**(1): p. 12-20.

190. Nimmanwudipong, T., Runnebaum, R.C., Block, D.E., and Gates, B.C., *Catalytic Conversion of Guaiacol Catalyzed by Platinum Supported on Alumina: Reaction Network Including Hydrodeoxygenation Reactions.* Energy Fuels, 2011. **25**(8): p. 3417-3427.

191. Bui, V.N., Laurenti, D., Afanasiev, P., and Geantet, C., *Hydrodeoxygenation of guaiacol with CoMo catalysts. Part I: Promoting effect of cobalt on HDO selectivity and activity.* Appl. Catal., B, 2011. **101**(3-4): p. 239-245.

192. Huber, G.W., Chheda, J.N., Barrett, C.J., and Dumesic, J.A., *Production of liquid alkanes by aqueous-phase processing of biomass-derived carbohydrates.* Science, 2005. **308**(5727): p. 1446-50.

193. Zhao, C., He, J., Lemonidou, A.A., Li, X., and Lercher, J.A., *Aqueous-phase hydrodeoxygenation of bio-derived phenols to cycloalkanes.* J. Catal. , 2011. **280**(1): p. 8-16.

194. Bui, V.N., Laurenti, D., Delichère, P., and Geantet, C., *Hydrodeoxygenation of guaiacol.* Appl. Catal., B, 2011. **101**(3-4): p. 246-255.

195. Weingarten, R., Tompsett, G.A., Conner Jr, W.C., and Huber, G.W., *Design of solid acid catalysts for aqueous-phase dehydration of carbohydrates: The role of Lewis and Brønsted acid sites.* Journal of Catalysis, 2011. **279**(1): p. 174-182.

196. Hunger, M., Freude, D., and Pfeifer, H., *Magic-angle spinning nuclear magnetic resonance studies of water molecules adsorbed on Bronsted- and Lewis-acid sites*

in zeolites and amorphous silica-aluminas. Journal of the Chemical Society, Faraday Transactions, 1991. **87**(4): p. 657-662.

197. Ravenelle, R.M., Schüβler, F., D'Amico, A., Danilina, N., van Bokhoven, J.A., Lercher, J.A., Jones, C.W., and Sievers, C., *Stability of Zeolites in Hot Liquid Water.* The Journal of Physical Chemistry C, 2010. **114**(46): p. 19582-19595.

198. Su, L., Liu, L., Zhuang, J., Wang, H., Li, Y., Shen, W., Xu, Y., and Bao, X., *Creating Mesopores in ZSM-5 Zeolite by Alkali Treatment: A New Way to Enhance the Catalytic Performance of Methane Dehydroaromatization on Mo/HZSM-5 Catalysts.* Catalysis Letters, 2003. **91**(3-4): p. 155-167.

199. Williams, P.T. and Besler, S., *The influence of temperature and heating rate on the slow pyrolysis of biomass.* Renewable Energy, 1996. **7**(3): p. 233-250.

200. Ben, H. and Ragauskas, A.J., *Comparison for the compositions of fast and slow pyrolysis oils by NMR characterization.* Bioresource Technology, (0).

201. Mu, W., Ben, H., Ragauskas, A., and Deng, Y., *Lignin Pyrolysis Components and Upgrading—Technology Review.* BioEnergy Research, 2013: p. 1-22.

202. Zhang, L., Liu, R., Yin, R., and Mei, Y., *Upgrading of bio-oil from biomass fast pyrolysis in China: A review.* Renewable and Sustainable Energy Reviews, 2013. **24**: p. 66-72.

203. Bridgwater, A.V., Meier, D., and Radlein, D., *An overview of fast pyrolysis of biomass.* Organic Geochemistry, 1999. **30**(12): p. 1479-1493.

204. Ben, H., Pan, S., Berg, A., and Ragauskas, A., *HSQC-NMR fingerprint analysis of pyrolysis oils produced from tannin, pine bark and residue.* Under preparation.

205. Ben, H. and Ragauskas, A.J., *Comparison for the compositions of fast and slow pyrolysis oils by NMR characterization.* Bioresour Technol, 2013. **147**: p. 577-84.

206. Pindoria, R.V., Megaritis, A., Messenböck, R.C., Dugwell, D.R., and Kandiyoti, R., *Comparison of the pyrolysis and gasification of biomass: effect of reacting gas atmosphere and pressure on Eucalyptus wood.* Fuel, 1998. **77**(11): p. 1247-1251.

207. Maggi, R. and Delmon, B., *Comparison between 'slow' and 'flash' pyrolysis oils from biomass.* Fuel, 1994. **73**(5): p. 671-677.

208. Yaman, S., *Pyrolysis of biomass to produce fuels and chemical feedstocks.* Energy Conversion and Management, 2004. **45**(5): p. 651-671.

209. Bridgwater, A.V. and Cottam, M.L., *Opportunities for biomass pyrolysis liquids production and upgrading.* Energy & Fuels, 1992. **6**(2): p. 113-120.

210. Ben, H., Mu, W., Deng, Y., and Ragauskas, A.J., *Production of renewable gasoline from aqueous phase hydrogenation of lignin pyrolysis oil.* Fuel, 2013. **103**(0): p. 1148-1153.

211. Marker, T.L. and Petri, J.A., *Gasoline and diesel production from pyrolytic lignin produced from pyrolysis of cellulosic waste*, U.S. Patent, Editor. 2006, UOP LLC, Des Plaines, IL(US): United States of America.

212. Vispute, T.P. and Huber, G.W., *Production of hydrogen, alkanes and polyols by aqueous phase processing of wood-derived pyrolysis oils.* Green Chemistry, 2009. **11**(9): p. 1433-1445.

213. Gao, D., Hwang, H.T., and Arvind, A. *Catalytic Hydrodeoxygenation of Bio-Oil*. in *American Institute of Chemical Engineering Conference (AIChE)*. 2012. Pittsburg, PA.

214. Wildschut, J., Mahfud, F.H., Venderbosch, R.H., and Heeres, H.J., *Hydrotreatment of Fast Pyrolysis Oil Using Heterogeneous Noble-Metal Catalysts.* Industrial & Engineering Chemistry Research, 2009. **48**(23): p. 10324-10334.

215. Daystar, J., Reeb, C., Venditti, R., Gonzalez, R., and Puettmann, M.E., *Life-Cycle Assessment of Bioethanol from Pine Residues via Indirect Biomass Gasification to Mixed Alcohols.* 2012.

216. Huang, F., Singh, P.M., and Ragauskas, A.J., *Characterization of Milled Wood Lignin (MWL) in Loblolly Pine Stem Wood, Residue, and Bark.* Journal of Agricultural and Food Chemistry, 2011. **59**(24): p. 12910-12916.

217. Wang, H., Male, J., and Wang, Y., *Recent Advances in Hydrotreating of Pyrolysis Bio-Oil and Its Oxygen-Containing Model Compounds.* ACS Catalysis, 2013. **3**(5): p. 1047-1070.

218. Lu, Q., Dong, C.-q., Zhang, X.-m., Tian, H.-y., Yang, Y.-p., and Zhu, X.-f., *Selective fast pyrolysis of biomass impregnated with ZnCl2 to produce furfural: Analytical Py-GC/MS study.* Journal of Analytical and Applied Pyrolysis, 2011. **90**(2): p. 204-212.

219. Vispute, T.P. and Huber, G.W., *Breaking the Chemical and Engineering Barriers to Lignocellulosic Biofuels.* International Sugar Journal, 2008: p. 110, 138, 140, 142, 146, 148-149.

220. Elliott, D.C. and Hart, T.R., *Catalytic Hydroprocessing of Chemical Models for Bio-oil.* Energy & Fuels, 2008. **23**(2): p. 631-637.

221. Zhou, B., *Cleaning the catalyst by solvent extraction, drying, calcining, and contacting with an organo-metallic complex to break down large metal agglomerates; hydrogenation catalysts*. 2002, Google Patents.